

Impact of the Supplementary Cementitious Materials on the kinetics and microstructural development of cement hydration

THÈSE N° 6417 (2015)

PRÉSENTÉE LE 30 JANVIER 2015

À LA FACULTÉ DES SCIENCES ET TECHNIQUES DE L'INGÉNIEUR
LABORATOIRE DES MATÉRIAUX DE CONSTRUCTION
PROGRAMME DOCTORAL EN SCIENCE ET GÉNIE DES MATÉRIAUX

ÉCOLE POLYTECHNIQUE FÉDÉRALE DE LAUSANNE

POUR L'OBTENTION DU GRADE DE DOCTEUR ÈS SCIENCES

PAR

Elise Marie Jeanne BERODIER

acceptée sur proposition du jury:

Prof. D. Damjanovic, président du jury
Prof. K. Scrivener, directrice de thèse
Prof. R. J. Flatt, rapporteur
Prof. D. E. Macphee, rapporteur
Dr T. Matschei, rapporteur



ÉCOLE POLYTECHNIQUE
FÉDÉRALE DE LAUSANNE

Suisse
2015

Liquid/solids, smooth/rough, natural/artificial, ancient/modern, base/spirit – concrete has a
tendency [...] to be two opposite things in once.
Adrian Forty

Acknowledgements

This thesis dissertation relies also on interactions and time spent with many people. I would like to express my sincere gratitude to each of them.

My first thank goes to Prof. Karen Scrivener who gave me the opportunity to do this work in her lab at EPFL. I would like to thank her for the discussions which improved the quality of my work. She also gave me the great opportunity to be involved in Nanocem, the industrial-academic research network on cement and concrete and which funded this thesis.

I would like to thank all the members of Nanocem for the valuable discussions. I specially want to thank Dr. Thomas Matchei, Prof. Donald McPhee, Dr. Duncan Hedfort, Dr. Patrick Juilland, Prof. Jorgen Skibsted, Dr. Ellis Gartner and Prof. Robert Flatt. I would also like to thank Marie Alix who makes these Nanocem events so fruitful.

Another important acknowledgement goes to the undergraduated EPFL students Nicholas, François, Félix and Damien for their excellent work and stimulating questions. It was a great experience to manage those projects.

Je voudrais remercier chaleureusement l'équipe du Centre de Microscopie de l'EPFL pour leur aide dans la préparation des échantillons. Egalement Carlos Morais et Dr Paul Bowen du LTP pour leur aide dans la caractérisation des matériaux cimentaires.

I was lucky to work with a very friendly and productive team at the Laboratory of Construction Materials and I would like to sincerely thank all my colleagues. You made my PhD time a delightful experience!

I would like to specially thank my officemates Pawel and Aslam for their support, everyday jokes; my former officemates Théo and Cédric; mes copines de labo Amélie et Berta pour leur aide, encouragements et toutes les discussions qui ont amené nos conclusions; Julien et Mo pour avoir organisé les sorties et les voyages qui marqueront ces 4 années; John pour avoir sauvé mon ordinateur plus d'une fois et surtout pour sa créativité vidéographique; Mathieu, pour toujours avoir été disponible pour mes questions et Arnaud pour son aide avec les mesures de NMR. Un grand merci à Maude et Anne Sandra pour votre soutien, l'organisation des voyages, ski-seminaire et labhike et pour les jolis défis sportifs relevés ensemble! I would like to thank the post-doc team: Cédric, Ruben, Hadi, Aurélie and specially Cyrille for the thesis corrections which contributed to the quality of this work. Merci à Emmanuelle pour son aide et ses conseils avec le nouveau microscope du labo. Un très grand merci à Lionel, Jean et Tonio qui ont toujours été là pour m'aider et me donner de précieux conseils. I also want to thank Ashley for giving me the opportunity to present my work as a Pecha Kucha at the WISH (Women in Science and Humanities) foundation event. Merci Marie-Alix pour tes encouragements et tes conseils.

Katrina was a great coworker with who I shared the excitement and the stress before the meetings. I would like also to thank Sandra, Lidija, Emilie, Camille and Mateja for the stimulating scientific discussions and for the fun we had discovering new countries.

L'Ecole Polytechnique Fédérale de Lausanne est un endroit idéal pour s'ouvrir à d'autres sujets. Merci à Prof. Ortelli de m'avoir accueillie dans son module d'architecture; Merci à Laure, Maria et Ines mes partenaires architectes, qui m'ont initié à la réalisation de projets d'architecture. Un grand merci également à Dr. Julien Grisel pour son enthousiasme et son soutien.

Je voudrais remercier tous mes amis d'ici et d'ailleurs qui m'ont accompagnée pendant ces 4 années de travail

Merci à Anaïs, Laure, Claire, Jérémie, Pierre, Yvan, Camille et Guillaume qui m'ont accompagnée depuis le début (28 ans déjà)!! Et que je retrouve toujours avec autant de plaisir.

Merci à Fabiola, Lucile, Amandine, Carole et Natalia qui ont toujours su me (re)donner le sourire!!

Merci à Lucian pour les pauses cafés et le beach volley près du lac.

Merci à Marion et Aurélien pour les régulières séances d'abdo-fou rire.

Merci à Adèle pour avoir guidé mes premiers pas en Suisse.

Merci à Anaïs de m'avoir si chaleureusement accueillie.

Merci à Luis, it was a wonderful surprise that we met again in Switzerland and working in the same field!

Un gros merci à Maude pour son soutien de chaque jour et toutes ses petites attentions!

Un immense merci à Berta, ma super copine-coloc pour son amitié, son soutien et tous les supers moments que nous avons partagés chaque jour (et tous les autres à venir...)!!!

Je remercie vivement toute ma famille, mes parents, mon frère, ma soeur et ma grand mère pour m'avoir soutenu tout au long de mon parcours, de m'avoir laissé la liberté de faire des études que j'aime. Un très grand merci aussi à ma cousine Aline pour ses nombreux encouragements et ses recettes brain power boost!

Last but not least! Un immense merci à Xavier qui m'a donné beaucoup d'énergie et d'idées tout au long de ce travail et avec qui la vie est chaque jour plus pétillante!

Lausanne, December 18th 2014

Élise Bérodiér

Abstract

Supplementary cementitious materials (SCMs) are currently used to replace part of the clinker to reduce the environmental impact of cement and to favor the use of local materials.

Two representative SCM have been used in this work – slag and fly ash. Each one corresponds to one of the SCM categories: blast furnace slag is a hydraulic material while siliceous fly ash is a pozzolanic material. A hydraulic material sets and hardens under water while pozzolans need calcium hydroxide (also referred as Portlandite) and water to produce hydrates. As a consequence when slag or fly ash is blended with clinker, its reaction occurs in addition to the cement reaction.

This work aims to study the impact of the SCMs on cement hydration to get a generic knowledge on the changes in kinetics and microstructural development when SCMs replace a part of the Portland cement. These changes are important as they can modify the microstructure and change the long term properties. It is interesting to quantify and understand these effects to predict their performance and improve these sustainable cements.

A large part of the reaction of clinker phases takes place within two days after the mixing with water. During the same period, slag and fly ash particles are not yet reacting, however they can enhance the hydration of the clinker phases. Using inert quartz powders with different fineness, our results show a clear relation between the inter-particle distance and the kinetics of the acceleration period. This can be explained by the shearing between particles which increases as the inter-particle distance decreases. The micrographs showed that reducing the distance or increasing the mixing speed produces more nucleation sites of C-S-H on the grains surfaces.

The study of limestone indicates that limestone powder has an additional effect beyond the effect of increasing the shear produced by other SCMs. The nucleation density is much higher on limestone surface and the morphology of C-S-H is changed to individual needles. The arrangement of the atoms at the surface of limestone seems to explain the increased nucleation.

In blended systems, the peak during the deceleration period has sometimes been considered as marking the beginning of the reaction of SCM. In this work, we showed that the peak only corresponds to the second dissolution of C_3A although the SCM substitution level changes the kinetics of this reaction. It has been shown that this effect is caused by the faster depletion of sulfate ions, due to the faster reaction of clinker phases and faster formation of C-S-H. A part of the sulfate is adsorbed on the C-S-H structure. This leads to the faster depletion of sulfate in the solution and change the morphology of C-S-H. Our results showed that the adsorption of sulfate promotes the growth of C-S-H as we observed needles diverging from nucleation sites. When the sulfate desorbs the C-S-H needles grow more parallel to each other. This effect was confirmed with the observation of alite where sulfate is not present. The results from 1H NMR showed that the structure itself of C-S-H is affected: few gel pores are formed in presence of sulfate.

Over the course of hydration, C-S-H fills the space available between the grains. Once the capillary pores reach a size of 6-8nm, the formation of C-S-H is slowed down and the capillary pores do not reduce

further in size. The stabilization of the pore size was explained by the increase of the supersaturation index for precipitation in these small pores. ^1H NMR results suggest that the C-S-H might grow by forming extra intersheets. In blended systems, the restriction of space also limits the reaction of slag and fly ash, thus explaining the lower degree of reaction of SCM in blended systems at high replacement levels. A similar slow-down of the kinetics was observed for unblended systems. This suggests that similar mechanisms are controlling the kinetics in both systems. The main difference between blended and unblended systems is the filling ability of the hydrates. The clinker reaction is more effective than slag or fly ash, however the reaction of slag is more efficient than that of fly ash in modifying the porosity.

Keywords: blended systems, cement hydration, microstructure, C-S-H

Résumé

Les matériaux alternatifs (SCM) sont utilisés aujourd'hui pour substituer une partie du clinker, le matériau brut du ciment ordinaire, afin de diminuer l'impact environnemental du ciment et d'utiliser des matériaux locaux.

Dans ce travail deux matériaux alternatifs, le laitier de haut fourneau et la cendre volante ont été étudiés. Ils représentent les principales catégories de SCM actuellement utilisées; respectivement les matériaux hydrauliques et pozzolaniques. Les matériaux hydrauliques réagissent avec l'eau de façon similaire au ciment. Les pozzolans nécessitent de l'eau, de l'hydroxide de calcium, aussi appelée Portlandite, pour réagir. Quand le ciment est mélangé avec le laitier ou la cendre volante, leur réactions s'ajoutent à celle de l'hydratation du ciment.

Le but de cette thèse est de comprendre l'impact des matériaux alternatifs sur l'hydratation du ciment. Quels sont les changements de cinétique de réaction et les modifications opérées sur la microstructure? Ces informations sont fondamentales pour améliorer ces ciments écologiques et prédire leurs futures propriétés.

L'hydratation du ciment se déroule principalement dans les deux jours après le mélange avec l'eau. Pendant cette même période, le laitier et les cendres volantes ne sont généralement pas encore réactifs. Néanmoins il s'avère que des particules inertes peuvent accélérer l'hydratation du ciment. Dans ce travail, nous avons utilisé des poudres de quartz de taille différente pour simuler les particules inactives. Nous démontrons que la réactivité du ciment est augmentée en fonction de la distance moyenne entre les particules. En effet, les matériaux alternatifs sont généralement broyés plus finement que le ciment, et donc réduisent la distance entre toutes les particules par rapport à un mélange fait uniquement de ciment. L'effet de la distance entre les particules a été relié à l'intensité des forces de friction induites lors du malaxage de la pâte. Plus la friction est forte, plus de nucléus sont observés à la surface des grains de ciment et de quartz.

Nos résultats sur le calcaire broyé et mélangé au ciment montrent que le calcaire favorise la nucleation du C-S-H bien plus que tout autres matériaux; y compris le ciment. Cet effet semble être dû à l'arrangement des atomes en surface.

Le pic durant la période de décélération de l'hydratation du ciment a parfois été attribué à la réaction du SCM. Il a été montré dans ce travail, que ce pic est le résultat de la seconde dissolution du tricalcium d'aluminate (C_3A), bien que le SCM modifie la cinétique de cette réaction. Cet effet est causé par le manqué d'ions sulfate. Dans les systèmes contenant SCM et ciment, les ions sulfates sont moins nombreux et plus rapidement consommés pour continuer à bloquer la réaction du C_3A . En effet, une grande partie des ions est adsorbée à la surface des C-S-H. Ceci a pour conséquence d'avancer la seconde dissolution du C_3A et de modifier la morphologie du C-S-H. La structure divergente des aiguilles de C-S-H connue dans les pâtes de ciment, peut maintenant être expliquée par l'adsorption des ions sulfates. Lors de la désorption, les aiguilles fusionnent entre elles. La morphologie obtenue est similaire à celle des C-S-H dans les pâtes d'alite ou de C_3S . La structure propre du C-S-H observée par

^1H NMR est altérée par la présence de sulfate: il y a moins de pores de gel pour une même quantité de couches de C-S-H.

Au cours de l'hydratation, le C-S-H remplit petit à petit l'espace disponible entre les grains. Lorsque les pores capillaires atteignent la taille de 6-8 nm, le C-S-H n'arrive plus à se former par précipitation et la cinétique d'hydratation devient très lente. Dans ces petits pores l'index de supersaturation qui contrôle la formation du C-S-H est augmenté ce qui rend la précipitation plus difficile. Les mesures de porosité et de ^1H NMR suggèrent que le C-S-H continue alors de se former en créant dans sa propre structure des nouvelles inter-couches.

Dans les systèmes mélangeant SCM-ciment, le manque d'espace disponible pour la croissance des hydrates, limite également la réaction du laitier et des cendres volantes. Ce résultat explique la faible réaction des SCMs dans les systèmes à haut taux de substitution. La grande différence entre les systèmes mélangés et le ciment pur est la façon dont les hydrates remplissent l'espace. La réaction du clinker est plus performante que celle du slag ou du fly ash. Cependant le laitier est plus efficace que le fly ash pour réduire la porosité.

Mots clés: ciments mélangés, hydratation du ciment, microstructure, C-S-H

Contents

Acknowledgement	v
Abstract	vii
Résumé	ix
Content	xi
List of Figures	xiii
List of Tables	xvii
Glossary	xix
Chapter 1 – Introduction	1
1. Introduction	2
1.1. Supplementary cementitious materials	3
1.2. Limitations for the use of SCMs	5
2. Motivation and objectives of the thesis	5
3. Chapter overview	6
4. References	6
Chapter 2 – Materials and Methods	7
1. Raw materials	8
1.1. Portland cement	8
1.2. Alite	9
1.3. Choice of the inert filler	10
1.4. Supplementary cementitious materials	11
2. Methods	13
2.1. Characterization of the raw materials	13
2.2. Sample preparation	16
2.3. Methods to follow the kinetics of reaction	17
2.4. Methods to assess the microstructural development	19
3. References	27
Chapter 3 – Effect of mineral additions on acceleration period	29
1. Literature review	30
1.1. Parameters affecting the nucleation and growth mechanism	32
1.2. Filler effect	34
2. Studied mixes	35
3. Results	37
3.1. Microstructure development in alite and cement paste containing quartz	37
3.2. Effect of the surface provided by inert particles on the kinetics	41
3.3. Effect of the water/solids ratio	43
3.4. Shearing effect on the microstructure and kinetics	45

3.5. Effect of common SCM	50
4. Summary	61
5. References	64
Chapter 4 – Factors affecting the second aluminate reaction	67
1. Literature review	68
1.1. The second aluminate dissolution in cement paste	68
1.2. Interaction between sulfate and C-S-H	70
1.3. Effect of SCMs on the second reaction	72
2. Studied mixes	73
3. Results	74
3.1. Control of C ₃ A reaction by gypsum content	74
3.2. Effect of gypsum depletion on C-S-H	79
3.3. Discussion on the gypsum effect on C-S-H	83
5. Summary	84
6. References	86
Chapter 5 – Hydration at later ages (>1 day)	89
1. Literature review	90
1.1. Kinetics and mechanisms	90
1.2. Impact of SCM on the microstructural development	93
2. Mixes studied	96
3. Factors controlling the later hydration	97
3.1. Cement paste	97
3.2. Blended systems	101
4. Evolution of pore	113
4.1. Phase assemblages	114
4.2. Filling ability	115
4.3. Discussion	120
5. Summary	121
6. References	123
Chapter 6 – Conclusions & Perspectives	125
1. Filler effect	125
2. Impact of Slag and Fly ash	125
3. Impact of limestone	126
4. Nucleation and growth of C-S-H	126
5. Later age	127
6. Perspectives	127
Appendix 1: Effect of temperature on nucleation and growth of C-S-H	129
Appendix 2: Calculation of the supersaturation index of C-S-H	131
Appendix 3: Fitting the kinetics at later age	133
Curriculum Vitae	135

List of Figures

Figure 1.1: Urban and rural population of the world	2
Figure 1.2: Comparative relative energy and CO ₂ per building material	2
Figure 1.3: Ternary diagram of the chemical composition of Portland cement, Slag and Fly ash	3
Figure 2.1: Cement grain and detail of the surface	8
Figure 2.2: Particle size distribution of cement	9
Figure 2.3: Alite grains and detail of the surface	10
Figure 2.4: Isothermal calorimetry of 40% replacement of quartz, rutile and corundum compared to Slag	10
Figure 2.5: Particle size distribution of the fillers	11
Figure 2.6: Particle size distribution of the quartz powders	12
Figure 2.7: a) Slag grain b) Limestone grain	12
Figure 2.8: Particle size distribution of the six SCMs used	12
Figure 2.9: Effect of the variation of the imaginary component k on slag particle size distribution	15
Figure 2.10: Reproducibility of the particle size distribution measurements of cement grains	16
Figure 2.11: Results from the BET measurement. Five points	17
Figure 2.12: The acceleration period is characterized by the slope of the linear part of the curve	18
Figure 2.13: BSE image of quartz-alite paste	20
Figure 2.14: Method used to prepare SEM samples	21
Figure 2.15: Effect of the carbon coating on the same sample	21
Figure 2.16: Grey level from the BSE polished section image	22
Figure 2.17: Polished section of cement paste with BSE	22
Figure 2.18: Interaction volume	23
Figure 2.19: Example of EDX analysis on C-S-H composition	23
Figure 2.20: Comparison of the pattern on fresh slice and <i>in situ</i> preparation	24
Figure 2.21: Comparison of the phase evolution between the normalized peak area method and the Rietveld refinement	24
Figure 2.22: Typical curves from MIP experiments done up to 400MPa	26
Figure 2.23: Relaxation time of the different water population in cement paste from 1 day to 62 days	27
Figure 2.24: Microstructural model from Feldman and Sereda	27
Figure 3.1: Typical isothermal calorimetry curve of cement hydration	29
Figure 3.2: Cement hydrated for 3 hours, 6 hours and 10 hours	31
Figure 3.3: X-ray microscopy images during the reaction of silica gel in NaOH and CaCl ₂ solution	32
Figure 3.4: Relation between rate of the acceleration period and the specific surface area of alite particles.	32
Figure 3.5: Increase of the acceleration rate with mixing speed.	33
Figure 3.6: Initial proportion of the mixes studied	34
Figure 3.7: Calorimetry curve of 40% Quartz alite system	38
Figure 3.8: Microstructure in quartz-alite paste at 1 hour on a) alite grains b) quartz grain, 3 hours on c)alite d)quartz and 5 hours on e)alite grains f)quartz grain	39
Figure 3.9: Microstructure in quartz-cement pastes at 5 min a) quartz surface b) cement surface; at 2 hours c) quartz surface d) cement surface; at 5 hours e) quartz surface f) cement surface	40

Figure 3.10: Effect of increasing the replacement of quartz in cement paste	41
Figure 3.11: Slope value of the acceleration curve as a function of the total surface of solids	41
Figure 3.12: Comparison of the surface effect between quartz and alite	42
Figure 3.13: Effect of the water/solid ratio on kinetics	43
Figure 3.14: Effect of water/cement ratio in blended systems	44
Figure 3.15: Effect of the water/solids ratio	44
Figure 3.16: Simulation of the packing in blended paste	45
Figure 3.17: Slope value as a function of the inter-distance between particles	46
Figure 3.18: Effect of mixing speed on cement paste and 70% quartz PC	46
Figure 3.19: Effect of mortar on kinetics	47
Figure 3.20: Micrographs of cement pastes, mortars and quartz – cement paste	48
Figure 3.21: Simplistic scheme of the shear between two particles	49
Figure 3.22: Slope value as a function of the estimated shear rate	50
Figure 3.23: Calorimetry curves of blended systems with fly ash, slag and quartz	51
Figure 3.24: BSE image of slag – cement	51
Figure 3.25: Grains from slag-cement paste and detail of the surface	52
Figure 3.26: Fly ash – cement systems at 2 hours	53
Figure 3.27: Slope value as a function of the total surface of SCM	54
Figure 3.28: Calorimetry curves of limestone- cement pastes compared to quartz- cement paste	55
Figure 3.29: CaCO ₃ content in Limestone-cement paste and limestone – C ₃ S paste	55
Figure 3.30: Micrographs in limestone PC paste. Limestone surface at a) 5 min c) 1 hour e) 5 hours and cement surface at b) 5 min d) 1 hour and f) 5 hours	56
Figure 3.31: TEM in bright field mode of limestone – C ₃ S paste at 10 hours of hydration	57
Figure 3.32: Slope value as a function of the total surface of limestone	58
Figure 3.33: Effect of the shear rate between SCM particles on the slope value	58
Figure 3.34: Limestone surface at 1h30 of hydration	59
Figure 3.35: Limestone surface at the main peak	59
Figure 3.36: (101.4) surface of calcite	60
Figure 3.37: Comparison of atomically resolved and Fourier-transformed images of calcite cleavage plane	60
Figure 4.1: Comparison of the calorimetry curves of alite (left) and Portland cement (right)	68
Figure 4.2: The renewal of C ₃ A dissolution at 20°C corresponds to the anhydrite depletion	68
Figure 4.3: Concentrations in the pore solution in PC at w/c 0.35	69
Figure 4.4: Optimal gypsum content on the mechanical strength	70
Figure 4.5: 14A Tobermorite structure	71
Figure 4.6: Mechanisms proposed by Barbarulo for sulfate adsorption on C-S-H surface sites	71
Figure 4.7: Microstructure at 16 hours of c) C ₃ S paste and f) PC. The presence of sulfates changes the microstructure	72
Figure 4.8: Effect of additional gypsum on 40% Slag PC systems (left) the C ₃ A peak is progressively delayed (right) the peak area is similar for all the systems	73
Figure 4.9: Isothermal calorimetry curves of quartz – cement paste showing the enhancement of the second C ₃ A dissolution	74
Figure 4.10: Effect of gypsum on the kinetics of 70% quartz PC system	75

Figure 4.11: Gypsum content detected by in situ XRD (a) 70% Quartz PC (b) same system with 2% additional gypsum	75
Figure 4.12: Cumulative heat as a function of the time of the onset of C ₃ A peak	76
Figure 4.13: S/Ca ratio in 70% Quartz cement paste. Sulfate ions are adsorbed on the C-S-H structure and are released gradually during the deceleration period	76
Figure 4.14: BSE image: quartz and cement grains	77
Figure 4.15: Isothermal calorimetry curves (left) acceleration does not affect the shoulder peak (right) water/solids ratio enhance the peak	77
Figure 4.16: Sulfate content in the pore solution in cement paste and 70% quartz-cement paste	78
Figure 4.17: Comparison of the effect of quartz, fly ash and slag on the C ₃ A dissolution peak	79
Figure 4.18: Evolution of the different water populations (capillary water, interlayer water, gel water and water in the solids including Portlandite, AFt AFm	80
Figure 4.19: Change of the C-S-H morphology in plain cement	81
Figure 4.20: Change of the C-S-H morphology in 70% Quartz PC system	81
Figure 4.21: Change of the C-S-H morphology in 70% Quartz PC with 2% gypsum	81
Figure 4.22: Change of the C-S-H morphology in 70% Quartz PC with 6% gypsum	81
Figure 4.23: Evolution of the gypsum content from in situ XRD	82
Figure 4.24: S/Ca ratio in a) PC 70% Quartz and b) PC 70% Quartz + 2% Gypsum added	82
Figure 4.25: Morphology of the C-S-H in PC (left) compared in alite i.e. no gypsum (right)	83
Figure 4.26: Effect of sulfate on the kinetics of second reaction of C ₃ A. Proposed mechanisms to explain the kinetics and the microstructure	85
Figure 5.1: Stages over the course of cement hydration	90
Figure 5.2: (left) Hydrated C ₃ S grains at the main peak. C-S-H layer is covering the whole surface of the grains (right) Formation of the gap between the silicate phase and the product layer	91
Figure 5.3: Impingement of the hydrates between two grains	91
Figure 5.4: C-S-H growth at the different stage of hydration	92
Figure 5.5: Prediction of the phase assemblage by thermodynamics simulation with GEMS of a cement paste with increasing slag content and fly ash content	93
Figure 5.6: Interface fibrils / foil-like morphology in the Fly ash-cement paste after 3 years	94
Figure 5.7: Water populations (left) volumetric composition of cement paste (right) water populations from ¹ H NMR	95
Figure 5.8: Pore structure development in blended systems	95
Figure 5.9: Initial proportion of the mixes of slag-quartz-cement and fly ash-quartz-cement	97
Figure 5.10: Proposed delimitation of the kinetics regimes	98
Figure 5.11: Correlation between calorimetry and chemical shrinkage of cement paste w/c 0.4	98
Figure 5.12: Deceleration rate dependent on the water/cement ratio	99
Figure 5.13: Effect of the water/cement and water/solids ratios	100
Figure 5.14: Micrographs at 7 days of hydration of a) PC w/c 0.4; b) PC w/c 0.6. At this stage the PC 0.4 paste is already well filled whereas in PC 0.6 some outer space remains	100
Figure 5.15: Pore structure development in cement paste w/c 0.4	101
Figure 5.16: Cumulative heat curves of cement, 40% quartz PC, 40% Fly ash PC and 40% slag PC	102
Figure 5.17: Degree of hydration of cement at 28 days with increasing the proportion of slag	102
Figure 5.18: Degree of hydration of cement at 28 days with varying the proportion of fly ash	103
Figure 5.19: Cumulative calorimetry curve of slag-quartz-cement systems	104
Figure 5.20: Contribution of slag in slag – quartz PC	105

Figure 5.21: Effect of increasing the water/solids ratio in slag-cement systems	106
Figure 5.22: Degree of reaction of fly ash in Fly ash – quartz – cement systems with w/s 0.4, unless otherwise stated	107
Figure 5.23: Portlandite content in fly ash- quartz- cement pastes	108
Figure 5.24: Micrographs at 28 days a) 10%slag-30%quartz cement b) 40% slag cement	108
Figure 5.25: Micrographs at 28 days a) 10% Fly Ash PC b) 40% Fly ash PC	109
Figure 5.26: Cumulative and pore size distribution curves from MIP of a) and b) PC, c) and d) 40% Slag PC, e) and f) 40% Fly ash PC	110
Figure 5.27: The reaction of slag (a) and fly ash (b) is limited in the systems where the critical radius reaches 6 nm	111
Figure 5.28: Cumulative heat curves of cement, 40% quartz PC, 40% Fly ash PC and 40% slag PC	112
Figure 5.29: Chemical shrinkage: kinetics slow down when the critical radius stabilizes	112
Figure 5.30: Decreasing pore entry radius, increase the pressure and thus the SI	113
Figure 5.31: Comparison of the phase volume calculated from GEMS of PC at 28 days	114
Figure 5.32: Volume of the phases in the Fly ash – quartz cement systems at 90 days	115
Figure 5.33: MIP curves of Fly ash – Quartz PC systems a) cumulative porosity b) Pore size distribution	115
Figure 5.34: Pore volume in slag PC pastes as a function of the critical radius	116
Figure 5.35: Pore volume reduction and critical radius a) and b) in cement paste; c) and d) in Slag-cement system e) and f) in fly ash cement system	117
Figure 5.36: Effect of increasing w/s ratio on MIP curve at 28 days of PC, 40%Slag and 40% Fly ash systems at 60 days	118
Figure 5.37: Microstructure of PC at 28 days a)w/s 0.4 b)w/s 0.6; 40% Slag at 28 days c) w/s 0.4 d) w/s 0.6 40% Fly ash e) w/s 0.4 f)w/s 0.6	119
Figure 5.38: Detail of the microstructure (left) 40% Slag PC system at 28 days (right) 40% Fly ash PC system w/s 0.6 at 28 days	120
Figure 5.39: ¹ H NMR on the Slag – Quartz PC systems. Gel water/interlayer ratio decreases with increasing slag amount	121
Figure 5.40: Microstructural development during the hydration	122
Figure 6.1: Compressive strength of slag-quartz-PC systems	128
Figure A1.1: Calorimetry curves of cement paste at 5°C, 20°C and 60°C	130
Figure A1.2: Micrographs of cement paste at different temperature	131
Figure A2.1: Concentration of elements in the pore solution	131
Figure A3.1: Chemical shrinkage of cement and 40% slag cement pastes	133
Figure A3.2: Fitting of the late age rate	134

List of Tables

Table 2.1: Chemical composition of the Portland cement	8
Table 2.2: Mean diameter and S.S.A of Portland cement	9
Table 2.3: Chemical composition of alite	9
Table 2.4: Mean diameter and Specific surface area of the quartz powders	11
Table 2.5: Mean diameter and specific surface area of the SCMs	12
Table 2.6: Chemical composition of the SCMs used	13
Table 2.7: Refractive index of the mineral phase	14
Table 2.8: Refractive index of the cementitious materials	14
Table 3.1: Mix design of quartz-cement systems	36
Table 3.2: Mix design for w/s study	36
Table 3.3: Concentration of calcium during induction period in limestone-cement and quartz-cement paste	54
Table 4.1: Atomic percent of some elements on cement and quartz grains	77
Table 5.1: Mixes for the study of kinetics	96
Table 5.2: Mixes used to isolate the effect of SCM	96
Table 5.3: Enthalpies of the three major reactions in cement hydration	105
Table 5.4: Comparison of the degree of reaction of fly ash from mass balance calculation and thermodynamic simulation	107

Glossary

Abbreviations

Definition

Cement notation

C	Calcium Oxide CaO
S	Silicon dioxide SiO ₂
A	Aluminium oxide Al ₂ O ₃
F	Iron oxide Fe ₂ O ₃
H	Water H ₂ O
\$	Sulfate SO ₃

Cement phase

C ₃ S	Tricalcium silicate
C ₂ S	Dicalcium silicate
C ₃ A	Tricalcium aluminate
C ₄ AF	Tetracalcium aluminoferrite
CH	Portlandite ou Calcium hydroxide
C-S-H	Calcium silicate hydrate
AFt	Ettringite
AFm	Monosulfo/carboaluminate

OPC or PC	Ordinary Portland Cement
SCM	Supplementary Cementitious Materials
doR	degree of reaction
doH	degree of hydration
w/c	water-to-cement ratio
w/s	water-to-solids ratio

Methods

MIP	Mercury Intrusion Porosimetry
SEM	Scanning Electron Microscopy
TEM	Transmission Electron Microscopy
PSD	Particle Size Distribution
NMR	Nuclear Magnetic Resonance
XRD	X Ray Diffraction
TGA	Thermogravimetry Analysis

Chapter 1

Introduction

Cement production is currently facing two main challenges: reduction of the environmental impact of cement and increasing its availability. Clinker substitution is a promising strategy to solve both issues. A part of the clinker is replaced by alternative materials, called Supplementary Cementitious Materials (SCMs). The impact of these materials on the cement hydration is the central topic of this thesis. Two representative SCMs have been used in this work – fly ash and slag. The current knowledge about these materials is summarized in this chapter. Many open questions related to their reactivity and their impact on cement hydration, are unsolved and justify this work.

1. Introduction	2
1.1. Supplementary Cementitious Materials	3
1.2. Limitations for the use of SCMs	5
2. Motivation and objectives of the thesis	5
3. Chapter overview	6
4. References	6

1. Introduction

Concrete is a unique building material. It results from the reaction between cement and water. This material was first used in Ancient Greece and re-developed in the mid- XVIII century. Today it is the most used material for construction. The success of cement comes from several factors but mainly ease of production, widespread availability of the raw materials and its capacity to build durable infrastructure.

In 2007, for the first time in history, more people were living in urban areas than in rural areas and this trend continues (Figure 1.1). UN Habitat estimates that 2 billion more people will need housing in 2030. Therefore cities must improve their infrastructures and their stock of decent housing. The large majority of these constructions are made with concrete which is currently the most adequate material to build fast and safe megacities.

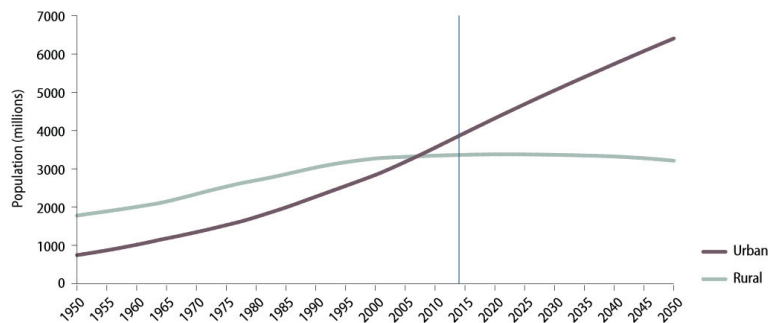


Figure 1.1: Urban and rural population of the world from UN[1]

The current consumption is around 3 tons of concrete per person per year and the overall amount is estimated to double by 2050 [2]. The main issue is the CO₂ emission from cement production. Although the emissions per kg of cement or concrete produced are lower than most building materials (Figure 1.2), the scale of production is such that it represents currently 5-8% of the global CO₂ emissions from human activity.

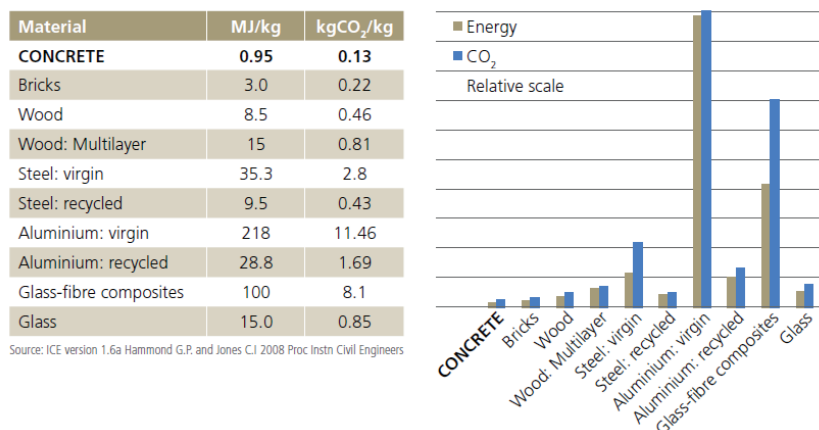


Figure 1.2: Comparative relative energy and CO₂ per building material

In 2008, cement makers through World Business Council for Sustainable Development recognized the urgency to reduce CO₂ emissions from cement industries and requested the International Energy

Agency to evaluate long term options to lower the environmental impact [2]. Improving energy efficiency, use of alternative fuels, use of alternative material to clinker and capture of CO₂ emissions were the main strategies considered. The main source of CO₂ in cement production comes from the raw materials. Cement is produced by the calcination of limestone and clay at high temperature. During this process, limestone (CaCO₃) decomposes and emits CO₂ (CaCO₃ → CaO + CO₂). Therefore, the biggest challenge of the cement industry is to produce more cement with less clinker.

The most realistic solution to achieve this goal is to blend the clinker with other materials. This saves directly CO₂ emissions as less clinker is needed. There is, however, a limitation in that only some materials can be used to replace cement. These materials must develop cementitious properties to maintain the mechanical properties of the concrete. These materials are called Supplementary Cementitious Materials (SCMs).

1.1. Supplementary Cementitious Materials (SCMs)

Natural pozzolans, fired clay, crushed bricks or pottery have been found in Antique mortars. They were the first SCMs used. The most famous example of the use of SCMs is the Pantheon Coliseum in Rome where a mix of lime and pozzolane was used for the dome. This monument built in CE 125 shows the outstanding lifetime of concrete, provided by the contribution of SCMs to the cement hydration.

The good performance is the result of the chemical reaction of the SCM which can be hydraulic or pozzolanic. In general SCM used today can be classified in these two categories of materials. In this work we used one SCM representative of each category: blast furnace slag as hydraulic material and siliceous fly ash as pozzolanic material.

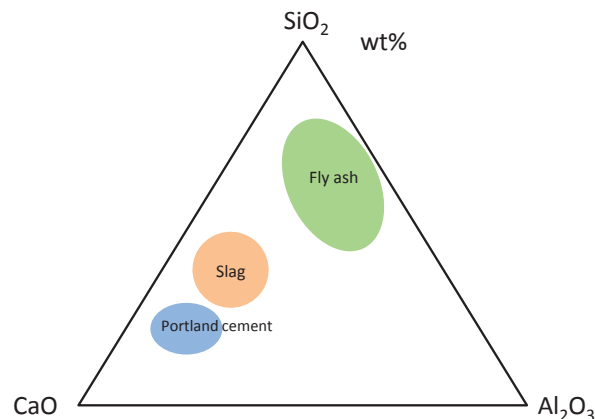


Figure 1.3: Ternary diagram of the chemical composition of Portland cement, Slag and Fly ash

Slag and fly ash are both by-products from industry. Slag comes from the iron industry. During the process of iron making, a non-metallic liquid forms and floats on the molten iron. This liquid made of the impurities of coke and clays is separated from the liquid metal and quenched. After drying and grinding, the finished product is called ground granulated blast furnace slag.

Fly ash is the residue produced by the burning of coal in power plants. Coal is pulverized in fine particles and burnt in a boiler. During the combustion, heat and a molten residue are generated. Heat is extracted on one side and the flue gas is cooled down. The residue hardens in spherical glassy particles. The lighter particles are collected and are the “fly ash”.

As it can be seen in Figure 1.3, slag and fly ash have very different chemical composition. The slag is homogeneous and composed mainly of CaO (40%) SiO₂ (35%) Al₂O₃ (8 – 20%) MgO (1-18%) which is quite similar to Portland cement. Fly ash is a heterogeneous material mainly amorphous and containing small amount of crystalline phase. The crystalline phases are quartz, mullite, hematite, melilite or others. The characterization of the amorphous content is more delicate but can be seen as an alumina-silica glass containing modifiers elements (Ca, Na, K, Mg, Fe).

The different chemistry and the glass content lead to hydraulic or pozzolanic material. Slag as a hydraulic material, sets and hardens under water. It is, consequently, the hydration of the material which produces cementitious hydrates. Whereas fly ash is a pozzolanic material and reacts only if there is calcium hydroxide and water to produce hydrates with cementitious properties.

Therefore both materials are able to compensate the dilution of clinker by producing themselves hydrates however their reactions involves changes in the clinker hydration.

The replacement by slag or fly ash changes the kinetics of hydration[3]. The hydration of the clinker component is usually enhanced in blended systems. At early age (<1day), this effect is termed the filler effect as the SCM particles are not yet reacting [4]. The significant influence of the fineness of the SCM particles has been interpreted as more surface area where calcium silicate hydrates, the main hydrate in cement paste, can precipitate. This change is important as it can modify the microstructure and change the long term properties. It is interesting to quantify this effect and know if SCM with different surface chemistry have a different influence.

Blended systems are known to have better durability properties than Portland cement. These properties are closely related to the permeability and ion transport which are determined by the microstructure. The analysis of the pore structure at later ages has shown that the blended system and specially slag-cement system have a more refined porosity. Although the total amount of pores in the blend is higher than in Portland cement, the size of the pores is usually lower at later age (28 days). The hydrates formed in blended systems are similar to those in Portland cement. The main hydrate is still C-S-H although its chemical composition is changed. Therefore, the refinement of the porosity cannot be simply explained by a change of the phase assemblage. The understanding of the microstructural development in blended system is important to optimize the use of SCM. Several studies have reported that increasing the replacement of SCM decreases its own reaction. The replacement level of SCM in blended systems is therefore relatively limited.

Many researchers have studied blended systems with SCMs from diverse origins. However the generic microstructural development of blended systems is still not well understood. There are several explanations for that.

First, the mechanisms controlling the hydration of Portland cement are not totally understood. It is consequently difficult to identify the changes in a more complex system.

Secondly most authors described the effect of a specific SCM regarding the changes of the microstructure, compressive strength, and evolution of the phase assemblage but have not established generic knowledge.

Thirdly, although the SCMs have a slower reaction, they contribute to cement hydration from the very beginning. Most of the studies reported long term changes caused by the introduction of SCM. However the early hydration is a crucial step for the later properties, we need to study the effect of SCM on the totality of the hydration process.

1.2. Limitations for the use of SCMs

SCMs present many benefits: they save directly CO₂ emission, promote the use of local/waste materials and develop even better properties than pure cement for some applications.

However three main issues currently limit their use:

- There is limited availability of good quality SCMs
- There is a maximal replacement level beyond which the strength decreases
- The slow strength development at early age caused by the slow reactivity

A better understanding of the impact of SCMs of the hydration process can help to overcome these limitations.

2. Motivations and objectives

This work aims to study the impact of the SCMs on cement hydration to get a generic knowledge on the changes in kinetics and microstructural development when SCMs replace part of Portland cement. These effects were studied over the cement hydration process to determine the mechanisms taking place in blended systems.

SCMs particles have two impacts over the course of hydration. First they are inert and then they become reactive materials. Using quartz-cement system, we dissociated the effect of filler (inert particles) from the SCM reaction.

The main points that this work aims to elucidate are:

- Do all the inert particles have similar filler effects?
- What are the effects of inert particles on the kinetics and microstructure?
- How do the cement and SCM reactions act on each other?
- What are the kinetics of SCM reaction in the blended systems?
- How is the microstructure modified by the SCM reaction?

The work presented here is a part of a Nanocem core project investigating the impact of the SCM in the blended paste. The associated work which was done by Katrina Newlands in Aberdeen University focused on the reactivity itself of SCM. She investigated how the chemical composition of the SCM and its local environment influence its dissolution. This core project falls within the major challenge to be

able to predict the performance of blended systems based on the composition of cement and SCM used and the working conditions (temperature, etc)

3. Chapter overview

The impact of the SCM has been studied for each fundamental steps of the cement hydration. Therefore the thesis structure refers to the main hydration stages and has been divided as following:

Chapter II describes the methods and the materials used in this work.

Chapter III reports on the effect of filler and SCMs on the acceleration period. The filler effect has been quantified and the mechanisms behind this effect have been clarified.

Chapter IV focuses on the deceleration period. The second C_3A reaction is affected by the presence of SCM. The gypsum content is a key parameter and leads to changes on C-S-H.

Chapter V explains the significant contribution of SCM on the microstructure at later ages (from 1 day to 28 days). The questions on how reactions of SCM affect the microstructure and more importantly, how the distribution of hydrates from the reaction of SCM changes the overall porosity are developed and resolved.

Chapter VI presents and discusses the main conclusions deduced from this work.

4. References

1. United-Nations, ed. *World Urbanization Prospects: The 2014 Revision, Highlights*. 2014, United Nations.
2. World Business Council for Sustainable development and International Energy Agency, *Cement Technology Roadmap 2009 : Carbon emissions reductions up to 2050*. 2009, IEA publications.
3. Gutteridge, W.A. and J.A. Dalziel, *Filler cement: The effect of the secondary component on the hydration of Portland cement: Part 2: Fine hydraulic binders*. Cement and Concrete Research, 1990. **20**(6): p. 853-861.
4. Gutteridge, W.A. and J.A. Dalziel, *Filler cement: The effect of the secondary component on the hydration of Portland cement: Part I. A fine non-hydraulic filler*. Cement and Concrete Research, 1990. **20**(5): p. 778-782.

Chapter 2

Materials and Methods

This chapter describes the characterization of the materials and the description of the methods used in this work.

The composition of the material was analyzed by X-Ray Fluorescence and their crystalline content was quantified by XRD. The particle size distribution was measured by laser diffraction and their specific surface area by the BET method.

1. Raw materials	8
1.1. Portland cement	8
1.2. Alite	9
1.3. Choice of the inert filler	10
1.4. Supplementary Cementitious Materials (SCMs)	12
2. Methods	13
2.1. Characterization of the raw materials	13
2.1.1. Particle size distribution	13
2.1.2. Specific surface area	15
2.2. Sample preparation	16
2.2.1. Preparation of the pastes	16
2.2.2. Preparation of the mortars	17
2.3. Methods to follow the kinetics of the reaction	17
2.3.1. Isothermal calorimetry	17
2.3.2. Chemical shrinkage	18
2.3.3. Chemical composition of the pore solution	18
2.4. Methods to assess the microstructural development	19
2.4.1. Observation at early age	19
2.4.2. Observation of polished section at later ages	21
2.4.3. Energy dispersive X-ray spectroscopy	22
2.4.4. X-ray diffraction	23
2.4.5. Mercure intrusion porosimetry (MIP)	24
2.4.6. Neutron Magnetic Resonance	26
3. References	28

1. Raw materials

1.1. Portland cement

Grey Portland cement, CEM I 52.5 type supplied by Holcim (Siggenthal) was used for all the pastes. The chemical composition measured by Riteveld XRD and XRF are shown in Table 2.1. Figure 2.1 shows the morphology of the cement grains, they have a mean diameter of about 16 μm (Table 2.2). The small particles on the surface observed in Figure 2.1 are the result of the grinding process. The methods to measure the particle size distribution and the specific surface area are described in the methods section.

Table 2.1: Chemical composition of the Portland cement

Phase composition %		XRF analysis [wt%]	
C ₃ S	69	SiO ₂	14.85
C ₂ S	4	Al ₂ O ₃	2.5
C ₃ Acubic	1.3	CaO	62.43
C ₃ Aortho	2.6	MgO	2.05
C ₄ AF	10	Fe ₂ O ₃	3.11
Calcite	1.5	Na ₂ O	2.76
Gypsum	1.3	K ₂ O	3.82
Other	4.6	TiO ₂	0.29
		SO ₃	5.54

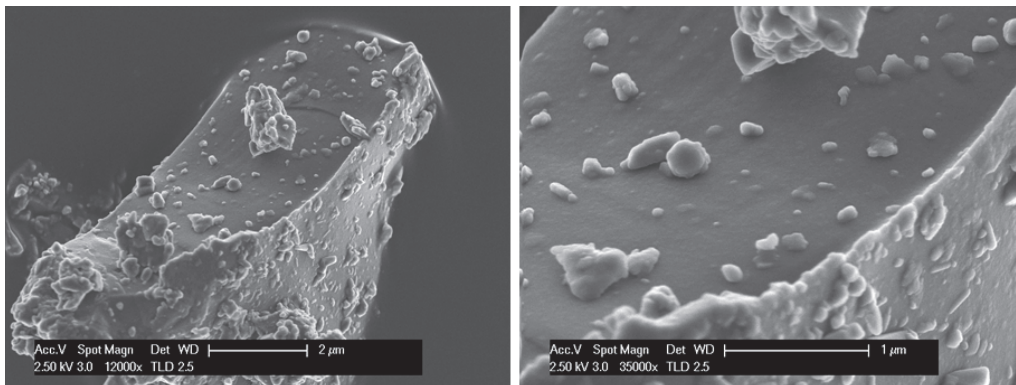


Figure 2.1: Cement grain and detail of the surface. Small particles are the results of the grinding process

Table 2.2: Mean diameter and SSA of Portland cement

	D ₅₀ (μm)	Specific surface area BET (m ² /g)
Cement	16	1.0

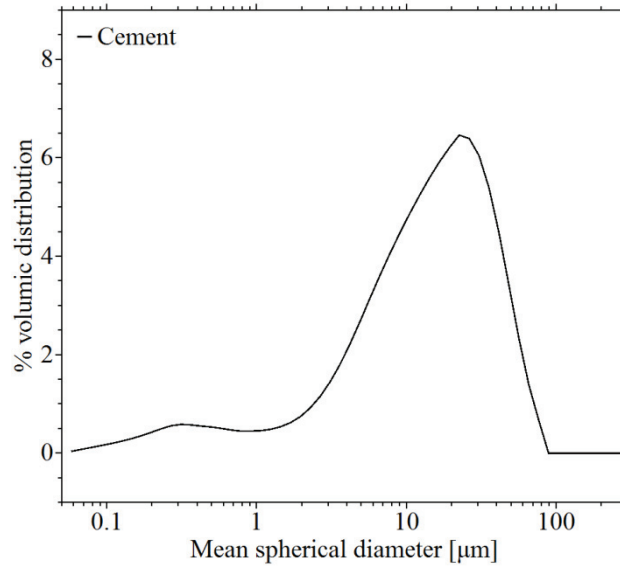


Figure 2.2: Particle size distribution of cement

1.2. Alite

Alite is the main component of cement clinker. This phase was used to compare the nucleation and growth of C-S-H in simpler systems.

Alite was synthesised by Berta Mota Gasso in our lab by several heating and grinding cycles as detailed in Quennoz work [1]. The chemical composition is shown in Table 2.3 and the morphology of the particles are shown in Figure 2.3.

Table 2.3: Chemical composition from XRF of alite

Chemical composition %	
CaO	77.5
SiO ₂	19.5
Mg	2.2
Al ₂ O ₃	0.5

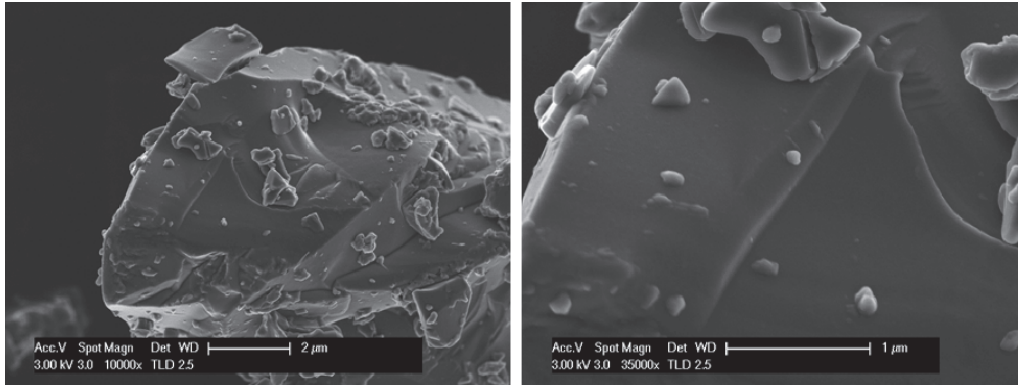


Figure 2.3: Alite grains and detail of the surface

1.3. Choice of the inert filler: Quartz

The filler material must be inert in cement paste conditions (e.g. pH 13, high alkalinity), easily available, preferably in a range on fineness. Among three selected materials (Rutile TiO_2 , Quartz SiO_2 , Corundum Al_2O_3) quartz was found to be the material best fitting the kinetics of slag (Figure 2.4). This was verified for a range of 10% to 90% of substitution level in the cement paste.

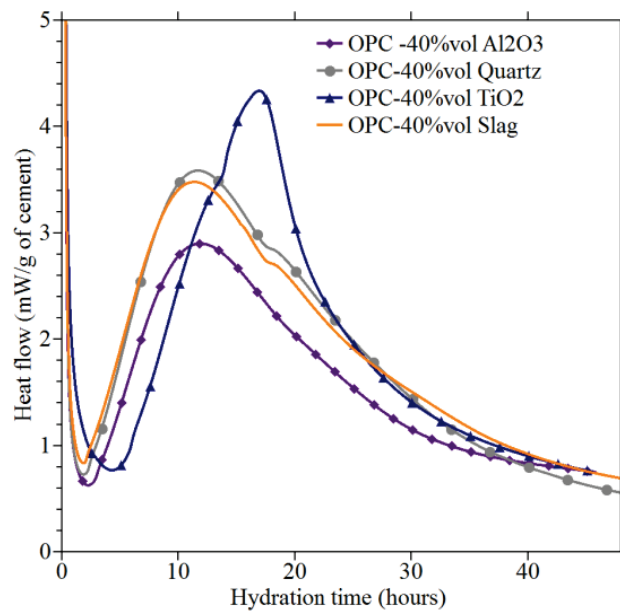


Figure 2.4: Isothermal calorimetry of 40% replacement of quartz, rutile, corundum compared to slag

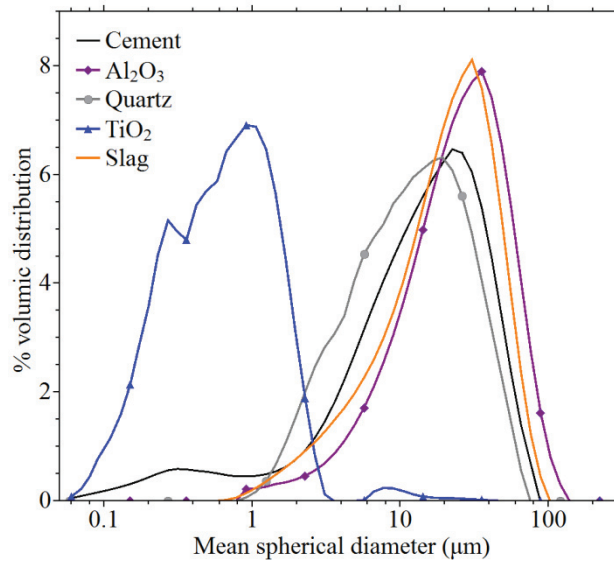


Figure 2.5: Particle size distribution of the fillers

^{29}Si NMR measurements proved that there was negligible reaction of the quartz in the quartz-cement paste even after 28 days (below 5%).

Three fineness of quartz powders were selected to study the effect of the size of the filler on the kinetics of hydration. The mean diameter and the specific surface area are shown and compared with cement in Table 2.4. As it can be seen in Figure 2.6 the distribution of the particle size is quite narrow.

Table 2.4: Mean diameter and Specific surface area of the quartz powders

	D_{50} (μm)	Specific surface area (m^2/g)
Quartz	18	0.79
	13	1.53
	4	3.48
Cement	16	1.0

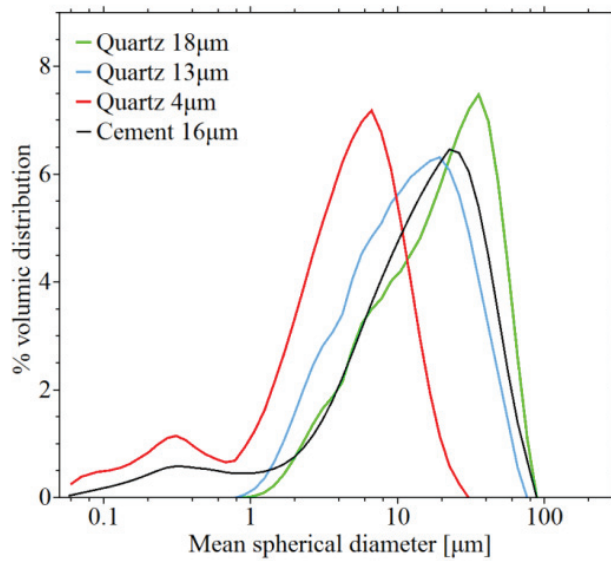


Figure 2.6: Particle size distribution of the quartz powders

1.4. Supplementary cementitious materials (SCMs)

There is a large variety of SCM currently used. Most of them are hydraulic or pozzolanic materials. We selected slag as hydraulic material and fly ash as pozzolanic material. Limestone was also studied although it falls into none of these categories but it is one of the most used filler in cement production. Therefore these common SCM were used as substitutes in the blends to quantify and study the possibility of different filler effect with the chemistry of the particles. The particle size distribution and the specific surface area obtained from BET measurements are shown in Figure 2.8 and Table 2.5. The chemical compositions of the SCMs by XRF are presented in Table 2.6.

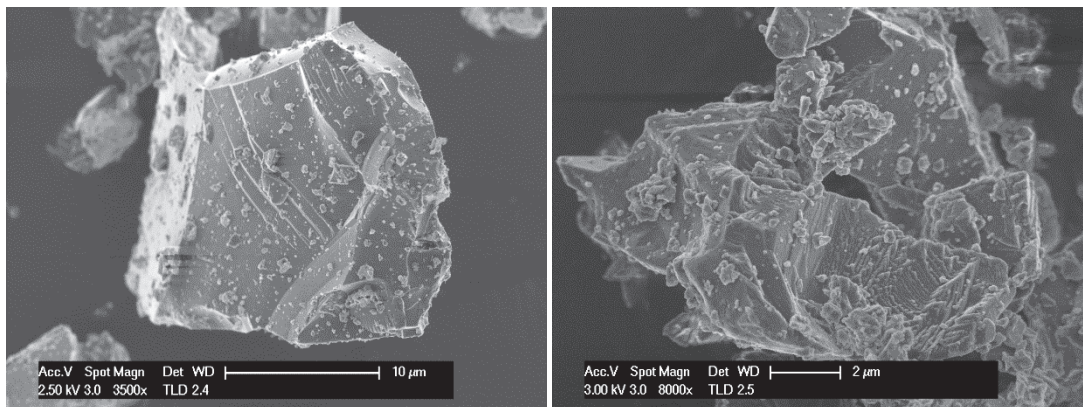


Figure 2.7: (left) slag grains, (right) limestone grain

Table 2.5: Mean diameter and specific surface area of the SCMs

	D ₅₀ (μm)	Specific surface area (m ² /g)
Cement	16	1.0
Slag	19.5	1.15
	18	1.01
Fly Ash	18.3	0.72
Limestone	18	0.55
	12	1.1
	3	3.49

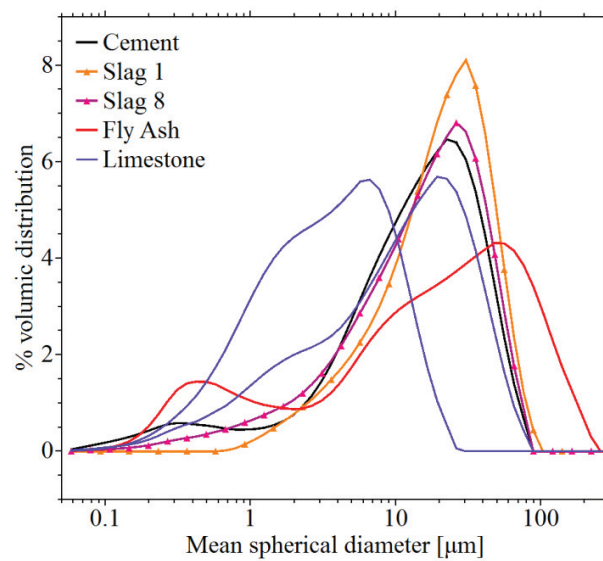


Figure 2.8: Particle size distribution of the 6 SCMs and cement used

Table 2.6: Chemical composition of the SCMs used

XRF analysis (wt%)	Limestone	Slag		Fly Ash T
		S1	S8	
SiO ₂	0	35.72	34.09	50.54
Al ₂ O ₃	0	11.94	19.87	24.7
CaO	60.09	41.38	33.01	5.07
MgO	0.48	7.45	9.73	2.88
Fe ₂ O ₃	0.03	0.84	0.45	9.29
Na ₂ O	0	0.26	0.25	1.05
K ₂ O	0.01	0.27	0.84	4.1
TiO ₂	0.01	0.51	0.9	0.95
SO ₃	0	1.38	0.75	0.71

2. Methods

2.1 Characterization of raw materials

2.1.1 Particle size distribution

The particle size distribution has been measured for all the materials by a laser diffraction supplied by Malvern Instrument.

The laser beam passes through the powder dispersed in a solution. The particle on the path of the beam scatters the light. Large particles scatter at small angles whereas the small particles scatter at large angles. Thus from the variation of the angular scattering of the light, the distribution of the particles from the powder can be deduced using the Mie theory. The particle size is reported as a volume equivalent sphere diameter.

The Mie model is usually used for the analysis of fine particles (<100µm) and requires the optical properties of the sample and the median used for dispersion.

For cementitious materials, isopropanol is used as the medium instead of water. Isopropanol avoid the hydration of the cementitious powder during the measurements and yields the best overall precision due to its good dispersant properties[2]. The refractive index of the medium and commom cementitious phases are reported in Table 2.7.

Table 2.7: Refractive index of the mineral phase

Mineral phase	Refractive index n
C ₃ S	1.72
C ₃ A	1.71
SiO ₂ amorphe	1.44
SiO ₂ (quartz)	1.53
Al ₂ O ₃	1.76
Fe ₂ O ₃	2.91
CaO (free lime)	1.84
MgO	1.74
Isopropanol	1.37

Cement, slag, fly ash do not have a single refractive index as they are composed of more than one phase. We used a composite refractive index based on the index of each phase contained in the material such as:

$$n_{material} = \sum_i \%vol_i \times n_i$$

The refractive index calculated for the materials used in this work are reported in Table 2.8.

Table 2.8: Refractive index calculated for the cementitious materials used

	Refractive index n (real part)	k (imaginary part)
Cement	1.7	0.1
Slag 1	1.59	0.1
Slag 8	1.56	0.1
Fly ash T	1.53	0.1

The imaginary component k of the refractive index corresponds to the ability of the material to absorb the light from the beam. In the literature a value of k is 0.1 for cement[3]. Same value was used for slag and fly ash as they contain very absorbing phase such as magnetite.

The fraction below $D_{(10)}$ is usually very sensitive to this parameter[4]. Figure 2.9 shows an example of the effect of different k values.

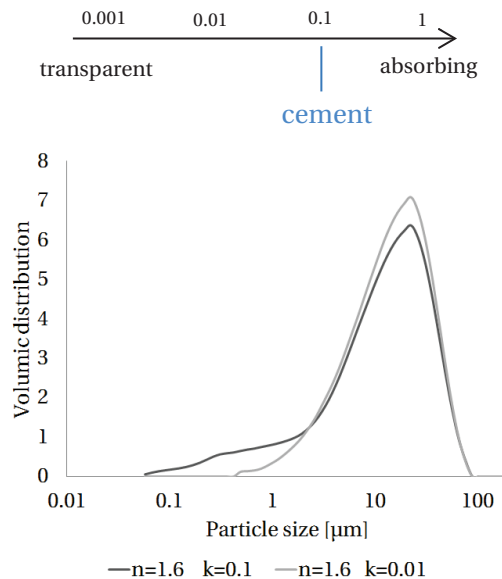


Figure 2.9: Effect of the variation of the imaginary component k on slag particle size distribution

Sample preparation

The optical model was selected according to the refractive index calculated for the material (Table 2.8). For instance for Portland cement, the best fitting optical model was SHE_3 which corresponds to $n=1.7$ $k=+0.1$ in medium $n=1.39$.

Prior experiment, the tube was cleaned with isopropanol three times. A few mg of the anhydrous material was dispersed in isopropanol until to reach the obscuration level of 12% on the Malvern machine. The measurement was repeated two times on the same sample. Then all the equipment was rinsed three times with isopropanol to remove the previous powder. And a new experiment was performed with a new sample of the material. All the measurements presented a good reproducibility (Figure 2.10).

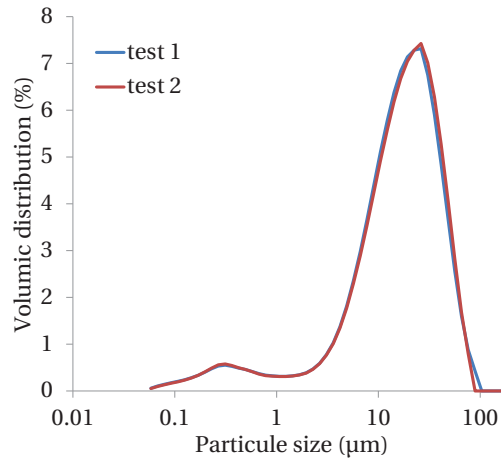


Figure 2.10: Reproducibility of the particle size distribution measurements of cement grains

2.1.2 Specific surface area

The specific surface area is the solid surface area per unit mass of this material. This value can be determined by the N₂ gas adsorption on the surface. The samples are prepared by heating while simultaneously evacuating or flowing gas over the sample to remove the liberated impurities. The prepared samples are then cooled with liquid nitrogen and analyzed by measuring the volume of N₂ gas adsorbed as a function of the pressure.

We used the multi-point method and treated the data according to the Brunauer, Emmet and Teller equation which describes the isotherm equation such as:

$$\frac{P}{[V_a(P_0 - 1)]} = \frac{C - 1}{V_m C} \times \frac{P}{P_0} + \frac{1}{V_m C}$$

where P and P₀ are the equilibrium with the sample surface and saturated pressures of N₂ (Pascal)

V_m is the volume of gas necessary to produce one monolayer on the sample surface (m³)

V_a is the measured volume of gas adsorbed on the sample (m³)

C is an intrinsic constant

Figure 2.11 shows the typical straight line obtained after the 5 measurements. From this relation we can calculate the volume of gas to cover the surface with one monolayer (V_m) and deduced the specific surface area like following:

$$S = \frac{V_m N_a s}{m \times 22400}$$

S is the specific surface area (m²/g)

N_a is the Avogadro number (mol⁻¹)

s is the adsorption cross section of the adsorbing species (m²)

22400 is the volume of 1 mole of N₂ at standard temperature and pressure (m³.mol⁻¹)

m is the masse of the sample (g)

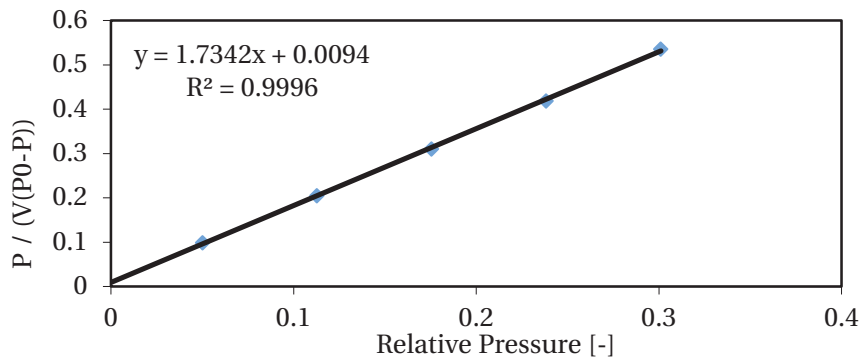


Figure 2.11: Results from the BET measurement. Five points

Sample preparation

Only anhydrous materials were analysed by BET. The powder was inserted in a glass tube. The amount of powder was adapted to have approximately more than 1 m² of surface to analyse. The sample was heated at 200°C and degassed for 8 hours. These conditions were found to give good reproducible results. Then the powder was cooled down to the room temperature for 10 minutes while the machine was calibrated. Thereafter the sample was cooled with liquid nitrogen and the measurement was started.

2.2 Sample preparation

2.2.1 Preparation of the pastes

Prior to hydration, the anhydrous cement was mixed with the mineral substitution (i.e. quartz, slag, fly ash, limestone) in a Turbula blender (Willy A. Bachofen AG, Switzerland) to obtain a homogeneous blend. About 80 grams of this anhydrous blend were mixed with deionized water (except when mentioned) at the desired water/solids ratio (0.4 and 0.6 for the blends and varying from 0.35 to 0.6 for pure cement). The pastes were mixed at 1600 rpm for 2 minutes. To study the effect of the mixing speed some samples were also mixed at higher speed (15000 rpm).

2.2.2 Preparation of the mortars

Mortars samples with the Portland cement used in cement paste were prepared with standard sand according to EN-196-1. The anhydrous powders were first well homogenized. And the deionized water was adjusted to obtain water/solids ratio 0.5.

2.3 Methods to follow the kinetics of reaction

2.3.1 Isothermal calorimetry

The hydration was followed by calorimetry (TAM Air, TA Instruments). This technique records the heat released from the sample and compares it to a reference sample. The reference sample should have a constant heat capacity similar to the measured sample.

In this study we used deionized water. The quantity required was calculated as:

$$m_{water\ ref} = \frac{C_{p\ paste} \times m_{paste}}{C_{p\ water}}$$

where C_p is the mass heat capacity of the material. For water $C_{p\ water} = 4.18\text{ J}\cdot\text{g}^{-1}\cdot\text{K}^{-1}$

The overall heat flow provides information on the kinetics of the hydration process.

In Chapter 3 the slope of the linear part of the acceleration was used to characterize the kinetics of the different systems (Figure 2.12).

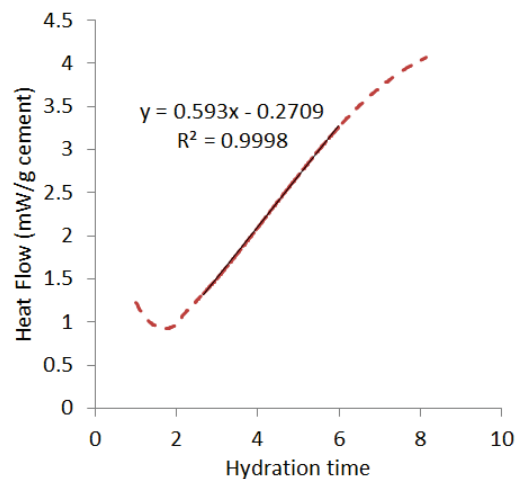


Figure 2.12: The acceleration period is characterized by the slope of the linear part of the curve

Sample preparation

Ten grams of paste were placed in the calorimeter. The instrument was maintained in a temperature controlled room to ensure the stability of the baseline. The measurements were carried out for 28 days. Beyond this time the heat released is so low that the calorimetry measure is not reliable.

2.3.2 Chemical shrinkage

Chemical shrinkage is related to the volume changes during the hydration process. The volume of the hydrates is lower than the initial volume of the reactants i.e. water, cement, SCM. This effect is due to the water binding in the hydrates which decreases the total volume. This technique is more convenient than isothermal calorimetry for long term hydration as the shrinkage measurement is cumulative.

Sample preparation

About 5 grams of mixed paste was placed into a plastic cylindrical bottle (2 cm of diameter, 5 cm height). The thickness of the paste was kept constant and thin enough to ensure the complete percolation (<1cm). To remove all the entrapped bubbles in the paste, the bottle was tapped manually and placed in an ultrasonic bath for 30 seconds. Then water was added drop by drop to minimize the disturbance of the top layer of the paste. Once the bottle was completely filled with water, it was sealed with a rubber stopper with a 10 mL pipette passing through it. The sealed system was maintained straight for a couple of minutes. On the top of the water level, few droplet of coloured oil were inserted with a syringe. The bottles were placed in a water bath at 20°C. The level of the coloured oil was recorded over 6 months. Three replicates for each system were prepared. The level of water in the pipette was similar for all the samples.

2.3.3 Chemical composition of the pore solution

The analysis of the element concentrations were done with inductively plasma optical emission spectroscopy (Schimadzu ICPE 9000), at the Central Environmental Laboratory of EPFL.

The solution is nebulized into a plasma source of Argon. The elements of the solution are released as free atoms which convert to excited ions. Their relaxation emits a photon at a characteristic wavelength. Therefore the wavelength can be used to identify the elements from the initial solution. Furthermore, the number of emitted photons is directly proportional to the concentration of the element in the solution.

Sample preparation

The sample was prepared according to the BASF protocol supplied by Nicoleau[5]. Fresh paste was cast into bottles (35 mm diameter, 50 mm height) sealed and stored at 20°C for pore solution extraction. The pore solution was extracted using a steel die device and pressure up to 70 kN. The liquid obtained was filtered using a 0.2 μm filter. About 3.3 mL was diluted in a solution with HNO_3 acid to prevent precipitation.

2.4 Methods to assess the microstructural development

2.4.1 Observations of the microstructure at early age

The morphology of the hydration products was studied with a FEI XLF-30 SFEG-SEM. The source of the beam in this microscope is a field emission gun. This kind of electron gun produces a more coherent beam and a high brightness and thus allows higher resolution at low energies compared to the conventional thermal emission (such as tungsten filament). This device was suitable for our observations of nano, micro-structure on hydrated grains.

The topography i.e. the morphology of the hydrates was observed with secondary electrons. They are emitted from the inelastic collisions with electrons. An incident electron ejects an electron from the target atom with a low energy. Due to their low energy, only the electrons generated near the surface are detected. Consequently they convey surface information.

In this work we used cement mixed with other materials (quartz, slag...). Hence, the study of the microstructure development on the different surface requires the identification of the different materials. In this case, secondary electrons are not sufficient and the sample has to be observed first with backscattered electrons. Backscattered electrons are electrons from the primary beam that interact with the matter of the specimen. They are elastically scattered by atoms in the sample. This effect is dependent on the atomic number of the atom. The higher the atomic number the more backscattered electrons emitted leading to a bright zone.

Figure 2.13 shows a backscatter electron image of quartz-alite system. Quartz grains are the grey particles and alite the whiter ones.

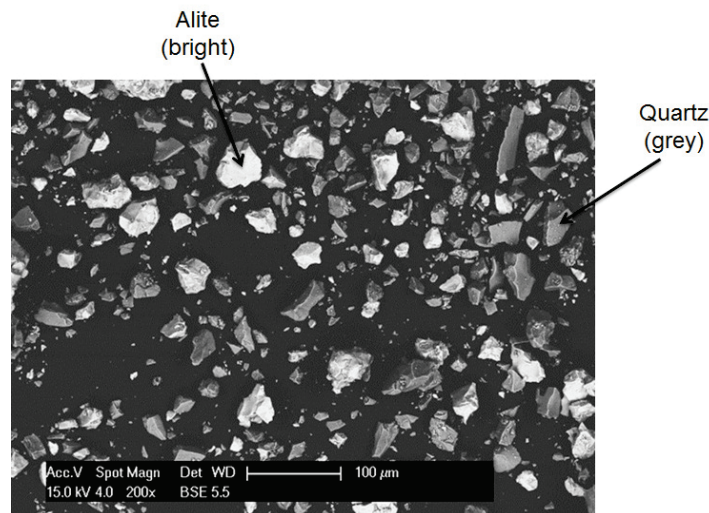


Figure 2.13: BSE image of quartz-alite paste. Bright grains are alite and grey grains are quartz

Sample preparation

The hydration of the pastes was stopped by solvent exchange with isopropanol which is known to be the best method for microscopy [6]. Figure 2.14 describes the method used. At the required times 0.2 g of the paste was removed from the sealed sample and put in a filtrating funnel with two filter papers (retention 5 μm). The funnel was immediately filled with isopropanol and the sample stirred in the funnel for 2 minutes. Then the isopropanol was removed with a vacuum pump. The washing was repeated four times. Once the isopropanol was removed, the dried paste was collected from the filter paper and stored under vacuum in a dessicator for 24 hours. SEM specimens were prepared from the dried powder. It was dispersed on an adhesive carbon tab and coated with a carbon layer of 15 nm. The microscope parameters are shown on the micrographs.

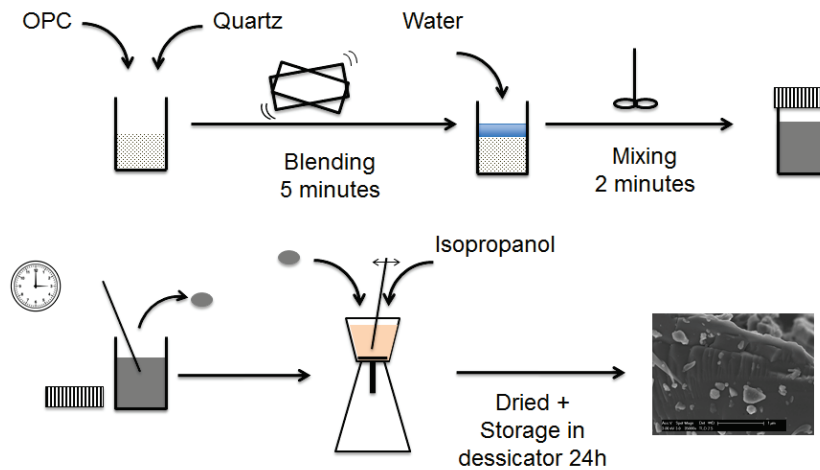


Figure 2.14: Methods used to prepare SEM samples

It is possible that the drying procedure induces some changes in the products but, as all the samples were prepared in similar conditions, qualitative comparison can be made. The conditions for high magnification observations required a carbon coating on the sample. A Zeiss Merlin microscope with different configuration has been used to determine the effect of the coating on the morphology of the hydrates (Figure 2.15). The sample without coating shows thinner and more delicate morphology. The C-S-H has a well-defined needle shape looking like a single crystal. The “globular agglomeration” effect is indeed induced by the carbon coating.

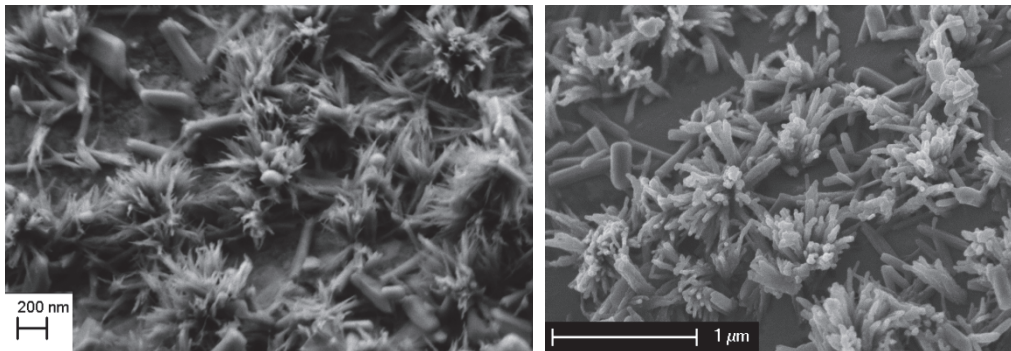


Figure 2.15: Effect of the carbon coating on same cement sample (left) no coating (right) carbon coating

2.4.2 Observation of polished sections at later ages

At later ages, fracture surfaces of hardened cement paste do not give much information. On the other hand, polished sections observed with backscattered electrons show well the distribution of the different phases (Figure 2.17). The difference of brightness or grey level allows the distinction of the major phases. Figure 2.16 shows the grey level from the Figure 2.17. The brighter zones correspond to anhydrous cement grains, grey phase is portlandite. The black areas are the pores filled of resin. The rest

is a mixture of C-S-H and different hydrated phases. The level of grey of C-S-H is related to its composition and density[7].

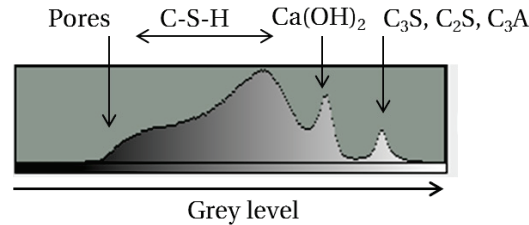


Figure 2.16: Grey level from the BSE polished section image

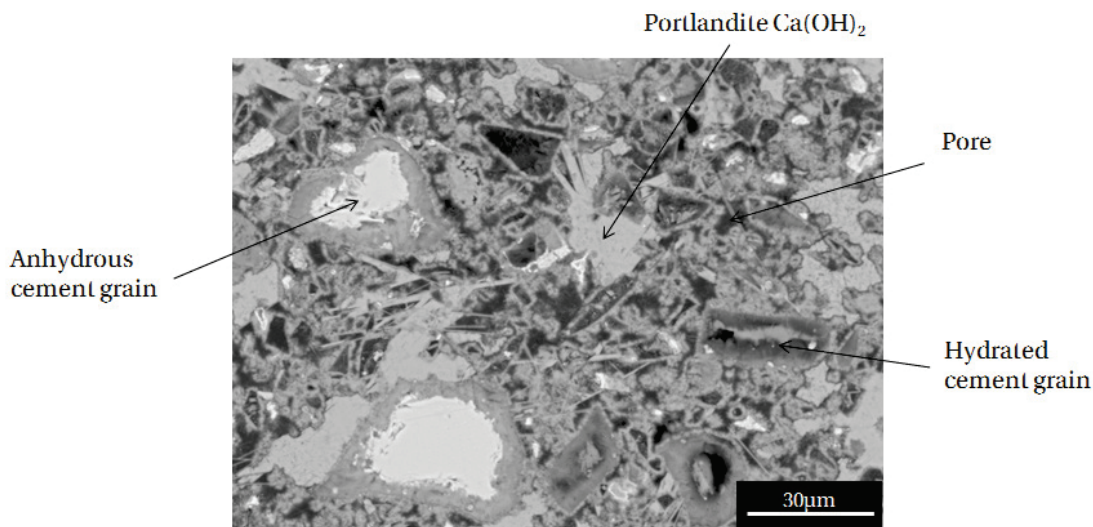


Figure 2.17: Polished section of cement paste with Backscattered electrons

Sample preparation

Fresh paste was cast into bottles (35mm diameter, 50mm height) cured under water and stored at 20°C. After 28 days, a slice of the hardened paste was cut. Then hydration was stopped by isopropanol exchange to preserve the microstructure [8]. The bulk sample was kept under vacuum pumping to remove all the isopropanol. Once dried, the sample was prepared for BSE observation by epoxy resin impregnation (EPOTEK-301) and polished with diamond powders down to 1µm. About 15nm carbon coating were put prior SEM observation.

2.4.3 Energy dispersive X-ray spectroscopy

Quantitative analysis of the chemistry of the sample can be achieved with the X-ray emitted from the interaction of the primary electrons and the sample. Each element produces an X-ray with a specific energy which allows the identification and quantification of each element. However as X-rays interact with the bulk sample, the volume of interaction has to be carefully considered (Figure 2.16). Basically the volume is about several µm in size. Nevertheless it has been demonstrated that the EDS

measurements done on SEM samples are in very good agreement with EDS on TEM sample where the volume of interaction is significantly limited[9].

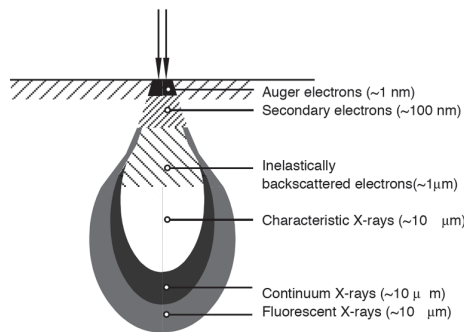


Figure 2.18: Volume interaction

EDS analysis is mainly used in hydrated cement to determine the composition of the C-S-H. C-S-H has a variable chemical composition and EDS provides information on the stoichiometry of the components. Figure 2.19 shows the typical plot Al/Ca versus Si/Ca. Each point represents one measurement. All the measurements give a cloud which represents the variability of the C-S-H composition in the sample. The extreme point of the cloud (for the highest Si/Ca) indicates the purest C-S-H composition. From this value 3 reference lines can be drawn and represent the inter-mix of C-S-H with AFm, AFt and CH hydrates.

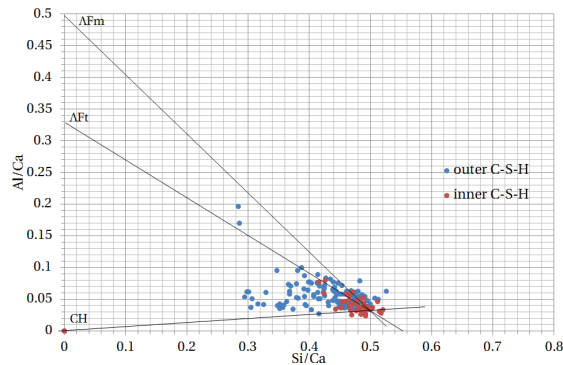


Figure 2.19: Example of EDX analysis on C-S-H composition

Sample preparation

The impregnated polished section was placed in a holder with a copper reference. Prior to any analysis, the detector was calibrated with the copper reference.

Recent work done in our lab optimized the conditions for better EDX analysis[9]. The voltage was 15kV and the spot size was tuned to obtain a constant current intensity (about 0.7-0.8 nA). 200 points on inner and outer products were analyzed for each sample.

2.4.4 X-ray diffraction

The X-ray diffraction technique is based on the scattering of the x-ray beam caused by the crystalline arrangement in the bulk specimen. Consequently only crystalline phase can be easily identified. To

quantify the phases, Rietveld analysis was done on the sample with the external standard method. The standard used in this work was rutile powder supplied by Kronos (2300 Titanium dioxide)

In situ experiments were done to follow the phase assemblage at early age. This technique requires a special device and the use of kapton film on the mixed paste to maintain the relative humidity during the hydration. Figure 2.20 compares the pattern on fresh slice and hydrating paste. Although the kapton film affects significantly the background, the peaks of the crystalline phases are similar to the fresh slice. The big advantage of in situ XRD is that the hydration can be followed from the beginning of the reaction whereas the fresh slices the analysis is limited to the time when the paste is stiff enough to be cut properly.

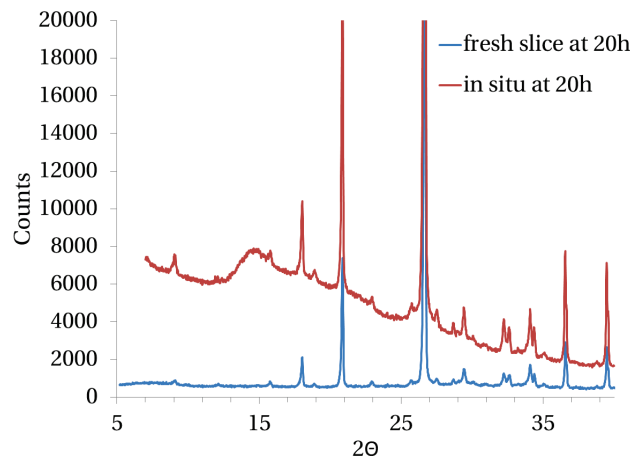


Figure 2.20: Comparison of the pattern on fresh slice and in situ preparation

Evolution of the gypsum and ettringite phases by Rietveld and normalized peak area methods are compared in Figure 2.21. We can see that the trend given by the normalized peak area is fairly good compared to the amount quantified from Rietveld analysis. It should be noted that the curve of the gypsum content is slightly less precise with respect to the quantification. We do not observe the small plateau between 10 to 12 hours. This is due to the very small amount of gypsum. The normalization by 100g of solids smooths the small variations.

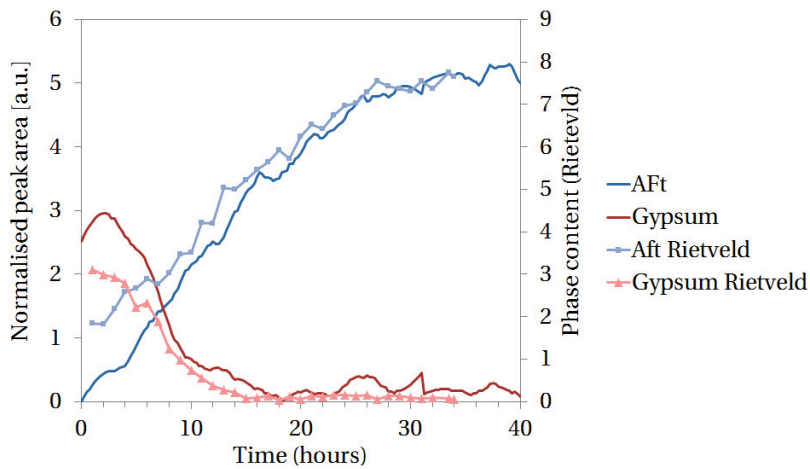


Figure 2.21: Comparison of the phase evolution between the normalised peak area method and the Rietveld refinement

Sample preparation for fresh paste

The samples were cast in plastic bottles and kept at room temperature during the curing time. One slice of the hardened paste cylinder was cut at the required hydration time and immediately inserted in the XRD holder. Standard XRD measurements were carried out with a Panalytical X'Pert Pro MPD diffractometer in a θ - θ configuration using $\text{CuK}\alpha$ source with a fixed divergence slit size of 0.5° . The X-ray tube was operated at 45 kV and 40 mA. The slice was scanned on a rotating stage between 4 and 65 [2θ] using an X'Celerator detector with a step size of $0.0167^\circ 2\theta$ and a time per step of 30s. The measurement lasts about 20 minutes and still the slice was near saturated after the test.

Sample preparation for in situ measurements

The sample was directly cast in the holder and covered with a film of kapton. Air bubbles were carefully removed by tapping the sample. It is important to note that any sample with bleeding can not be analysed with this technique. The sample was then placed in a chamber with controlled temperature. The XRD measurement was carried out each 16 minutes for 50 hours. Standard XRD measurements were carried out. The X-ray tube was operated at 45 kV and 40 mA. The sample was scanned between 4 and 40 [2θ] using an X'Celerator detector with a step size of $0.0167^\circ 2\theta$ and a time per step of 30s.

2.4.5 Mercury intrusion porosimetry

There are few techniques to characterize the pore structure of hydrated cement paste. One of the most used techniques is mercury intrusion porosimetry (MIP). This technique is based on the intrusion of a non-wetting fluid (mercury) into the connected pore structure under increasing pressure. The Washburn equation is used to relate the pressure to the entry pore size.

The interpretation of the MIP curve has been discussed due to the limitations of the technique and assumptions required [8, 10]. The most important of these is that MIP actually measures the pore entry size rather the real pore sizes. This effect is significant in cement paste as a high volume of pores are only accessible through a smaller pore. This effect is called ink-bottle effect in the literature and will overestimate the amount of small pores.

Figure 2.20 shows the typical results from the MIP analysis. Two interpretations of the results are used in this work: the cumulative pore volume curve and the pore entry size distribution curve. Both are shown in Figure 2.22. The first one is deduced from the intruded volume of mercury and gives the total connected pores volume in the entire specimen. The total pore volume can be read from the cumulative porosity for the smallest pore (i.e. highest pressure). The differential distribution curve is calculated from the cumulative pore volume curve. This plot has the advantage to clearly show the critical radius of the sample which is the inflexion point in the cumulative curve. It corresponds to the maximum of the sharp peak as described in Figure 2.22. In this study we used this critical radius to characterize the pore entry size of the connected porosity rather than the start of the turn up in the cumulative plot since it can be measured more accurately.

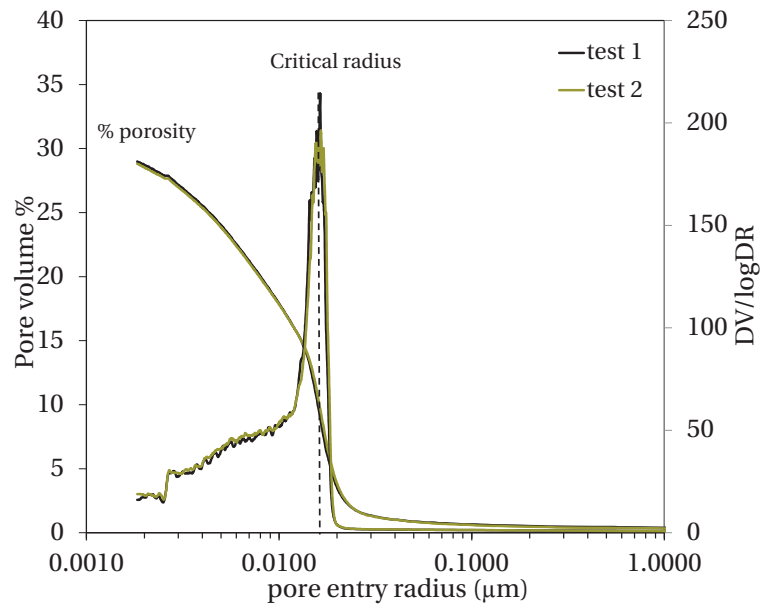


Figure 2.22: Typical curves from MIP experiment done up to 400MPa

Sample preparation

The sample was cast in plastic bottles and kept at room temperature during the curing time. One slice of the hardened paste cylinder was cut at the required hydration time and immersed in isopropanol for 6 days, renewed after 1 day. Then, the slice was dried and kept under vacuum before the test.

All the samples were crushed in small bits with similar weight for consistency (1g). The dried samples were placed in the dilatometer and the air was removed. The measurement was in two steps for two different populations of the pores. In the first step a pressure of 100kPa was applied to intrude larger pores. Then, the pressure is increased up to 400 MPa which allows intrusion of pore entries down to 2 nm.

2.4.6 ^1H NMR

^1H Nuclear Magnetic Resonance is a new technique in the cement field to study the porosity based on the water dynamics. The analysis of the relaxation time of the proton after the excitation pulse gives information on the mobility of the water molecules. Bulk water relaxes more slowly than bounded water. In cement paste four main populations of water have been identified as a function of their relaxation time (Figure 2.23).

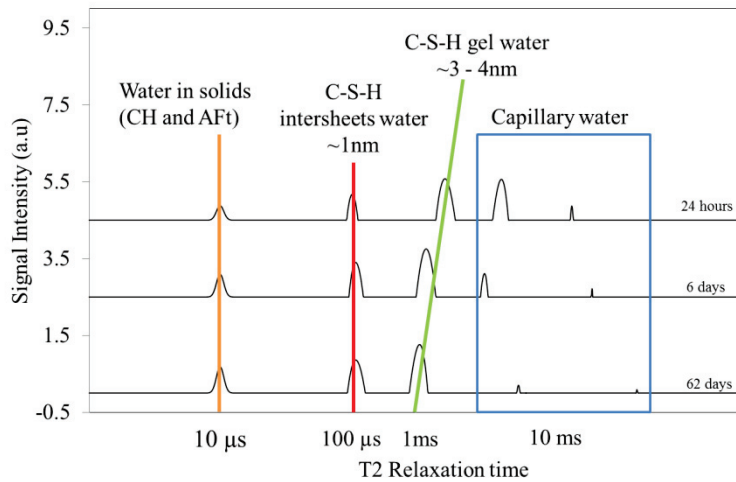


Figure 2.23: Relaxation time of the different water population in cement paste from 1 day to 62 days. Adapted from Muller[11]

Most of the techniques currently used are not able to quantify the nanoporosity of C-S-H such as C-S-H gel water and C-S-H intersheet water. Based on the model of Feldman and Sereda[12], the C-S-H gel water is a pore formed by the separation of the calcium silicate layers of the C-S-H (Figure 2.24, green triangles). The size of the gel pore decreases with the hydration time at early age and is constant thereafter (Figure 2.23). The C-S-H intersheets size is constant from the beginning of the hydration at 100 μ s. It corresponds to the water trapped between two calcium layers.

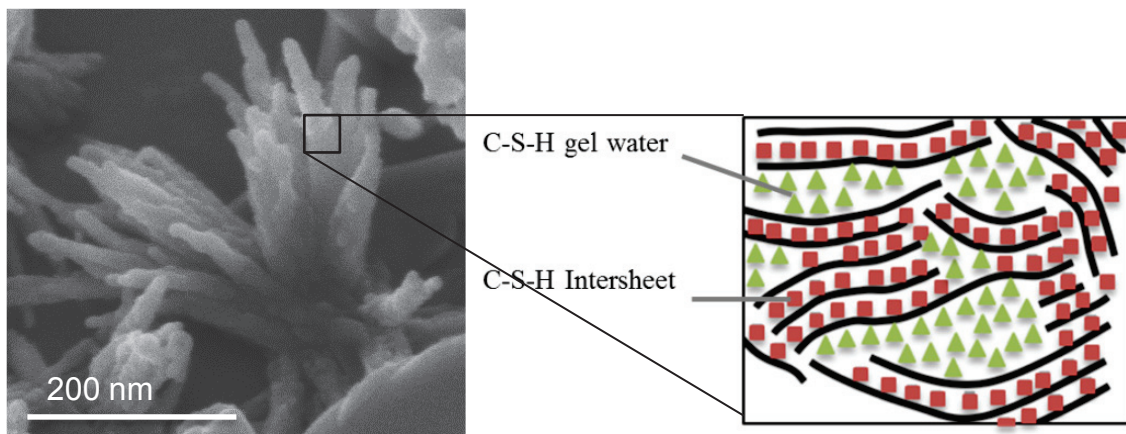


Figure 2.24: Microstructural model from Feldman and Sereda[12]. Scheme from Muller[11]

Sample preparation

The pastes were mixed according to the sample preparation previously described. About 0.35 cm³ of paste were placed into NMR tubes of 8 mm diameter. The tubes were then tightly sealed.

The NMR measurements were carried out on a Bruker Minispec NMR spectrometer operating at 7.5 MHz. The experiments and analysis of the relaxation time were done by A. Muller at EPFL LMC. The full description and detail on the signal sequences can be found in his thesis work [11].

3. References

1. Quennoz, A. and K.L. Scrivener, *Interactions between alite and C3A-gypsum hydrations in model cements*. Cement and Concrete Research, 2013. **44**(0): p. 46-54.
2. Ferraris, C.F., J.W. Bullard, and V. Hackley. *Particle size distribution by LASER diffraction spectrometry: application to cementitious powders*. in *Proceedings of the 5th world congress on particle technology, Orlando, FL*. 2006.
3. Cyr, M. and A. Tagnit-Hamou, *Particle size distribution of fine powders by LASER diffraction spectrometry. Case of cementitious materials*. Materials and structures, 2001. **34**(6): p. 342-350.
4. De Leeuw, G. and C. Lamberts, *Influence of refractive index and particle size interval on Mie calculated backscatter and extinction*. Journal of aerosol science, 1987. **18**(2): p. 131-138.
5. Nicoleau, L. 2012.
6. Zhang, J. and G.W. Scherer, *Comparison of methods for arresting hydration of cement*. Cement and Concrete Research, 2011. **41**(10): p. 1024-1036.
7. Gallucci, E., X. Zhang, and K.L. Scrivener, *Effect of temperature on the microstructure of calcium silicate hydrate (C-S-H)*. Cement and Concrete Research, 2013. **53**(0): p. 185-195.
8. Gallé, C., *Effect of drying on cement-based materials pore structure as identified by mercury intrusion porosimetry: A comparative study between oven-, vacuum-, and freeze-drying*. Cement and Concrete Research, 2001. **31**(10): p. 1467-1477.
9. Rossen, J., *Composition and morphology of C-A-S-H in pastes of alite and cement blended with supplementary cementitious materials*. 2014, Ecole Polytechnique Fédérale de Lausanne: Lausanne.
10. Diamond, S., *Mercury porosimetry: An inappropriate method for the measurement of pore size distributions in cement-based materials*. Cement and Concrete Research, 2000. **30**(10): p. 1517-1525.
11. Muller, A.C.A., *Charaterization of porosity and C-S-H in cement pastes by 1H NMR*, in *Faculté des Sciences et Techniques de l'Ingénieur*. 2014, Ecole Polytechnique Federale de Lausanne: Lausanne.
12. Feldman, R. and P. Sereda, *A new model for hydrated Portland cement and its practical implications*. Engineering Journal, 1970. **53**(8-9): p. 53-59.

Chapter 3

Effect of mineral additions on acceleration period

The reaction of the supplementary cementitious materials (SCM) usually starts after the main peak of the C_3S reaction. During the first hours of hydration in a paste containing ground clinker and SCM, the SCM particles are inert. This chapter focuses on this period when the SCM grains only act as filler. This concerns mainly the acceleration period. The objective of the work presented in this chapter is to:

- Quantify the filler effect of the most common SCMs. Do all SCMs have a similar filler effect?
- Identify which physical/chemical features of the SCM grains caused the filler effect.
- Explain the mechanism(s) behind the filler effect.

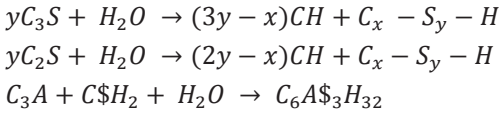
Part of this work has been published in 2014 in the Journal of the American Ceramic Society.

DOI: 10.1111/jace.13177

1. Literature review	30
1.1.Parameters affecting the nucleation and growth mechanisms	32
1.2.Filler effect	34
2. Mixes studied	35
3. Results	37
3.1.Microstructural development in alite and cement paste containing quartz	37
3.2.Effect of the surface provided by inert particles on the kinetics	41
3.3.Effect of the water/solids ratio on kinetics	43
3.4.Shearing effect on microstructure and kinetics	45
3.5.Effect of common SCMs	50
4. Summary	62
5. References	64

1. Literature review

Cement hydration consists of several chemical reactions occurring simultaneously and leading to the formation of a solid skeleton. The main reactions with cement notations are (see Glossary):



Most of these reactions are exothermic: the overall heat released can be thus recorded with a calorimetric device. A typical calorimetry curve of Portland cement is shown in Figure 3.1. The main reactions of hydration occur within the first 24 hours although the hydration will continue until exhaustion of reactants (> 1 year).

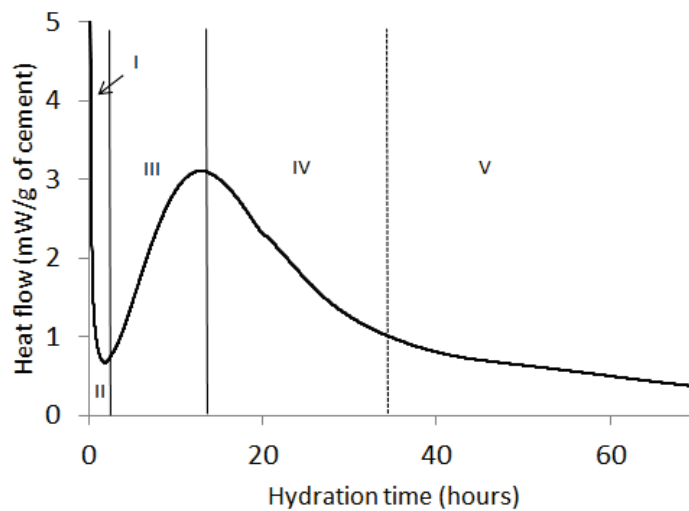


Figure 3.1: Typical isothermal calorimetry curve of cement hydration

The hydration curve is usually divided in 5 stages [1, 2]. One of the most important stages is the so-called “acceleration period” which corresponds to stage III in Figure 3.1. This period is of great interest due to the high amount of hydrates forming during this period.

The calcium silicate hydrate (C-S-H) is the main hydrate along with CH in hydrated cement paste. It forms connections between the cement grains leading to the setting and the strength development of the paste.

C-S-H clusters are forming rapidly on the surface grains after the contact with water. In few hours, the clusters of C-S-H grow in number and size to become fibrillar clumps which form sea-anemone like structures (Figure 3.2) [3]. The shape observed with SEM is reported as fibrillar and several terms have been used in the past to describe it: type I from Diamond or needles radiating from grains[2].

The nucleation and growth process of C-S-H is now well supported as the rate controlling mechanism of the acceleration stage [4, 5]. Recent advances in both experiments[6] and simulations[7] have brought new evidences to support this interpretation.

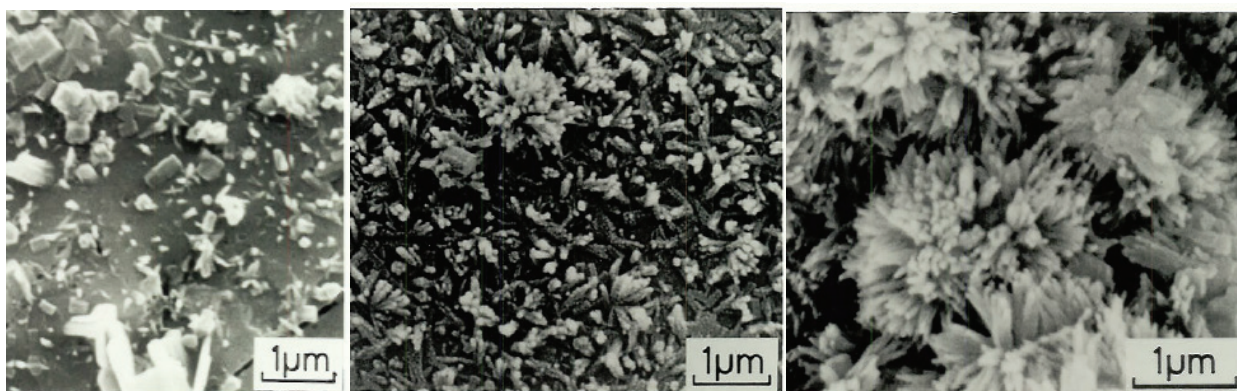


Figure 3.2: Cement hydrated for 3 hours, 6 hours and 10 hours from Scrivener[3]

Nucleation of C-S-H

Nucleation is a mechanism which creates new interfaces. The formation of these new interfaces requires extra energy which comes from the degree of supersaturation. The supersaturation is therefore the necessary condition for nucleation. A higher supersaturation leads to a faster nucleation rate.

The nucleation free energy barrier can be reduced on surfaces and hence nuclei can form on surface rather in the solution. This is referred as to heterogeneous nucleation. In cement hydration, nuclei are generally observed to form on cement grains rather than in the solution. This means that the nucleation of C-S-H is heterogeneous[8]. Surfaces favour nucleation when the substrate lower surface energy, *e.g.* has similar lattice or atomic structure than the growing new phase or catalyzes the formation of a bond with the new phase. C-S-H seeding seems to be a good substrate for C-S-H formation as it significantly increases the rate of nucleation and growth[6, 9].

Observation of the form or chemical composition of the first C-S-H is very limited at this scale. And most of the information is based on thermodynamics and indirect observations of species concentration. It is debatable whether C-S-H and CH which is the second main hydrate, are sharing a common nucleus. Gartner suggested that C-S-H would develop from $\text{Ca}(\text{OH})_2$ nuclei by adsorbing silicate ions[2]. A recent atomistic study on the CH had revealed that calcium-silicate complex is adsorbed at the Portlandite surface[10]. This phenomena seems to poison the growth of CH but seems to indicate that nucleation of C-S-H from CH is possible[11].

Growth of C-S-H

Once the nucleus is formed, it starts to grow. The growth rate is controlled by the kinetics of the process occurring at the solution-crystal interface. The morphology of the new phase depends on the growth rates of the different new surfaces.

The microstructural development of C-S-H through the acceleration period is not well established. The main issue which limits our understanding is that C-S-H is neither crystalline nor completely amorphous. There are different microstructural models suggested, which had led to different growth theories detailed in a recent review[12]. The main point of disagreement is whether the C-S-H is growing layer by layer[13] or by aggregation of randomly oriented units of C-S-H[14]. The latter is a mechanism proposed for diverse minerals such as CaCO_3 [15, 16].

The diverging structure sometimes called “sea-anemone” morphology observed in SEM micrographs during the acceleration period (Figure 3.2) has been compared to the products formed during the reaction of silica particles in a solution rich in calcium by Gartner[13]. Figure 3.3 shows the so-called sheaf-of-wheat structure obtained. The orientation of the needles or fibers on a common axis in each bunch suggests that they are growing from a common nucleus. This morphology was explained by Gartner as the consequence of the silicate vacancies that curve the needle from another one.

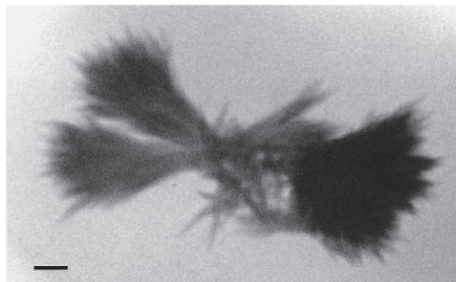


Figure 3.3: X-ray microscopy images during the reaction of silica gel in NaOH and CaCl₂ solution [14]. This morphology is very similar to the C-S-H morphology in cement paste

1.1. Parameters affecting the nucleation and growth mechanisms

Through experiments, several parameters have been identified to influence the kinetics of the reactions occurring over the acceleration period. Their effects are discussed regarding the mechanisms of nucleation and growth.

- Particle size of the alite/cement

The fineness of the clinker particles significantly affects the hydration kinetics. A higher hydration degree was found for cement with the smallest size [17]. Costoya [18] demonstrated that this effect is already significant at early age, and proportional to the total surface area of the particles. Figure 3.4 shows the relation between the rate during the acceleration period and the fineness of the alite particles: a doubling of the surface of alite powder leads to a doubling of the slope.

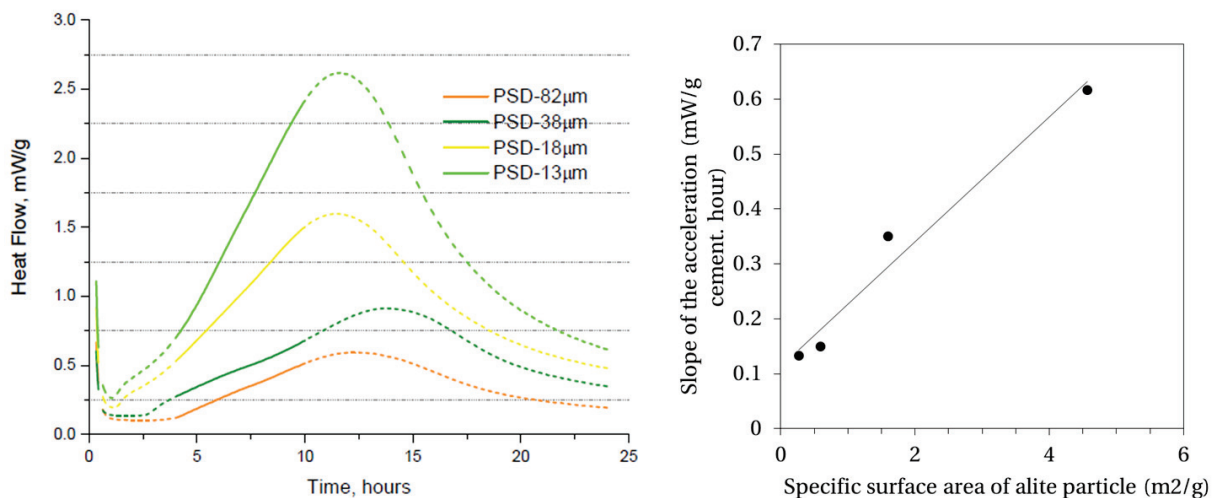


Figure 3.4: Relation between rate of the acceleration period and the specific surface area of alite particles. Adapted from Costoya[18]

– Mechanical mixing

Juilland [19] and Dollimore[20] both reported the important role of the mechanical mixing on kinetics. Figure 3.5 shows that when increasing the mixing speed, the kinetics of hydration are significantly changed at early age: the induction period is shortened and the acceleration period is earlier and steeper. The microstructure of the paste mixed at higher speed was more homogeneous and denser than at lower speed. Simulations support the hypothesis that the mechanical mixing leads to the formation of more nuclei of hydrates (C-S-H)[19]. The reduction of the double electrical layer around the grains or dislodging of pre-nuclei during the fast mixing are possible reasons for the increase in number of nucleation sites. The increase of the temperature caused by the friction of mixing was not enough to affect the kinetics. There are no direct observations of the increase of nucleation sites at this early age to confirm these hypotheses.

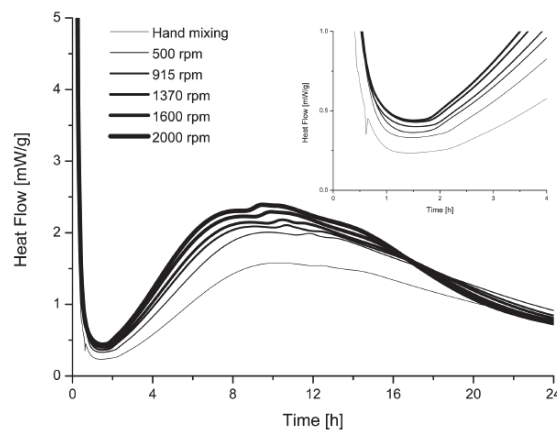


Figure 3.5: Increase of the acceleration rate with mixing speed. From Juilland[19]

– Temperature

The kinetics of cement hydration at early age is sensitive to the temperature: it becomes much faster with increasing temperature. As a result, more heterogeneous microstructure is observed caused mainly by an increase of the density of C-S-H with temperature [21, 22]. Below 50°C, the phase assemblage and the mechanisms governing hydration are maintained [22-24]. Therefore nucleation and growth of C-S-H is still expected to be the rate controlling mechanism.

– Accelerator/retardator admixtures

These chemical admixtures are mainly used to control the setting time, reduce the water content. They affect the kinetics of hydration at early age. Although admixtures are now widely used in concrete production, there are still outstanding questions regarding their effect on hydration mechanisms [25]. There are several possible mechanisms which might be specific to different chemicals. Poisoning nucleation or growth[26], change of CH [27] or C-S-H morphologies [28, 29] are currently the main hypothesis proposed in literature.

– Mineral additions

By-products or natural materials are more and more used in the cement industry to reduce the amount of clinker. These reactive materials [30-33] or inert particles [34-36] are reported to accelerate the rate of

the acceleration period of cement hydration. In 1990 Gutteridge [37] observed that before SCMs reacted, the hydration of the clinker phases was already enhanced. He demonstrated that the physical presence of particles enhanced the hydration of the clinker phases and even inert particles have this effect. This effect is called the *filler effect*.

This effect has been attributed to the increase of the number of nucleation sites provided by the extra surface from the particles.

1.2. Filler effect

The sole physical presence of SCM enhances the hydration of the clinker phases. This effect is usually referred as the filler effect. The replacement level of the SCM and its fineness have been shown to be the major factors affecting the hydration kinetics [35, 36]. Based on these observations several mechanisms have been put forward to explain the filler effect [38-40].

The first mechanism is related to the dilution of cement. The replacement of ground clinker by other materials means that relatively more space is available for the formation of hydrates from the clinker hydration [38, 39]. The cement is therefore diluted compared to plain clinker cement paste that is assumed to affect the kinetics and the microstructure development.

The second mechanism suggested is the heterogeneous nucleation of C-S-H on the filler surface [8, 35, 37, 41-43] as there is a clear dependency on the surface provided by the SCM particles. Most of the models assume that the rate of growth is constant [4, 12, 44]. The enhancement of the hydration rate during the early age is supposed to be due to the increase of nucleation sites of C-S-H [45].

Studies have qualitatively compared the effect of different types of SCM or inert filler [34, 36, 46]. Kadri *et al.*[36] focused on different inert fillers. They reported that quartzite had no accelerating effect compared to alumina powder and limestone. However, the replacement level of the fillers in the blended systems was 10% which is rather low to assess the accelerating effect. Poppe [34] and Oey [47] observed that limestone affected the hydration kinetics more than quartz. Although both studies show differences in the efficiency of filler, no explanations were proposed.

A few microscopic observations have confirmed the growth of C-S-H at early age on SCM surfaces. Stark *et al* [48] observed the nucleation directly on quartz, calcite and C_3S surfaces. The surfaces of the hydrated C_3S , quartz and calcite had different coverings of C-S-H. This emphasizes that the chemical nature of the surface can affect the C-S-H nucleation. The morphology of the C-S-H might be also affected as a C-S-H layer instead of needles-like morphology was observed on carbon nanotubes [49].

So far there is no explanation on the different effects of filler, or quantitative comparison between SCMs. Most of the studies used kinetic data such as isothermal calorimetry or consumption of the main clinker phases to study the filler effect. The microscopic observations are rare despite giving useful complementary information.

2. Mixes studied

The acceleration period is controlled by the C-S-H nucleation and growth. The increase of the slope in the acceleration period caused by the SCM and others parameters has been attributed to the larger number of growing C-S-H. The SCM are usually assumed to provide surfaces where C-S-H can nucleate. The evidence comes from the increase in kinetics with the fineness of the particles. Thus, the filler effect is seen to be proportional to the surface area. However these effects have not been well quantified. In this study we want to:

- Verify if hydrates are able to nucleate and grow on filler grains,
- Which hydrates can form?
- Do they have similar morphology and growth rates as on cement grains?
- Quantify the filler effect of the most common SCMs

The first step was to study the influence of inert particles with quartz and then confirm/disprove the findings with common SCMs.

2.1. Study with alite

Quartz-alite system is a simpler system compared to quartz-cement system since alite hydration produces only two hydrate phases (Portlandite Ca(OH)_2 and, calcium silicate hydrate C-S-H). Therefore before using blended systems with cement, quartz-alite systems were used to better observe the C-S-H growth on quartz and alite grains.

Alite and quartz powder were mixed together. Quartz replaced 40 % by mass of the solid content. Water was added to the anhydrous mix to reach a water/solids ratio of 0.4. The pastes were mixed in batches of 5g in a plastic vessel owing to the limited reserve of alite. The paste was hand mixed for 2 minutes.

2.2. Study with quartz in cement paste

To investigate the impact of the surface area of the filler Portland cement (CEM I 52.5) was mixed with different sized quartz powders ($d_{50} = 4, 13$ and $18 \mu\text{m}$) and the replacement level for each quartz was from 10% to 70%. The water/solid ratio was constant at 0.4.

There is debate as to whether it is best to consider water to solids ratio by weight or volume. Even though there is some difference in density between clinker (3.1 g/cm^3) and quartz (2.65 g/cm^3) the differences in water to solid ratio by volume are relatively small and are taken into account in the analysis.

Table 3.1: Mix design of quartz-cement systems

Mix	Weight		Volume	
	w/c	w/s	w/c	w/s
10% Quartz	0.44	0.4	1.38	1.22
20% Quartz	0.5	0.4	1.55	1.20
40% Quartz	0.66	0.4	2.07	1.16
50% Quartz	0.8	0.4	2.48	1.14
70% Quartz	1.3	0.4	4.13	1.11

2.2.1. Effect of the water/solids ratio

Four quartz-PC systems were used to investigate the effect of w/s ratio while the total surface provided by quartz was kept constant.

From the specific surface measurements, 10% of Quartz (4 μ m) provides same total surface area of quartz than 20% of Quartz (13 μ m).

Table 3.2: Mix design for w/s study

Mix	Weight	
	w/c	w/s
10% Quartz (4 μ m)	0.44	0.4
20% Quartz (13 μ m)	0.5	0.4
Add 10% Quartz (4 μ m)	0.4	0.36
Add 20% Quartz (13 μ m)	0.4	0.32

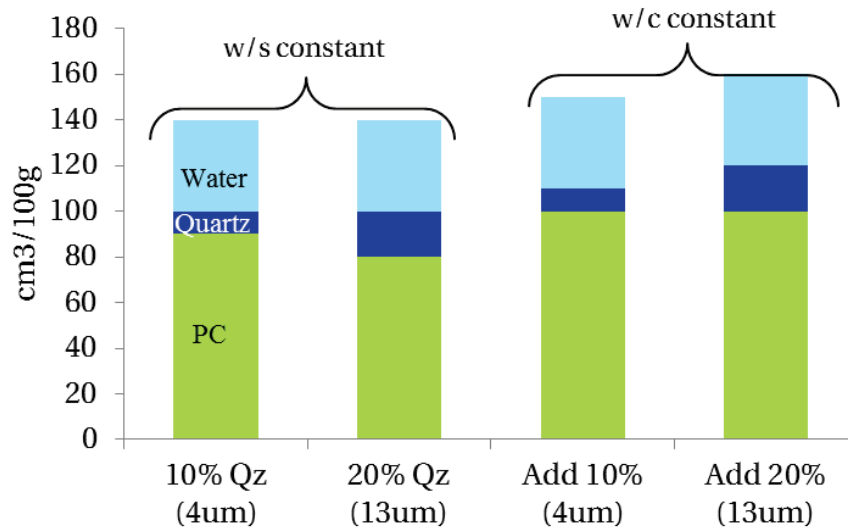


Figure 3.6: Initial proportions of the mixes studied

Pastes with Portland cement were also used with different water/solids ratio from 0.35 to 0.6 to complement this study.

2.2.2. Study with common SCMs

One siliceous Fly ash and two hydraulic slags were used to study the filler effect of SCM. Limestone powders were also used as substitutes in the blends. Limestone is known to have a marked effect on the early hydration kinetics. The level of substitution was from 20% to 70% in the paste. The water/solids ratio was maintained at 0.4.

3. Results

3.1. Microstructural development in alite and cement pastes containing quartz

3.1.1. Microstructure in alite-quartz paste

In the set of micrographs in Figure 3.8 we can observe the microstructure development on alite and quartz surface in alite-quartz paste. After hydration for 1 hour, the surface of the quartz remains identical to its unhydrated state. The presence of small quartz particles from the grinding on the surface could be confused with potential C-S-H at early stage (Figure 3.8.a).

After further hydration at 3 hours, C-S-H and Portlandite at early stage of growth are clearly visible on the quartz surface (figure 3.8 c and d). The presence these small particles (50 nm) on the quartz surface indicates that ionic species are available everywhere in the solution and confirm that quartz surface acts as a substrate for the heterogeneous nucleation of the hydrates. From the calorimetry curve plotted in Figure 3.7, at 3 hours we are still observing a microstructure during the induction period. Thus C-S-H seems to already nucleate in the induction period on the quartz grains.

Figure 3.8. e and f depicts the surfaces of both quartz and alite after 5 hours of hydration. On the alite grains, C-S-H is more abundant and sometimes mixed with CH crystals. Unlike quartz, the alite surface is covered by many etch pits that becomes larger and more abundant with time. Usually at the base of the C-S-H phase large pits were found (figure 3.8.e). The hydrates seem located and distributed randomly on both surfaces. The morphology of the C-S-H: straight needles growing perpendicular to the surface.

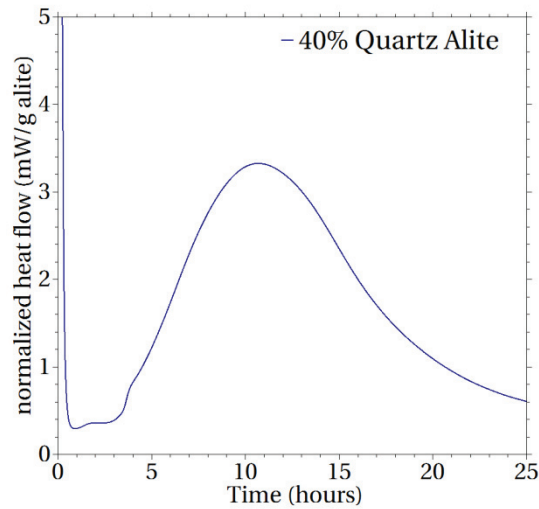


Figure 3.7: Calorimetry curve of 40% Quartz alite system

3.1.2. Microstructure in quartz-cement systems

Figure 3.9.a) and b) shows the surface of the quartz and cement grains from quartz-cement paste after 5 minutes of hydration. Small particles can be seen on both surfaces. A few of these can be identified as ettringite (hexagonal rods) or Portlandite (hexagonal plates). However most of the particles seem to be blobs thought to be C-S-H. Although the diversity of the first formation of C-S-H prevent a quantification of C-S-H nucleation sites on both surfaces (quartz and cement), the distribution of the number of nucleation sites seems similar on quartz and cement surface.

By 2 hours, more ettringite crystals and the C-S-H have started to grow with needle-like morphology (Figure 3.9.c,d). Ettringite forms in the water filled space as well as on the surface and falls onto the surface on drying [3]. Larger crystals are found when the growth was in the water-filled space.

After hydration for 5 hours (Figure 3.9.e and f) the surface is more covered by products. The C-S-H is well defined as needles which diverge in a “sea anemone” type morphology which is a different morphology than that seen in quartz-alite paste (Figure 3.8. e and f) where the phase is forming convergent needles. The growth on the quartz is similar to that on the cement grains.

3.1.3. Summary

The difference in microstructure between alite and cement pastes are clear from our micrographs. Differences between alite and cement have also been reported at later ages [50, 51] but not at early age. It seems that the microstructure at later ages results in changes in the growth of C-S-H from the very beginning of the hydration. The sulfate ions available in the clinker would be responsible for the difference between alite and cement. This possible explanation is further developed in the next chapter (Chapter 4).

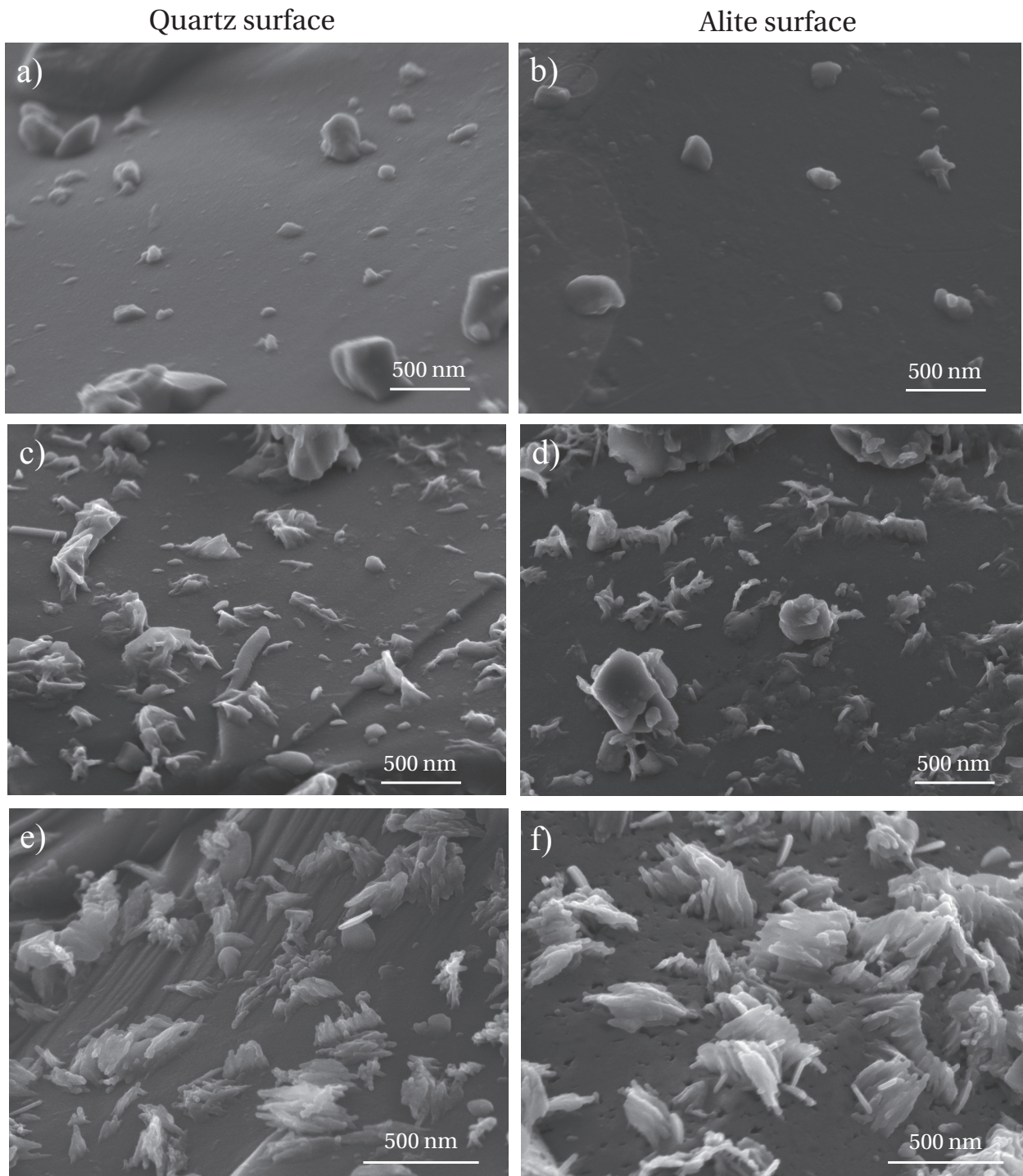


Figure 3.8: Microstructure in quartz-alite paste at 1 hour on a) and b), 3 hours on c) and d), 5 hours e) and f)

Quartz surface

Cement surface

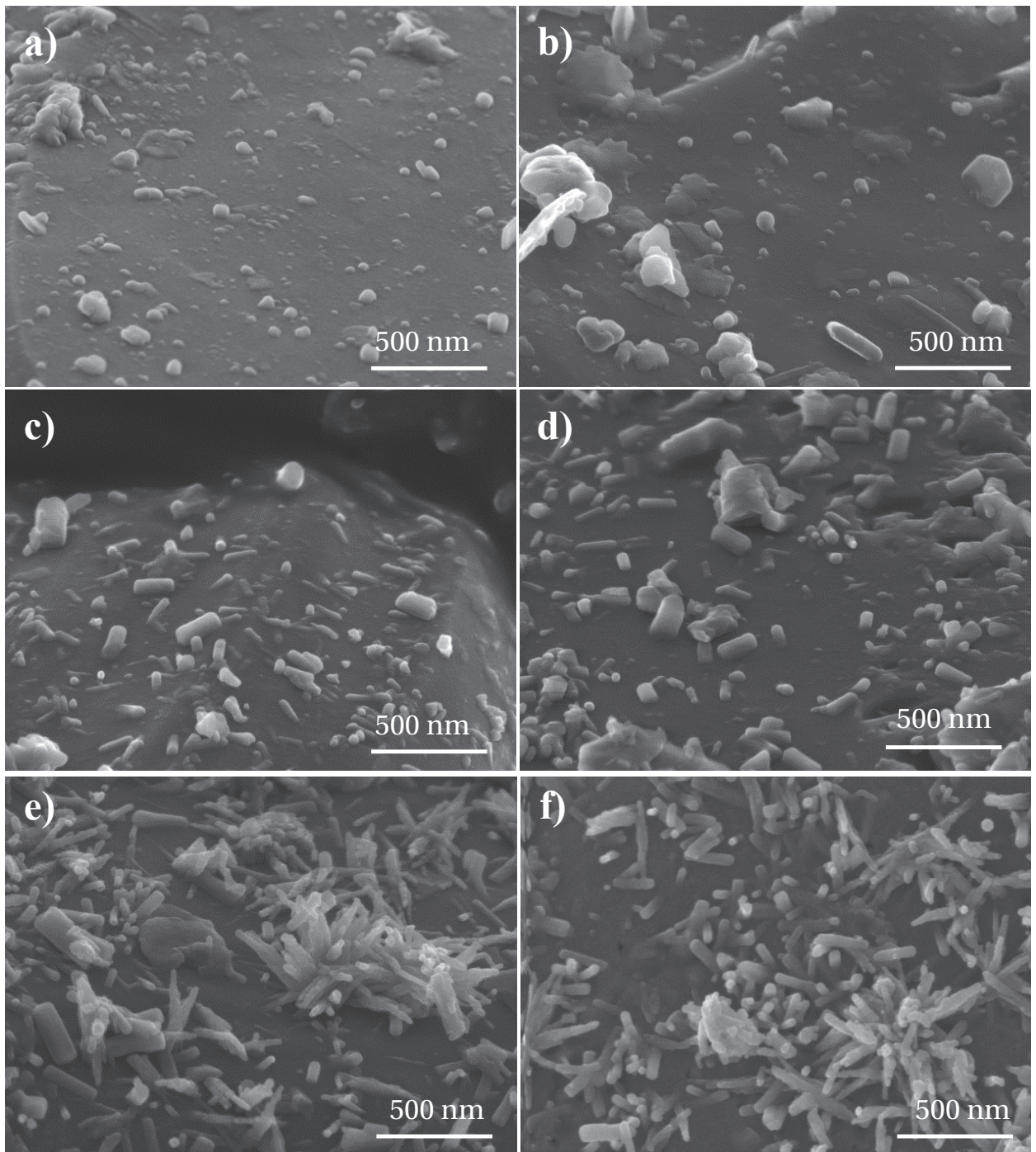


Figure 3.9: Microstructure in quartz-cement pastes at 5 min a) and b); at 2 hours c) and d); at 5 hours e) and f)

3.2. Effect of the surface provided by inert particles on kinetics

In this section we consider how the extra surface provided by the filler particle affect the kinetics of cement hydration. The kinetics is followed and quantified with isothermal calorimetry technique.

Figure 3.10 shows the heat flow curves during the first day of hydration for quartz-cement pastes, normalized by the plain Portland cement content which is the only reactive component. Although quartz is inert, the rate of reaction of the clinker component is enhanced. The main peak is higher and the acceleration slope steeper. The aluminate reaction, characterized by the shoulder during the deceleration period, is also enhanced by the replacement with quartz. This effect will be discussed in the next chapter (deceleration period).

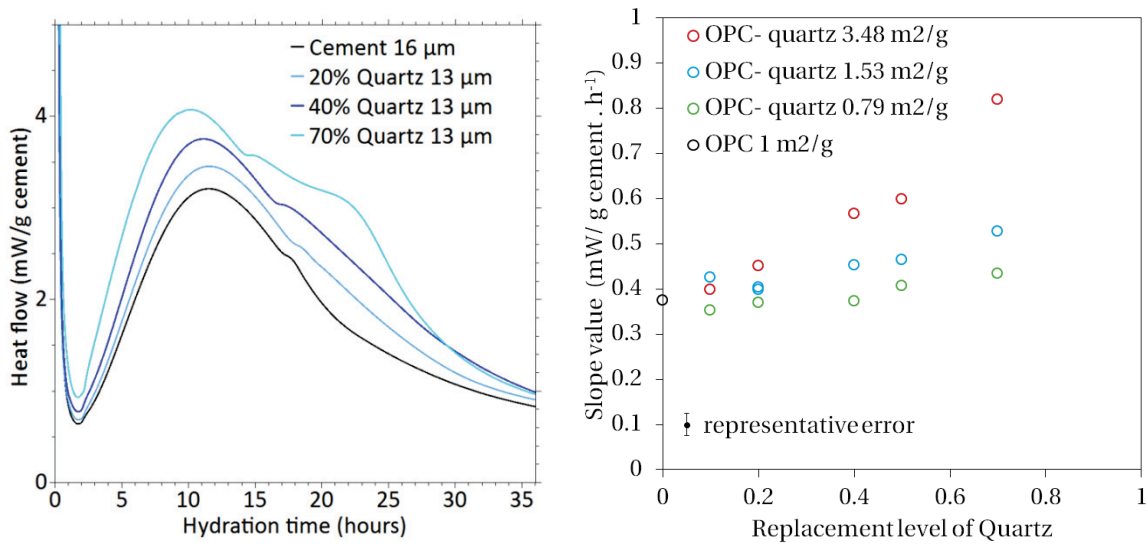


Figure 3.10: Effect of increasing the replacement of quartz in cement paste

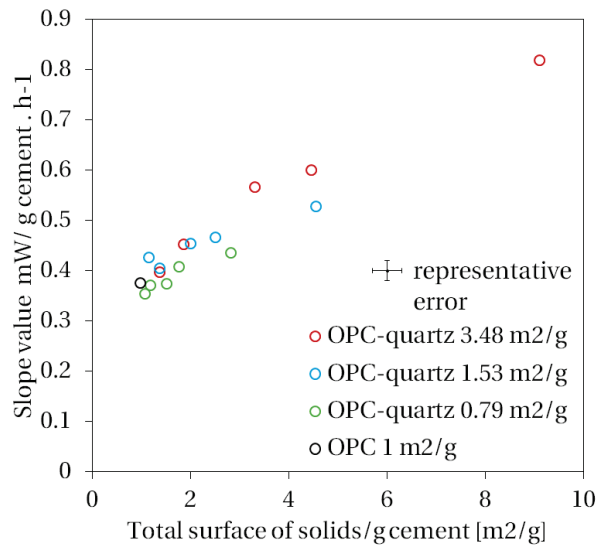


Figure 3.11: Slope value of the acceleration curve as a function of the total surface of solids

Figure 3.10 shows the slope value as a function of the replacement level for three fineness of quartz powder. For each quartz size, a relationship of increasing acceleration slope with the replacement level is observed. This indicates that the increase is dependent of the replacement and the quartz size. The quartz having slightly coarser specific area to cement leads to a solid surface nearly constant for different replacement. For this system the slope only slightly increases with replacement. This shows that the filler/cement ratio has little effect on the kinetics of cement hydration in this case.

In Figure 3.11 the slope of the acceleration period is plotted as a function of the surface provided by quartz. It is seen that there is a roughly linear increase of the slope with the surface of quartz per gram of cement in the paste. This effect is usually regarded as the increase of the surface available for the nucleation of C-S-H [4, 38, 45] as the rate of nucleation and growth of C-S-H is assumed to be the rate determining process during the acceleration period [4, 12, 52, 53].

However more detailed analysis of this relation shows that the impact of the extra quartz surface is quite low compared to the surface of the clinker grains. When the total surface is increased from $1\text{ m}^2/\text{g}$ (that of the plain cement) to $2\text{ m}^2/\text{g}$ the slope value only increases by about 20%. In comparison for different finenesses of plain cement it is seen that the acceleration slope for plain cement increases in direct proportion to the surface [18, 54] (Figure 3.12); a doubling of the surface leads to a doubling of the slope. If the only effect of the quartz was to provide extra nucleation sites, the efficiency of the quartz surface is only about one fifth that of the cement grains and we would expect to observe less C-S-H on quartz grains compared to cement grains. However this is in contradiction with our microscopic observations in the previous section (Figure 3.9).

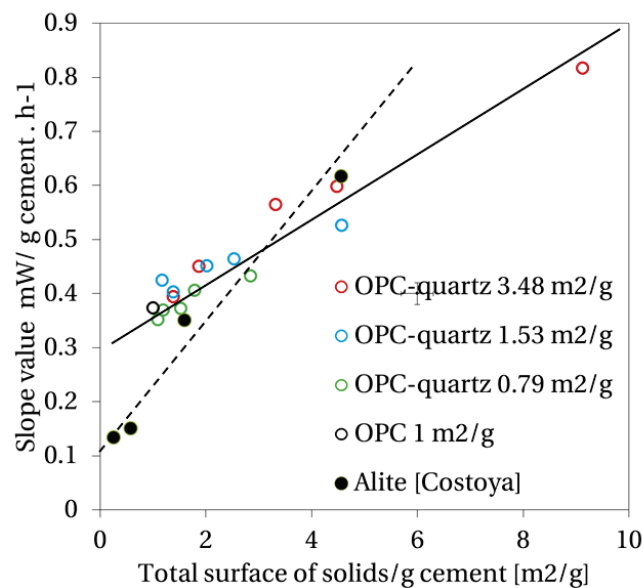


Figure 3.12: Comparison of the surface effect between quartz and alite

3.3. Effect of water/solids on kinetics

Figure 3.13 shows there is a noticeable effect of increasing water/solids ratio in cement paste on the kinetics of hydration. The main peak is slightly delayed and becomes broader: the rates of acceleration and deceleration are slower. Alkalis are known to affect the kinetics of hydration and when the w/c ratio increases, the concentrations of the dissolved ionic species (e.g. alkalis) are expected to decrease. Nevertheless, experiments with cement paste adjusted (w/c 0.6) with additional alkali show no effect on the hydration kinetics (Figure 3.13). So the changes in kinetics with w/c do not result from the decrease of the alkali concentration.

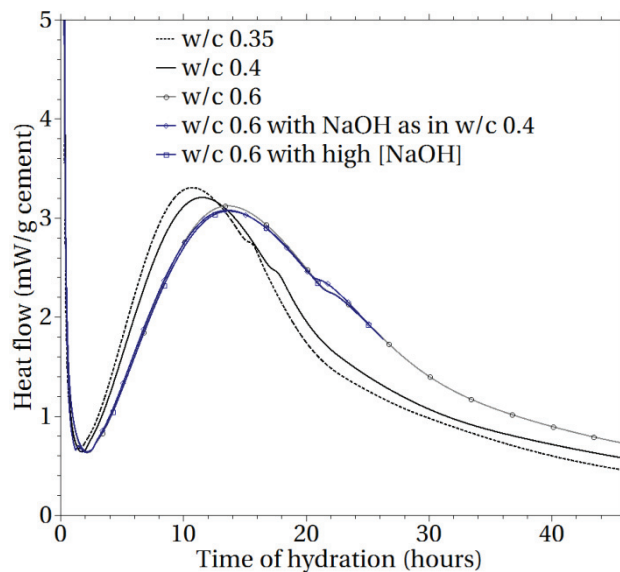


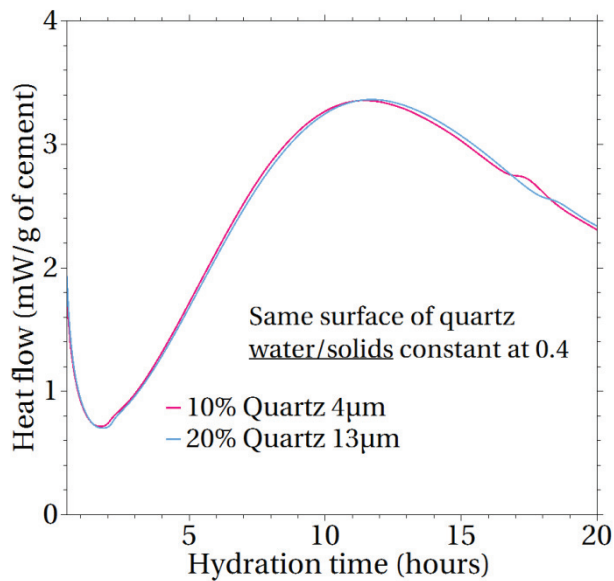
Figure 3.13: Effect of the water/solid ratio on kinetics of PC

In blended systems we can separate the water/solids from water/cement ratio.

Systems with 10% of finer quartz ($4\ \mu\text{m}$) and 20% of coarser quartz ($13\ \mu\text{m}$) were compared. These provide a similar surface area of quartz and thus provides similar surface for nucleation sites. Pastes were made with these two systems at the same water/solids ratio = 0.4. The w/c ratio was different due to the different level of replacement (10% replacement gives w/c=0.44 and 20% replacement gives w/c=0.5). Figure 3.14 shows the slope of the acceleration period of the systems with a similar surface area of quartz and w/s ratio. The results show that for similar surface area the slope of the acceleration is identical (although the replacement level was different in both systems i.e water/cement ratio different). Hence, this observation shows that water/cement ratio does not affect significantly the kinetic of the acceleration period.

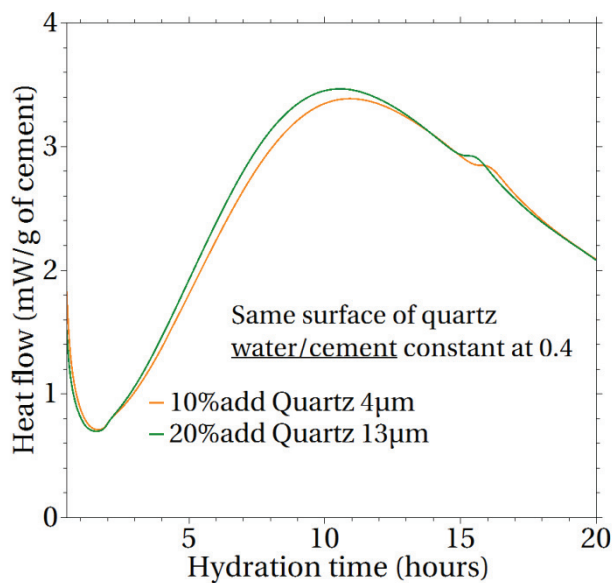
Similar systems were used: the surface area provided by quartz and the water/cement ratio were constant. Thus, in these two systems the cement is not diluted and the surface provided is the same; the water/solids ratio is the only parameter changed. (Figure 3.6). The curves plotted in Figure 3.15 and show that when the water/solids ratio is reduced, the slope of the acceleration is increased. This

indicates that it is the water/solids ratio rather than the water/cement ratio that has a more significant effect on the acceleration rate.



Mix	w/c	w/s	slope
10% Quartz (4um)	0.44	0.4	0.39 +/- 0.02
20% Quartz (13 um)	0.5	0.4	0.40 +/- 0.02

Figure 3.14: Effect of the water/cement ratio in blended systems. Water/solids ratio and surface provided by the quartz are constant



Mix	w/c	w/s	slope
10%add Quartz (4um)	0.4	0.36	0.42 +/- 0.02
20%add Quartz (13 um)	0.4	0.32	0.46 +/- 0.02

Figure 3.15: Change of the water/solids ratio. Surface provided by quartz and water/cement ratio are constant

The water/solids ratio in the paste determines the distance between the particles in the mix. Increasing the water/solids ratio corresponds to an increase in the distance between the grains. When filler with smaller size than cement is used to replace cement, the surface-to-surface distance which separates the particles is also reduced as illustrated in Figure 3.16.

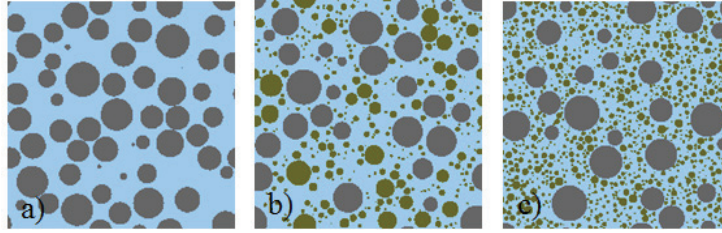


Figure 3.16: Simulation of the packing in a) PC paste b) PC+40% quartz with medium size c) PC + 40% quartz with smaller size. Grey spheres represent clinker grains, green spheres are quartz

The distance between the surface of particles (d_{BET}) can be written as [55, 56]:

$$\delta = d_{BET} \left(\left(\frac{\varphi}{\varphi_m} \right)^{-\frac{1}{3}} - 1 \right)$$

d_{BET} is the mean diameter from the specific surface area as

$$d_{BET} = \frac{6}{\text{Surface BET} \times \rho}$$

$$\text{Surface BET} = \frac{M_{cem}BET_{cem} + M_{filler}BET_{filler}}{M_{cement} + M_{filler}}$$

where

$\frac{\varphi}{\varphi_m}$ corresponds to the relative packing: where φ is the solid volume fraction and φ_m is the maximal packing fraction of the solids. φ_m can be calculated from the model of Hu and de Larrard [57]:

$$\varphi_m = 1 - 0.45 \left(\frac{d_{min}}{d_{max}} \right)^{0.19}$$

In cement paste φ_m is usually assumed to be of the order 0.64 [55]. Even in the case for the very fine quartz addition, the φ_m value only changes to 0.649.

Figure 3.17 shows the slope value as a function of the mean distance between the surfaces of the particles. The first observation is that all the systems (blended systems and plain cement systems), including variation in water to cement ratio, fall on the same curve. The smaller the distance, the higher the acceleration rate and this effect is independent of the nature of the particles: both quartz-cement and plain cement systems follow the same relation. This indicates that the acceleration rate is related to the distance between particles.

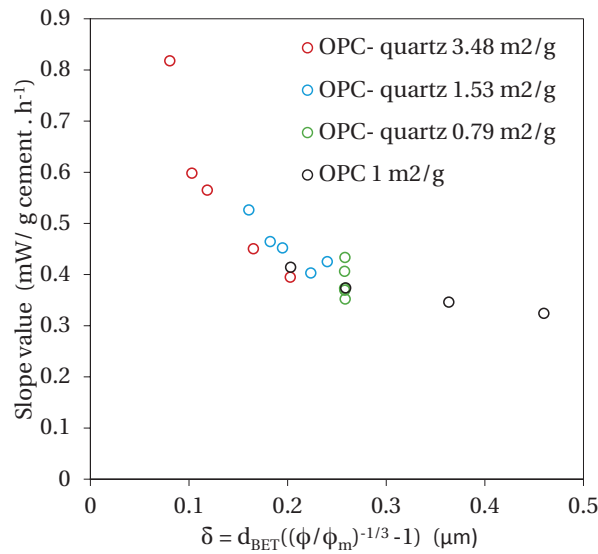


Figure 3.17: Slope value as a function of the inter-distance between particles

Several interpretations of this relation are possible, which may be related to either chemical or mechanical effects. For example, a smaller inter-particle distance will mean a shorter path for the diffusion of chemical species. This might improve the supply of the species and favor the nucleation and growth of the hydrates (i.e. higher acceleration rate). Nevertheless, the diffusion of the species in the pore solution is fast [58] and so is unlikely to be rate limiting. Furthermore, the distribution of C-S-H is quite homogeneous on the surface of all the particles. If diffusion was critical we would expect that quartz surface close to the cement grains have more nucleation sites and faster growth of C-S-H which is not observed. Mechanical reasons seem more plausible.

To investigate the mechanical reason related to the distance between particles, we used two mixes with a short (70% Quartz 4 μm leads to distance of 0.08 μm) and a larger mean distance (cement paste leads to distance of 0.25 μm) The results presented in Figure 3.18 show that the mechanical action of the mixing affects more the cement paste where there is a small distance between particles. In the paste where particle are closer, the impact of the shearing is much more important than in the cement paste.

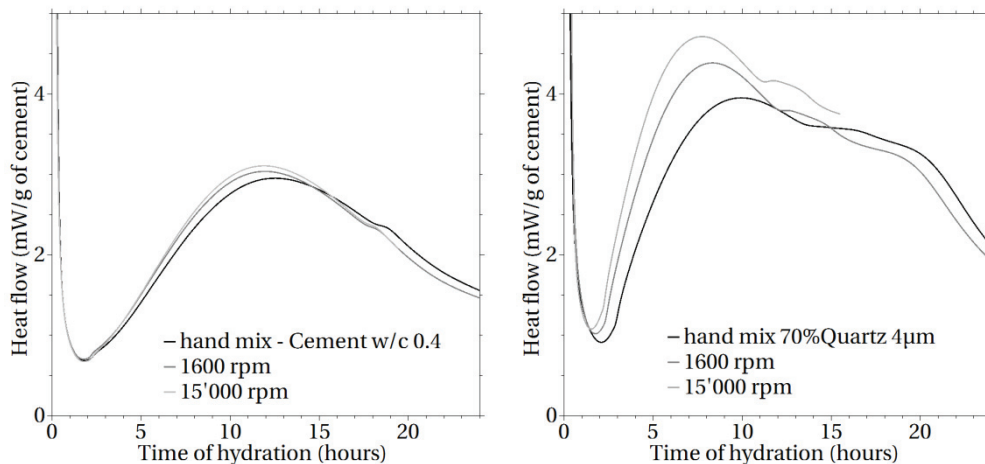


Figure 3.181: Effect of mixing speed on (left) cement pastes w/c 0.4 (right) 70% quartz of 4 μm

3.4. Shearing effect on microstructure and kinetics

Results on the both mixing and distance between particles suggest that the shearing during the mixing significantly influences the acceleration period. In this section we investigate further this effect on the microstructure.

Figure 3.19 shows the impact of increasing the shearing conditions. When cement is mixed as a mortar, the coarse sand particles increase the shearing condition during the mix. The total surface available for nucleation does not change much as the sand is too coarse to make a significant difference in the relative surface for heterogeneous nucleation [39]. However it can be seen in Figure 3.19 that the acceleration rate is significantly enhanced compared to cement paste. In fact, the increase in slope going from a paste to a mortar is as much as produced by the introduction of the quartz filler. This suggests that the shearing conditions in the mortar are similar to those in the quartz-cement paste.

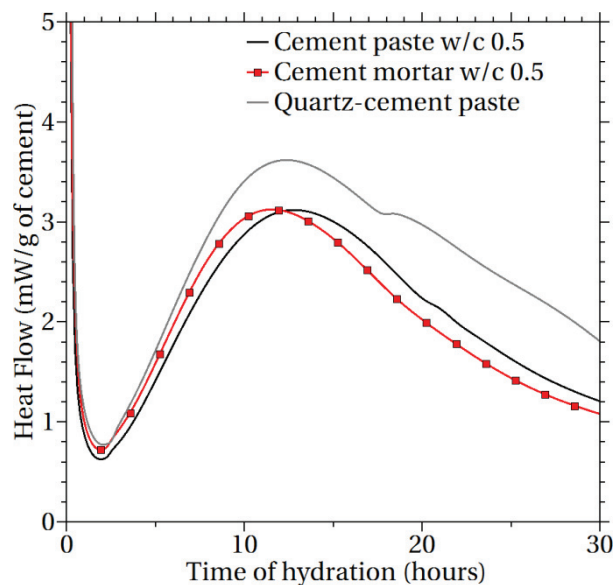


Figure 3.19: Effect of mortar on kinetics

Microscopic observations shown in Figure 3.20 reveal that in mortar the number of growth sites is increased. Figure 3.20(a) shows the surface of a cement grain in cement paste at 4 hours of hydration. C-S-H forms bushes distributed on the smooth surface at regular distances from each other. Ettringite crystals are also visible. In the mortar (see Figure 3.20(b)) the cement surface shows similar hydrates, mainly C-S-H and ettringite. However, here the surface is covered by many C-S-H at early stage and individual C-S-H needles everywhere. This indicates that increasing shearing generates more growing sites on the cement surface. This effect was also suggested by Juilland [19] to explain the denser microstructure in paste mixed in high shearing conditions.

The cement surface in the quartz-cement paste Figure 3.20(c) is seen to have a similar microstructure to the cement mortar Figure 3.20(b): C-S-H at different growing stage are distributed everywhere on the surface. This suggests that the introduction of quartz also increases shearing, which can result from the

reduction of the space between particles. Kinetics results and microstructural observations are in good agreement. Mortar and quartz-cement paste have a similar number of growing sites and comparable acceleration slopes. This illustrates well the relation between the nucleation density of C-S-H and the kinetics of the acceleration period.

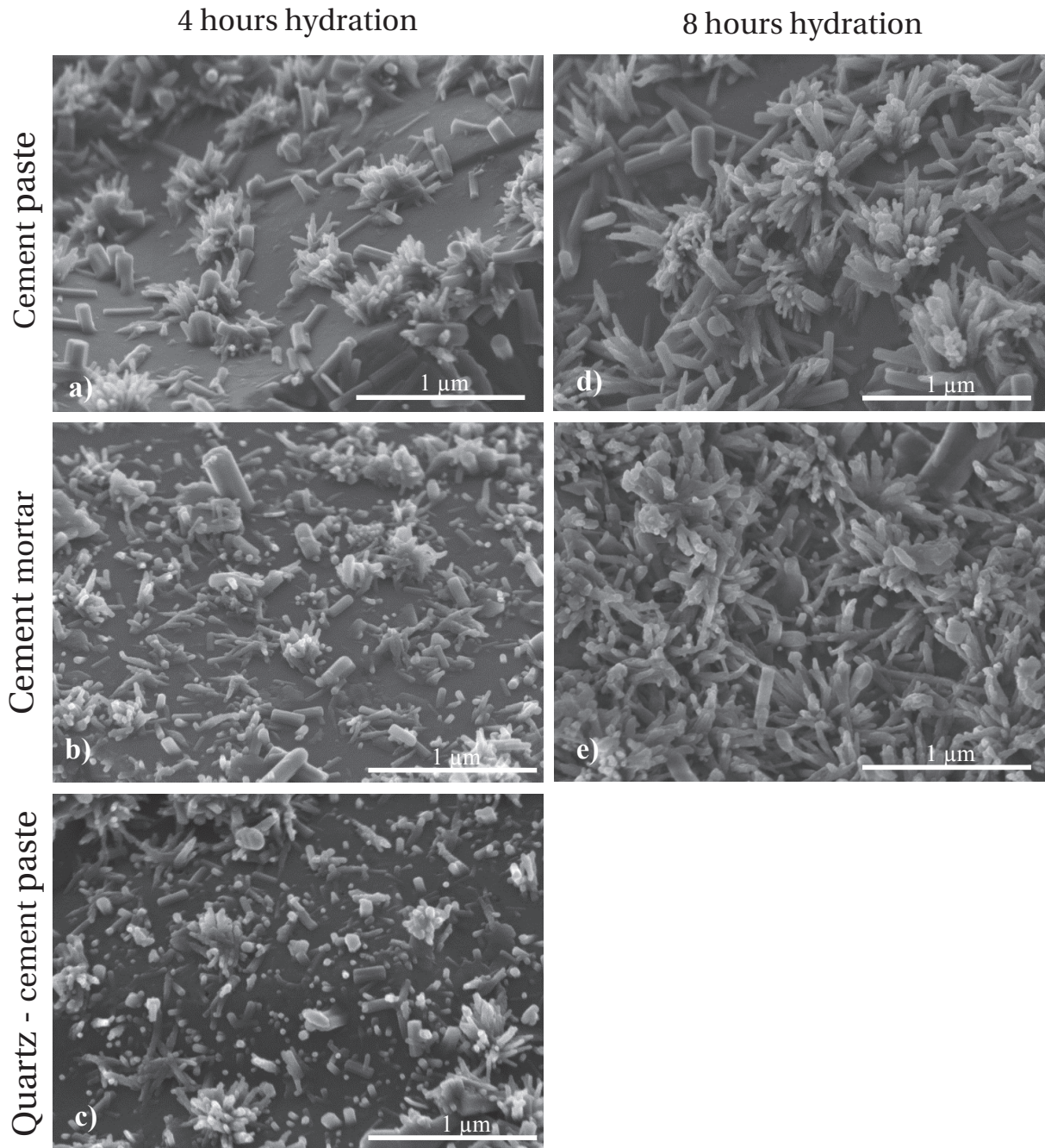


Figure 3.20: Micrographs of cement paste a) at 4 hours d) at 8 hours, cement mortar b) at 4 hours e) at 8 hours and quartz-cement paste c) at 4 hours

3.4.1. Shear rate calculation

We need to estimate the shear rate induced between the particles during the mixing procedure to demonstrate the effect of shearing on the kinetics. Within a reasonable approximation the mixing procedure is a simple shear case in laminar state.

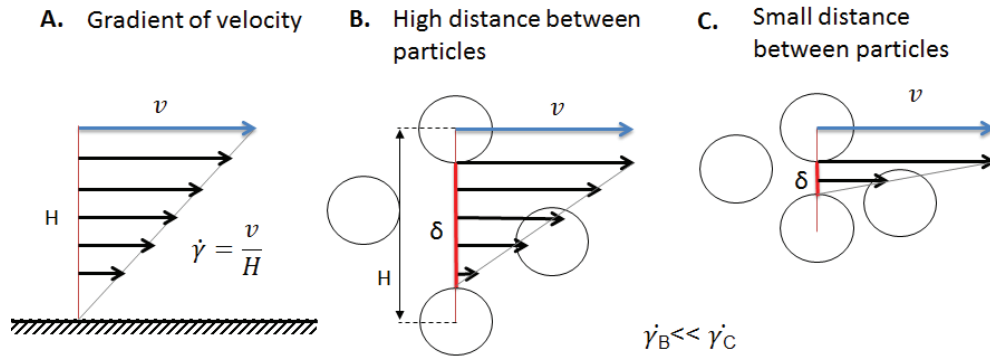


Figure 3.21: Simplistic scheme of the shear between two particles

In the case of simple shear (Figure 3.21.A.) two planes are parallel; one is moving the other is fixed. A gradient of velocity which defines a shear rate is applied in the distance which separates the two planes. In the case of paste, the planes are the grains of cement or quartz. The distance between the surfaces of the particles is δ rather than H , the distance between particle centers (Figure 3.21.B). The same shear rate is thus applied to a reduced distance which is the gap between the surfaces of the particles (figure 3.21.C). This can be translated by the following equation [59]:

$$\dot{\gamma}_{gap} = \dot{\gamma}_{ref} \frac{H}{\delta}$$

Where $\dot{\gamma}_{ref}$ is the shear rate induced by the mixing speed, 1600 rpm and 15000rpm produces respectively a shear rate of 335 s^{-1} from

$$\dot{\gamma}_{ref} = 2 \times (rpm \times 2\pi) \times \frac{R_1^2}{R_1^2 - R_2^2}$$

R_1 is the distance between the center of blade and the edge of the container. R_2 is the radius of the blade; H is the distance center to center between particles and δ is the mean distance between particles.

Figure 3.22 shows the relation between the slope value and the shear rate calculated between the grains. Our results describe a master curve which clearly shows that the slope value is increased as the shear rate produced in the gap between the particles increases.

The shear rate was increased in the sample with increasing the mixing rate from 1600 rpm to 15000 rpm that leads to respectively a shear rate of 335 s^{-1} and 3150 s^{-1} .

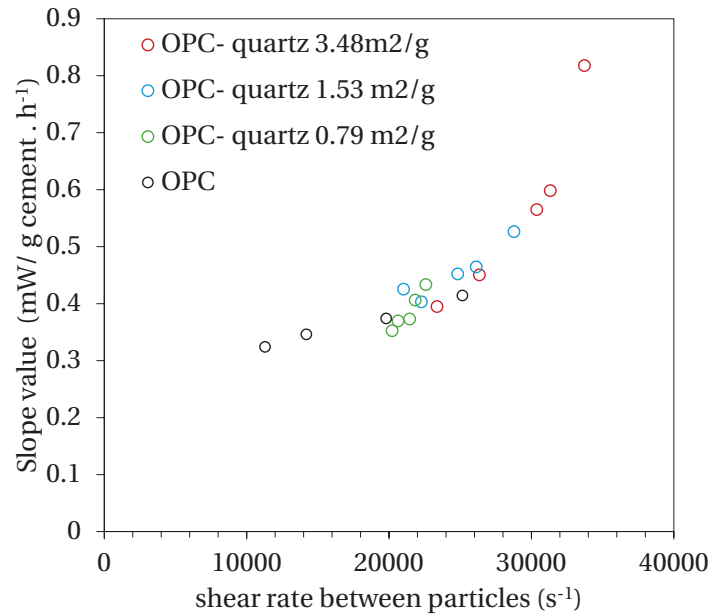


Figure 3.22: Slope value as a function of the estimated shear rate between the particles

3.5. Effect of common SCMs

The first part of this work was done with quartz as inert material. In this section we consider the filler effect of common SCMs (Slag, fly ash and limestone). We want to understand:

- Does SCM have a similar filler effect than quartz?
- Is there any effect of the chemical composition of the surface of the SCMs?

3.5.1. Slag and siliceous fly ash

Most commonly used SCMs are less reactive than cement. Figure 3.23 shows the kinetics of the hydration of the pastes with 40% substitution of plain cement by two slags and one fly ash in turn compared to the substitution of quartz at same level. All the curves are very similar to the quartz cement curve for the first 24 hours. This indicates that SCM particles are inert and have no impact on kinetics over this period.

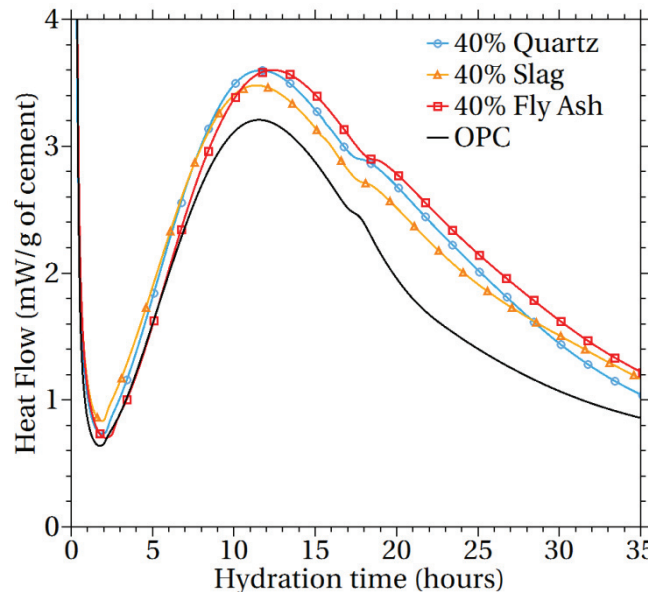


Figure 3.23: Calorimetry curves of blended cements with fly ash, slag and quartz

Microstructure in slag-cement systems

Figure 3.24 shows the BSE image of slag and cement grains. The chemical contrast of the two materials (i.e. slag and cement) is very similar and does not allow distinction between the grains. Thus, we cannot compare the development of the microstructure on the two surfaces. However, as it can be seen on Figure 3.25 the hydrates growing on random surfaces are similar to the microstructure found in quartz-cement system. This confirms that slag behaves like quartz at early age.

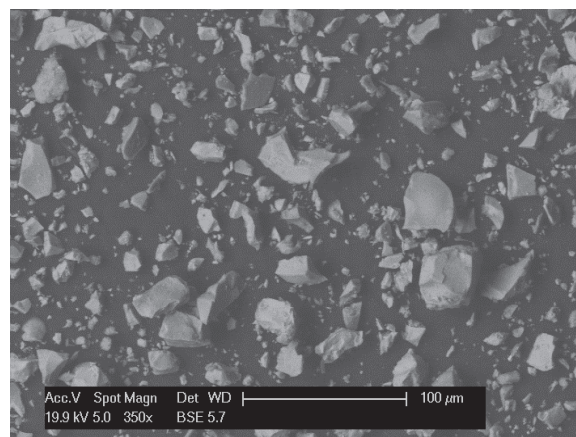


Figure 3.24: BSE image of slag-cement. The chemical contrast is very similar between the two materials.

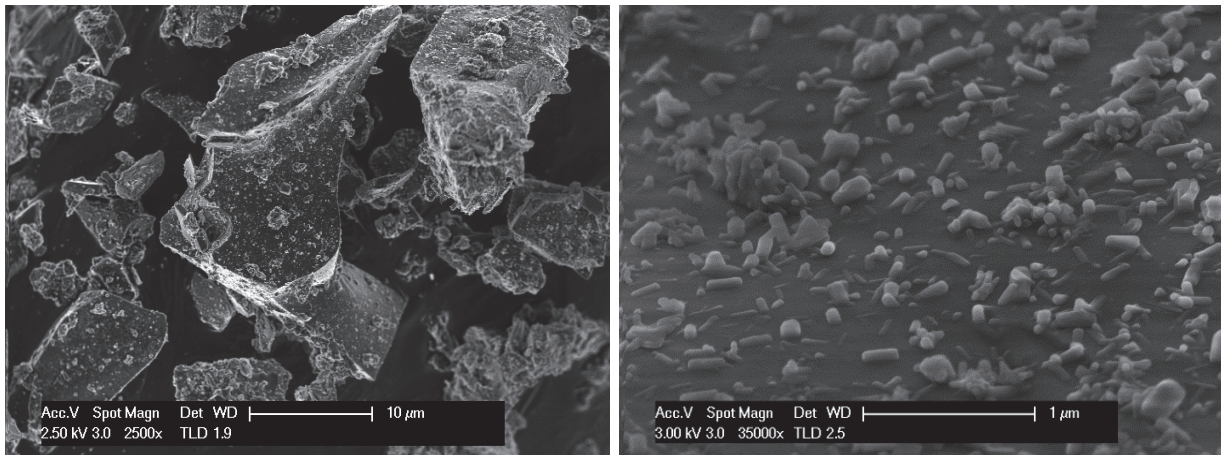


Figure 3.25: Grains from slag-cement pastes. On the left, detail of a representative surface

Microstructure in fly ash – cement system

Figure 3.26 show the development of the microstructure in fly ash- cement paste. On both cement and fly ash surface, the hydrates forming and their morphology are very similar and equivalent to those found in quartz-cement system. The structure might appear slightly coarse compare to the delicate C-S-H needles observed in quartz-cement paste. Actually this is due to the thicker carbon coating required for a good observation of the fly ash spheres.

At 7 hours of hydration (Figure 3.26 e and f), the surfaces are almost completely covered by hydrates, mainly C-S-H. The typical sea-anemone structure is clearly identified. From this set of micrographs the chemistry of the fly ash surface does not seem to have any impact on the microstructure development.

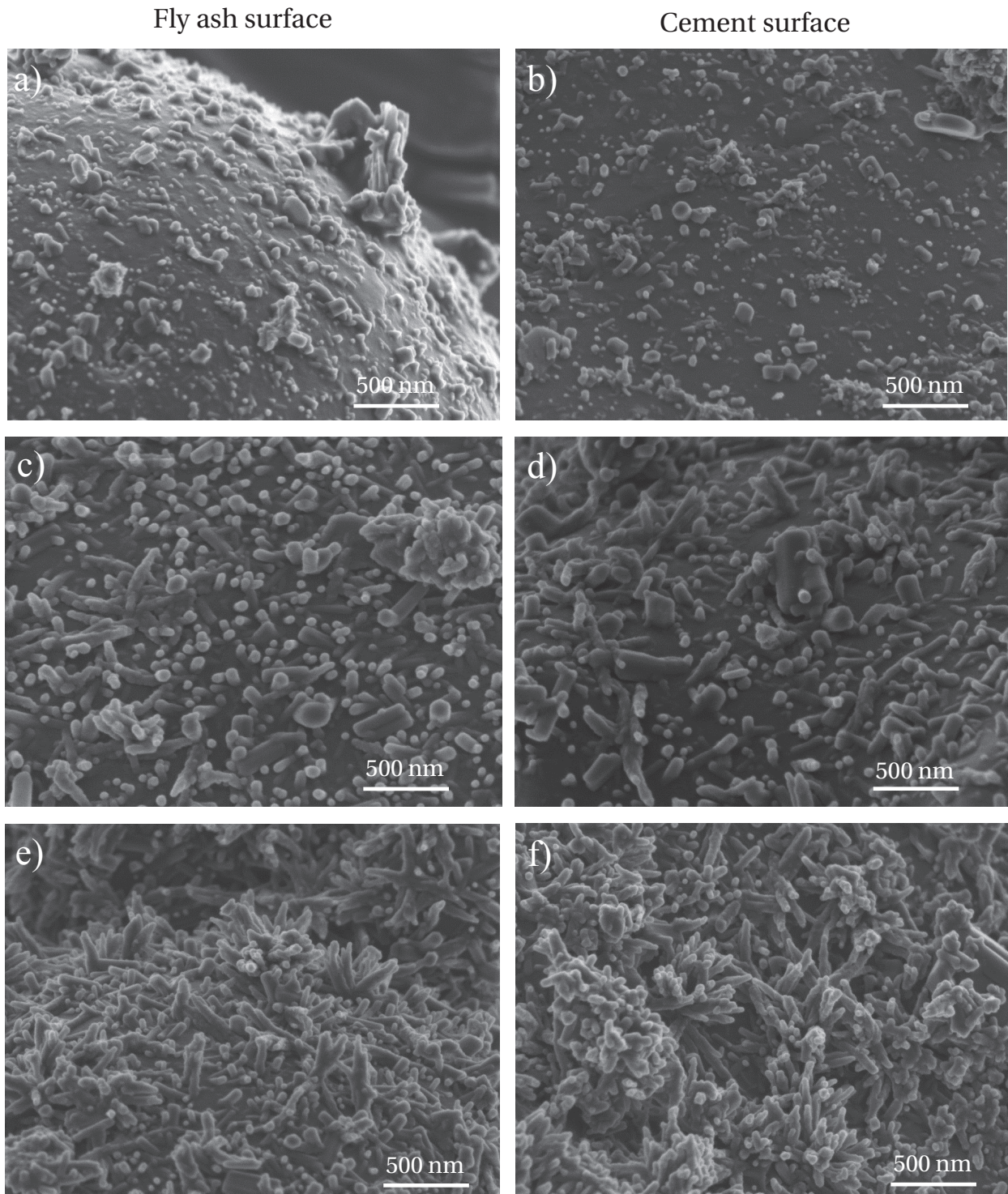


Figure 3.26: Micrograph of Fly ash cement systems a) and b) at 2 hours on c) and d) at 5 hours e) and f) 7 hours

Filler effect of slag and quartz on the kinetics

Figure 3.27 shows the slope of the acceleration period as a function of the shear rate between the particles for the substitution of the slags and the fly ash at different levels. It can be seen that all these systems follow the same trend as for quartz. When the surface of SCM is increased, the slope is raised. This relationship confirms the key role of the shearing at the mixing stage in blended systems.

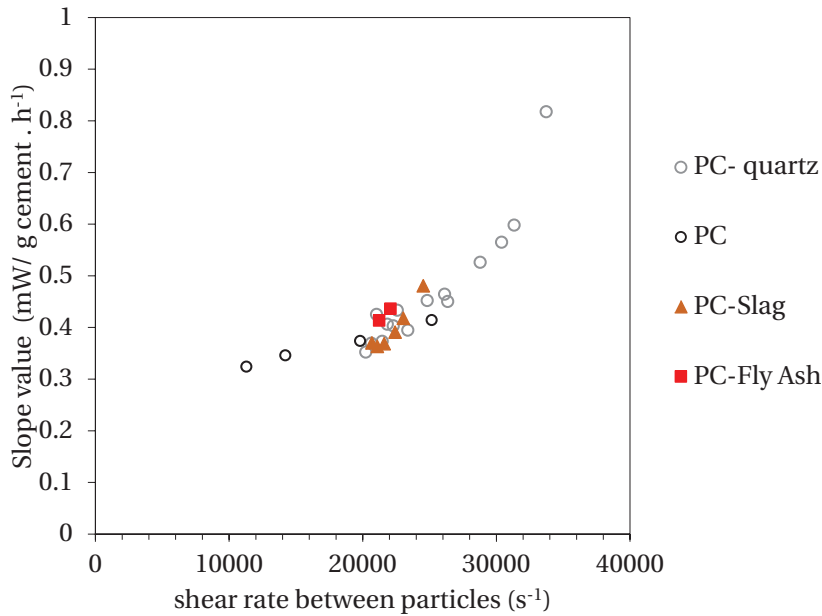


Figure 3.27: Slope value as a function of the shear rate between the particles

3.5.2. Limestone

Figure 3.28 shows the calorimetry curves of limestone-cement pastes. We can already notice that limestone has a different behavior than the other particles.

Compared to quartz-cement paste, the acceleration is higher and also the induction period is shortened. This means that the supersaturation is reached faster in the limestone system, probably because limestone dissolve slightly and release calcium ions [60]. This hypothesis is strongly supported by the higher concentration of calcium measured during the induction period in the limestone pastes compared to the reference with quartz (Table 3.3) and the TGA data (Figure 3.29) .

Table 3.3: Concentration of calcium during induction period in limestone-cement and quartz-cement paste

Induction period	[Ca] (mg/L)
OPC + 40% Limestone 15 μm	624
OPC + 40% Limestone 2 μm	630
OPC + 40% Quartz 13 μm	596

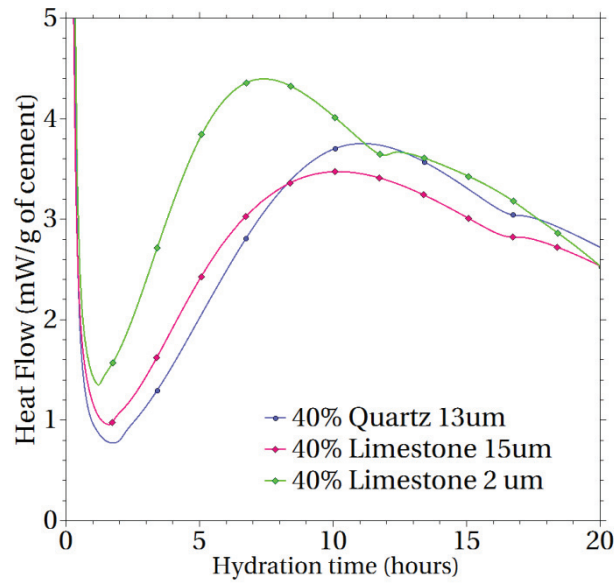


Figure 3.28: Calorimetry curves of limestone-cement pastes compared to quartz-cement

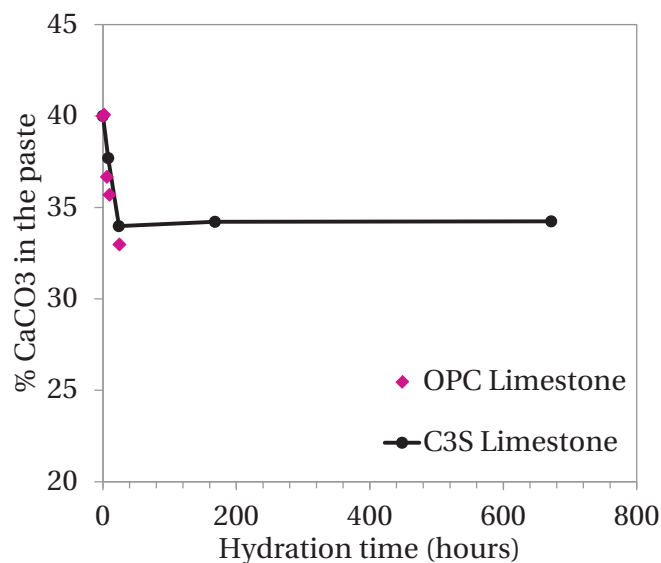


Figure 3.29: CaCO_3 content in OPC Limestone paste and C_3S Limestone paste. In both systems the limestone is dissolving (15%) in the first hours of hydration

Microstructure of limestone-cement blend

The micrographs in Figure 3.3 clearly show that limestone has a different effect on the nucleation of C-S-H compared to the previously observed SCMs (slag and fly ash).

After 5 minutes the limestone (Figure 3.30.a) and cement surfaces are similar (Figure 3.30.b)).

After 90 minutes, which corresponds to the end of the induction period (Figure 3.28), the limestone surface is completely covered with C-S-H at early age forming small particles (Figure 3.30.b)). This was

not observed for quartz or the other SCMs. At this stage, in the same sample, the cement grains have only a few dispersed growing first C-S-H. This microstructural observation indicates that C-S-H nucleates preferentially on limestone surface.

Figure 3.30.c) shows a limestone grain after 5 hours. C-S-H needles are growing densely perpendicular to the surface while the C-S-H on the cement grains shows the same divergent sea anemone morphology seen previously. In Figure 3.31 which shows limestone surface in C_3S -limestone system, it seems that the C-S-H are aligned along a certain direction meaning that limestone surface might provide a templating effect.

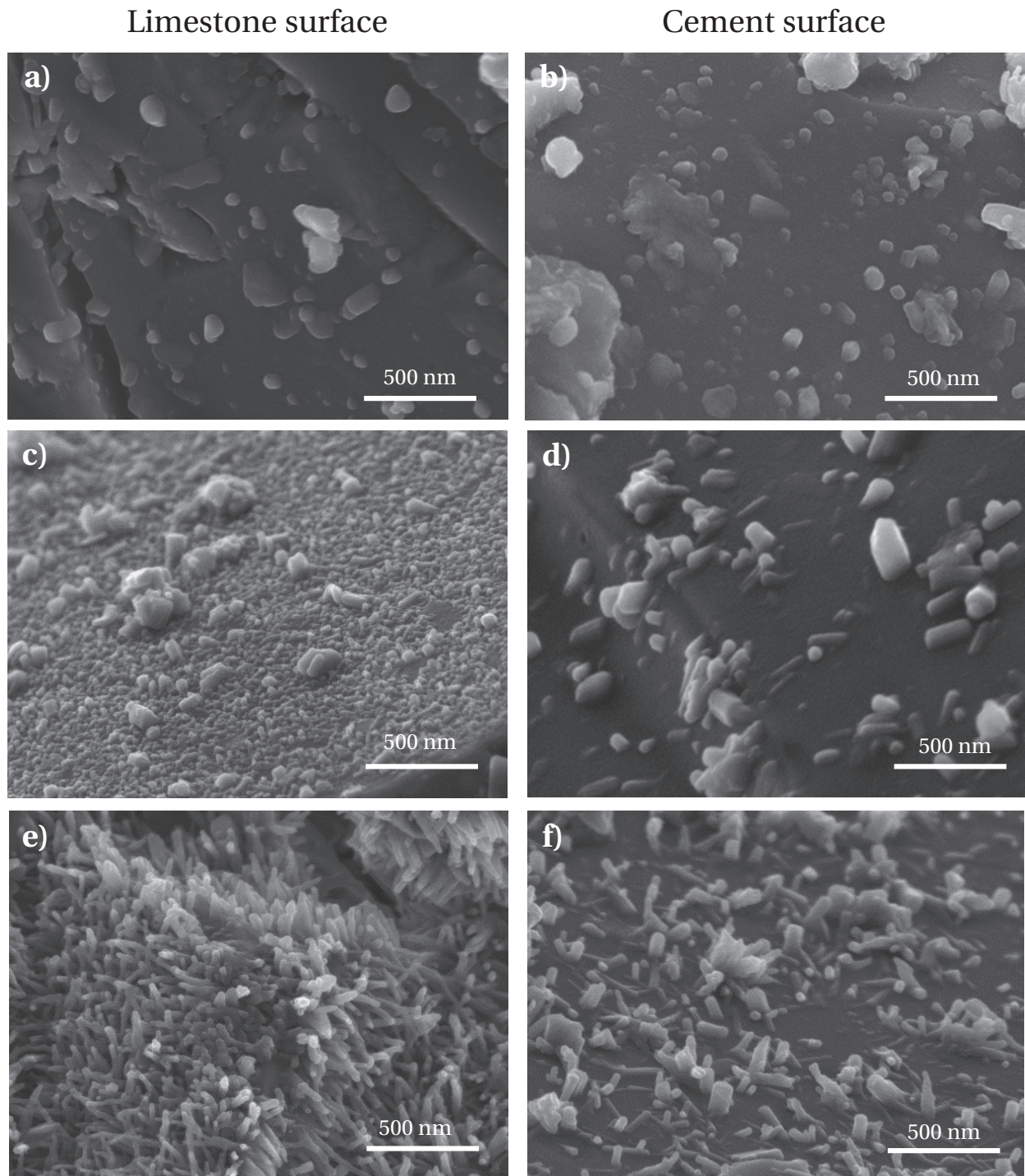


Figure 3.30: Micrographs in limestone PC paste. Limestone surface at a) 5 min c) 1 hour e) 5 hours and cement surface at b) 5 min d) 1 hour and f) 5 hours

The length of the C-S-H needles on both the cement and limestone surface seems similar. These observations are complemented by TEM images of a limestone- C_3S paste in Figure 3.31 from Amelie Bazzoni [61]. Unlike SEM micrographs, TEM images display the cross section of the sample. This makes it easier to compare the length of the C-S-H on the grains. Figure 3.31 shows the grains of C_3S and limestone at the time where the maximum heat flow is reached (~10 hours). The different morphology

of the C-S-H is clearly identified: individual needles perpendicular to the surface on limestone grains and different orientation of growth on C_3S grains. However, the length of the C-S-H needles is the same on both C_3S and limestone grains (about 300nm). Therefore, it appears that, limestone favors the nucleation of C-S-H while the growth rate on limestone and C_3S is similar. The observations in this limestone- C_3S system also rule out any role of aluminate in the higher nucleation on the limestone surface.

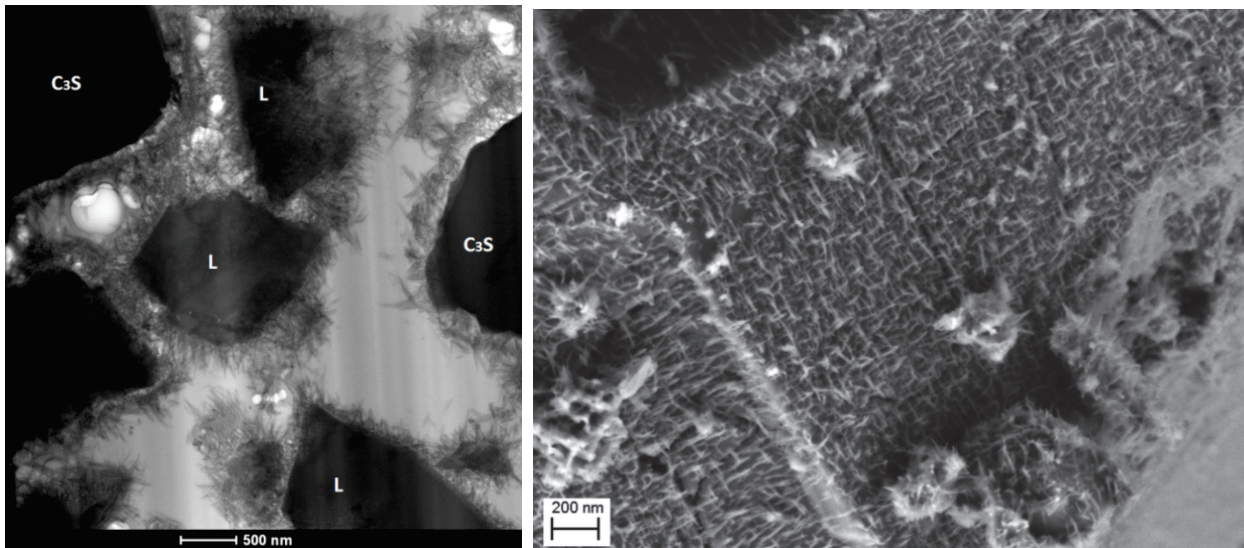


Figure 3.31: (left) TEM in bright field mode of limestone- C_3S paste at 10 hours of hydration. (right) SEM limestone in C_3S -limestone system. From A. Bazzoni [61]

Filler effect of limestone on kinetics

The points relating to the limestone systems shown in Figure 3.32 make it clear that limestone powders do not have the same filler effect as quartz, slag and fly ash. The efficiency of the surface of limestone for nucleation of C-S-H seems higher as the slope increases more than for quartz when the amount of surface provided is increased. The micrographs of limestone in Figure 3.29 indicated that there is a much higher density of first formed C-S-H on limestone surfaces than on cement. Consequently limestone has a larger accelerating effect on the hydration due to the high number of nucleation sites growing while the growth rate of individual needles on limestone seems not to be changed.

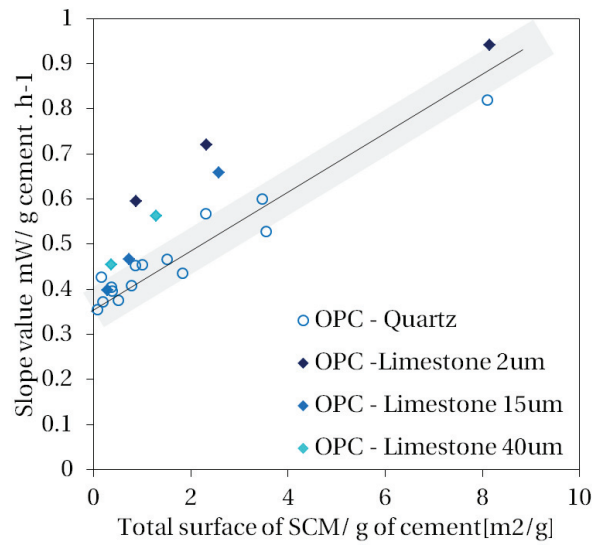


Figure 3.32: Slope value as a function of the total surface of limestone. The data does not fit the same trend than other fillers

Figure 3.33 shows the slope of the acceleration period as a function of normalized shear for the substitution of the slags, the fly ash, the limestone at different replacement levels. Compared to the others powders (quartz, fly ash, slag), the limestone does not fit the general trend.

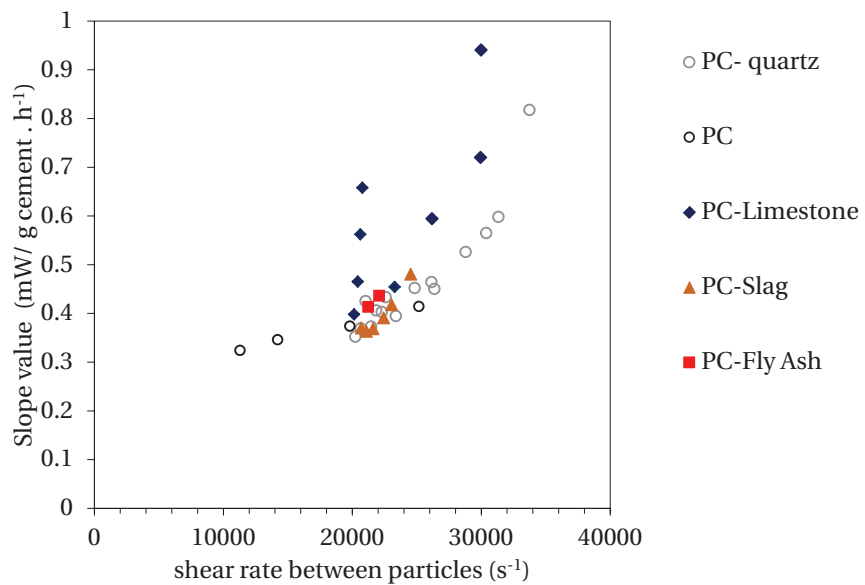


Figure 3.33: Effect of the shear rate between SCM particles on the slope value

Discussion on the effect of limestone and nucleation of C-S-H

Despite the wide use of limestone in cement production, its effect at early age did not attract so much attention. However our results show a high potential to increase the C-S-H nucleation.

- However it is also possible that Portlandite is first formed. As it can be seen in Figure 3.34 many CH crystal are observed on the limestone surface at the induction period. The presence of CH at this stage is not so marked in other systems studied. In the light of the recent work of Galmarini, CH crystal could catalyze the nucleation of C-S-H near the limestone surface[11]. Indeed, the calcium-silicate complex formed at the CH surface might be able to integrate silicate dimers and form C-S-H.

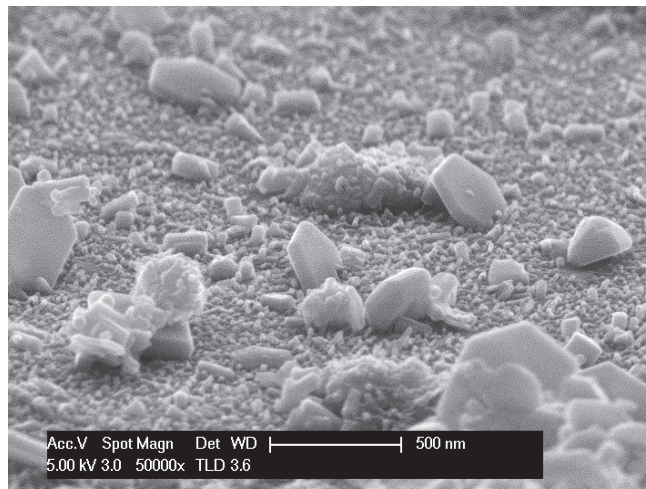


Figure 3.34: Limestone surface at 1h30. CH crystals are observed on the limestone surface at this stage.

- The visible alignment of C-S-H on limestone surface seems to indicate that there might also be a crystallographic effect. The micrograph in Figure 3.35, shows an alignment of the C-S-H along certain directions depending of the orientation of the surface. This seems to indicate that the atomistic configuration at the surface influences the growth morphology of the C-S-H.

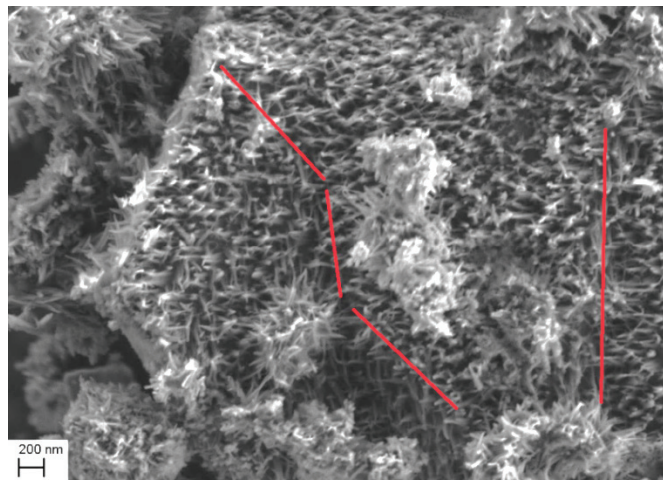


Figure 3.35: Limestone surface at the main peak. Different orientations of C-S-H are observed.

The arrangement of the atoms on the calcite surface might provide a “templating” effect which facilitates the nucleation of C-S-H.

The cleavage plane (101.4) of calcite contains both Ca^{+2} and CO_3^{-2} ions (see Figure 3.36) making the surface neutral with a low surface energy. This surface plane is always terminated by oxygen atoms. A recent study revealed that the polymorphs of CaCO_3 have different effect on the C-S-H nucleation[62]. Aragonite had no significant effect compared to calcite. In aqueous solution aragonite and calcite present different atom arrangement. The calcite surface is terminated by hydrogen [63] forming OH group, whereas the aragonite face is only terminated with calcium ions (Figure 3.37). This suggests that the strong OH bond on the calcite surface might catalyze or participate to the formation of C-S-H (or CH?) nuclei.

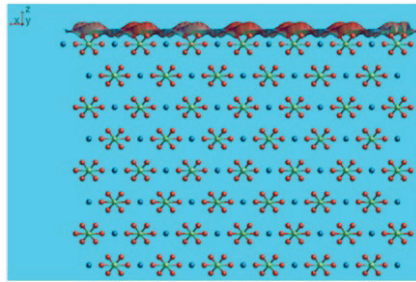


Figure 3.36: $(10\bar{1}4)$ surface of calcite not polar Blue atoms are Calcium, Green atoms are Carbon and Red are Oxygen. From Sekkal [64]

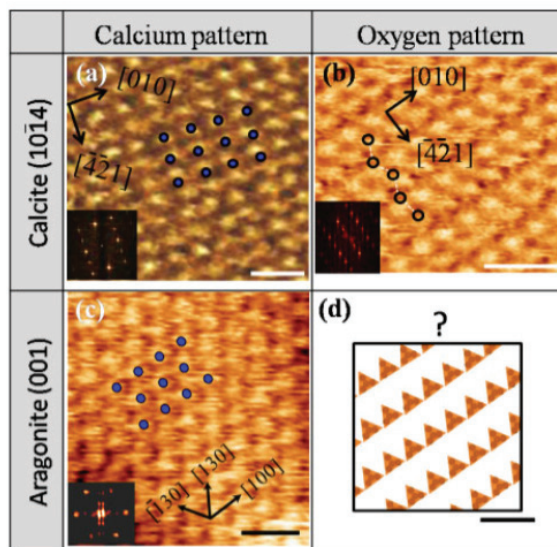


Figure 3.37: Comparison of atomically-resolved and Fourier-transformed images of calcite cleavage $(10\bar{1}4)$ and aragonite (001) faces. On calcite cleavage plane (a) latticed calcium layer (blue dot is a calcium atom) and (b) oxygen pattern. In aragonite (c) only calcium layer was observed (d) predicted image of oxygen pattern. No oxygen atoms are found when aragonite is in water. From Araki[65]

The structure of the C-S-H nuclei forming at very early age is not well established. If we consider whether the Tobermorite structure or the Jennite structure [66], in each case hydroxyl group is involved in the structure. It respectively bounds with silicate or calcium. From AFM data calcite surface is terminated by strong OH bound when immersed in water. Whereas the surface of cement, quartz or SCM are more susceptible to have weak OH bond (e.g. hydrolysis) which causes the dissolution of these materials. Therefore we can suppose that the OH group might play a role in the pre-nucleation of C-S-H.

4. Summary

This chapter reports on the filler effect during the acceleration period of the cement hydration.

- The kinetics and the development of the microstructure were studied in blended systems with quartz or SCMs. Our results show that fillers do accelerate the hydration of the clinker component in a blend, but this effect cannot be simply explained by the provision of extra surfaces for nucleation as formerly suggested.
- Microscopic observations show the nucleation density and the morphology of C-S-H are very similar across cement and quartz surfaces. This confirms that C-S-H is forming by a heterogeneous nucleation and that the species are available everywhere in the pore solution. The morphology of C-S-H seems rather dependent of the chemical composition of the phase (alite or cement).
- The results support the hypothesis that the acceleration slope is related to the nucleation and growth of C-S-H. The slope was steeper when a large density of growing C-S-H was found. Nevertheless, quartz surfaces only enhance the acceleration slope by 20% which is much less efficient compared to the cement surfaces. This is quite contradictory to the microscopic observations which show that the nucleation density of C-S-H was similar on quartz and cement.
- The results show a clear relation between the inter-particle distance and the kinetics of the acceleration period. This can be explained by the shearing between particles which increases as the inter-particle distance decreases. This explanation is supported by observations on mortars, where shear is increased by the presence of large sand grains, but the surface provided for nucleation is almost unchanged. Furthermore, increasing the shear rate by changing the mixing speed has quantitatively the same effect on acceleration.
- There are several possible explanations as to why higher shear produces more nucleation sites. High shear may disturb the double layer surrounding the cement grains when they are dissolving, moving ions from this gradient of concentration and better dispersing them through the mix. Recent experiments [67] have indicated that when the mixing speed is too low, there is an accumulation of ionic species close to the C_3S grains which decreases the dissolution rate. Consequently fewer ions are found in the solution at low mixing speed. It is also possible that critical C-S-H nuclei forming during the mixing time can be dislodged and displaced onto the surface and the pore space, as suggested by Juilland et al. [19].
- The study of limestone indicates that additional factors operate here to give a much higher density of C-S-H growing sites on limestone surfaces. Consequently limestone has a larger accelerating effect on the hydration due to the high number of C-S-H growing sites while the growth rate of individual needles on limestone is not changed. The increased nucleation on limestone surfaces may be related to the dissolution of this phase, but also to a favorable surface structure, providing a “template” for C-S-H precipitation.

5. References

1. Kondo, R. and M. Daimon, *Early Hydration of Tricalcium Silicate: A Solid Reaction with Induction and Acceleration Periods*. Journal of the American Ceramic Society, 1969. **52**(9): p. 503-508.
2. Gartner, E., et al., *Hydration of Portland cement*. Structure and performance of cements, 2002. **13**: p. 978-0.
3. Scrivener, K., *The development of microstructure during the hydration of Portland cement*, in *Metallurgy and Materials Science*. 1984, Imperial College of Science and technology: London.
4. Thomas, J.J., et al., *Modeling and simulation of cement hydration kinetics and microstructure development*. Cement and Concrete Research, 2011. **41**(12): p. 1257-1278.
5. Bishnoi, S. and K.L. Scrivener, *Studying nucleation and growth kinetics of alite hydration using μic* . Cement and Concrete Research, 2009. **39**(10): p. 849-860.
6. Thomas, J.J., H.M. Jennings, and J.J. Chen, *Influence of Nucleation Seeding on the Hydration Mechanisms of Tricalcium Silicate and Cement*. The Journal of Physical Chemistry C, 2009. **113**(11): p. 4327-4334.
7. Thomas, J.J., *A new approach to modeling the nucleation and growth kinetics of tricalcium silicate hydration*. Journal of the American Ceramic Society, 2007. **90**(10): p. 3282-3288.
8. Garrault-Gauffinet, S. and A. Nonat, *Experimental investigation of calcium silicate hydrate (C-S-H) nucleation*. Journal of Crystal Growth, 1999. **200**(3-4): p. 565-574.
9. Nicoleau, L., *New calcium silicate hydrate network*. Transportation Research Record: Journal of the Transportation Research Board, 2010. **2142**(1): p. 42-51.
10. Galmarini, S., et al., *Changes in portlandite morphology with solvent composition: Atomistic simulations and experiment*. Cement and Concrete Research, 2011. **41**(12): p. 1330-1338.
11. Galmarini, S., *Atomistic Simulation of Cementitious Systems*, in *Faculté des sciences et techniques de l'ingénieur*. 2013, Ecole Polytechnique Fédérale de Lausanne: Lausanne.
12. Bullard, J.W., *Mechanisms of cement hydration*. Cement and Concrete Research, 2010.
13. Gartner, E.M., *A proposed mechanism for the growth of C-S-H during the hydration of tricalcium silicate*. Cement and Concrete Research, 1997. **27**(5): p. 665-672.
14. Jennings, H.M., *A model for the microstructure of calcium silicate hydrate in cement paste*. Cement and Concrete Research, 2000. **30**(1): p. 101-116.
15. Niederberger, M. and H. Cölfen, *Oriented attachment and mesocrystals: non-classical crystallization mechanisms based on nanoparticle assembly*. Physical Chemistry Chemical Physics, 2006. **8**(28): p. 3271-3287.
16. Wang, T., H. Cölfen, and M. Antonietti, *Nonclassical Crystallization: Mesocrystals and Morphology Change of CaCO₃ Crystals in the Presence of a Polyelectrolyte Additive*. Journal of the American Chemical Society, 2005. **127**(10): p. 3246-3247.
17. Brown, P.W., *Effects of Particle Size Distribution on the Kinetics of Hydration of Tricalcium Silicate*. Journal of the American Ceramic Society, 1989. **72**(10): p. 1829-1832.
18. Costoya, M., *Kinetics and microstructural investigation on the hydration of tricalcium silicate*. 2008, EPFL: Lausanne.
19. Juilland, P., et al., *Effect of mixing on the early hydration of alite and OPC systems*. Cement and Concrete Research, 2012. **42**(9): p. 1175-1188.
20. Dollimore, D. and R. Mangabhai, *Effect of mixing time on heat evolution pattern of cement pastes*. Thermochemica Acta, 1985. **85**: p. 223-226.
21. Gallucci, E., X. Zhang, and K.L. Scrivener, *Effect of temperature on the microstructure of calcium silicate hydrate (C-S-H)*. Cement and Concrete Research, 2013. **53**(0): p. 185-195.

22. Kjellsen, K.O. and R.J. Detwiler, *Reaction kinetics of portland cement mortars hydrated at different temperatures*. Cement and Concrete Research, 1992. **22**(1): p. 112-120.
23. Lothenbach, B., et al., *Effect of temperature on the pore solution, microstructure and hydration products of Portland cement pastes*. Cement and Concrete Research, 2007. **37**(4): p. 483-491.
24. Kada-Benameur, H., E. Wirquin, and B. Duthoit, *Determination of apparent activation energy of concrete by isothermal calorimetry*. Cement and Concrete Research, 2000. **30**(2): p. 301-305.
25. Cheung, J., et al., *Impact of admixtures on the hydration kinetics of Portland cement*. Cement and Concrete Research, 2011. **41**(12): p. 1289-1309.
26. Peterson, V.K. and M.C.G. Juenger, *Hydration of Tricalcium Silicate: Effects of CaCl₂ and Sucrose on Reaction Kinetics and Product Formation*. Chemistry of Materials, 2006. **18**(24): p. 5798-5804.
27. Riding, K., D.A. Silva, and K. Scrivener, *Early age strength enhancement of blended cement systems by CaCl₂ and diethanol-isopropanolamine*. Cement and Concrete Research, 2010. **40**(6): p. 935-946.
28. Juenger, M., et al., *A soft X-ray microscope investigation into the effects of calcium chloride on tricalcium silicate hydration*. Cement and Concrete Research, 2005. **35**(1): p. 19-25.
29. Garci Juenger, M.C. and H.M. Jennings, *New insights into the effects of sugar on the hydration and microstructure of cement pastes*. Cement and Concrete Research, 2002. **32**(3): p. 393-399.
30. Kurdowski, W. and W. Nocuń-Wczelik, *The tricalcium silicate hydration in the presence of active silica*. Cement and Concrete Research, 1983. **13**(3): p. 341-348.
31. Wu, *Early stage hydration of slag cement*. Cement and Concrete Research, 1983. **13**(2): p. 277-286.
32. Wu, Z.-Q. and J. Young, *The hydration of tricalcium silicate in the presence of colloidal silica*. Journal of Materials Science, 1984. **19**(11): p. 3477-3486.
33. Langan, B., K. Weng, and M. Ward, *Effect of silica fume and fly ash on heat of hydration of Portland cement*. Cement and Concrete Research, 2002. **32**(7): p. 1045-1051.
34. Poppe, A.-M. and G. De Schutter, *Cement hydration in the presence of high filler contents*. Cement and Concrete Research, 2005. **35**(12): p. 2290-2299.
35. Land, G. and D. Stephan, *The influence of nano-silica on the hydration of ordinary Portland cement*. Journal of Materials Science, 2012. **47**(2): p. 1011-1017.
36. Kadri, E.H., et al., *Combined effect of chemical nature and fineness of mineral powders on Portland cement hydration*. Materials and structures, 2010. **43**(5): p. 665-673.
37. Gutteridge, *Filler cement: the effect of the secondary component on the hydration of portland cement*. Cement and Concrete Research, 1990. **20**: p. 778-782.
38. Lothenbach, B., K. Scrivener, and R.D. Hooton, *Supplementary cementitious materials*. Cement and Concrete Research, 2011. **41**(12): p. 1244-1256.
39. Lawrence, P., M. Cyr, and E. Ringot, *Mineral admixtures in mortars: Effect of inert materials on short-term hydration*. Cement and Concrete Research, 2003. **33**(12): p. 1939-1947.
40. Moosberg-Bustnes, H., B. Lagerblad, and E. Forssberg, *The function of fillers in concrete*. Materials and structures, 2004. **37**(2): p. 74-81.
41. Korpa, A., T. Kowald, and R. Trettin, *Hydration behaviour, structure and morphology of hydration phases in advanced cement-based systems containing micro and nanoscale pozzolanic additives*. Cement and Concrete Research, 2008. **38**(7): p. 955-962.
42. Kadri, *Combined effect of chemical nature and fineness of mineral powders on Portland cement hydration*. Materials and structures, 2010. **43**: p. 665-673.
43. Oey, T., et al., *The Filler Effect: The Influence of Filler Content and Surface Area on Cementitious Reaction Rates*. Journal of the American Ceramic Society, 2013. **96**(6): p. 1978-1990.
44. Scherer, G.W., J. Zhang, and J.J. Thomas, *Nucleation and growth models for hydration of cement*. Cement and Concrete Research, 2012. **42**(7): p. 982-993.

45. Gutteridge, W.A. and J.A. Dalziel, *Filler cement: The effect of the secondary component on the hydration of Portland cement: Part I. A fine non-hydraulic filler*. Cement and Concrete Research, 1990. **20**(5): p. 778-782.
46. Sharma, R.L. and S.P. Pandey, *Influence of mineral additives on the hydration characteristics of ordinary Portland cement*. Cement and Concrete Research, 1999. **29**(9): p. 1525-1529.
47. Oey, T., et al., *The Filler Effect: The Influence of Filler Content and Surface Area on Cementitious Reaction Rates*. Journal of the American Ceramic Society, 2013.
48. Stark, J., B. Möser, and F. Bellmann, *Nucleation and growth of C-S-H phases on mineral admixtures* in *Advances in Construction Materials 2007*, C.U. Grosse, Editor. 2007, Springer Berlin Heidelberg. p. 531-538.
49. Makar, *Growth of cement hydration products on single-walled carbon nanotubes*. Journal of the American Ceramic Society, 2009. **92**: p. 1303-1310.
50. Gallucci, E. and K. Scrivener, *Crystallisation of calcium hydroxide in early age model and ordinary cementitious systems*. Cement and Concrete Research, 2007. **37**(4): p. 492-501.
51. Kjellsen, K.O. and H. Justnes, *Revisiting the microstructure of hydrated tricalcium silicate—a comparison to Portland cement*. Cement and Concrete Composites, 2004. **26**(8): p. 947-956.
52. Taylor, H.F., *Cement chemistry*. 1997: Thomas Telford.
53. Scrivener, K. and A. Nonat, *Hydration of cementitious materials, present and future*. Cement and Concrete Research, 2011. **41**: p. 651-665.
54. De Weerd, K., et al., *Fly ash–limestone ternary cements: effect of component fineness*. Advances in Cement Research, 2011. **23**(4): p. 203-214.
55. Roussel, N., et al., *Steady state flow of cement suspensions: A micromechanical state of the art*. Cement and Concrete Research, 2010. **40**(1): p. 77-84.
56. De Larrard, F., *Concrete mixture proportioning: a scientific approach*. 2005: CRC Press.
57. Hu, C. and F. de Larrard, *The rheology of fresh high-performance concrete*. Cement and Concrete Research, 1996. **26**(2): p. 283-294.
58. Bullard, J.W., *A Determination of Hydration Mechanisms for Tricalcium Silicate Using a Kinetic Cellular Automaton Model*. Journal of the American Ceramic Society, 2008. **91**(7): p. 2088-2097.
59. Flatt, R. 2014.
60. Juilland, P., et al., *Dissolution theory applied to the induction period in alite hydration*. Cement and Concrete Research, 2010. **40**(6): p. 831-844.
61. Bazzoni, A., *Study early hydration mechanisms of cement by mean of electron microscopy*, in *LMC*. 2014, Ecole Polytechnique Fédérale de Lausanne: Lausanne.
62. Bentz, D.P.A., A; Barrett, T; Jones, S.Z; , *Multi-Scale Investigation of the Performance of Limestone in Concrete*. submitted in Construction and Building Material, 2014.
63. de Leeuw, N.H. and S.C. Parker, *Surface structure and morphology of calcium carbonate polymorphs calcite, aragonite, and vaterite: an atomistic approach*. The Journal of Physical Chemistry B, 1998. **102**(16): p. 2914-2922.
64. Sekkal, W. and A. Zaoui, *Nanoscale analysis of the morphology and surface stability of calcium carbonate polymorphs*. Scientific reports, 2013. **3**.
65. Araki, Y., et al., *Atomic-Resolution Imaging of Aragonite (001) Surface in Water by Frequency Modulation Atomic Force Microscopy*. Japanese Journal of Applied Physics, 2012. **51**(8S3): p. 08KB09.
66. Richardson, I.G., *Tobermorite/jennite- and tobermorite/calcium hydroxide-based models for the structure of C-S-H: applicability to hardened pastes of tricalcium silicate, β -dicalcium silicate, Portland cement, and blends of Portland cement with blast-furnace slag, metakaolin, or silica fume*. Cement and Concrete Research, 2004. **34**(9): p. 1733-1777.
67. Nicoleau, L., A. Nonat, and D. Perrey, *The di- and tricalcium silicate dissolutions*. Cement and Concrete Research, 2013. **47**(0): p. 14-30.

Chapter 4

Factors affecting the second aluminate reaction

During the deceleration period two main reactions overlap: the silicate reaction and the second aluminate dissolution. This chapter focuses on the second aluminate reaction. In blended systems the second reaction of C_3A is strongly affected by the SCM replacement. The reasons for these changes are yet not well understood despite the importance of this reaction for the development of mechanical strength.

The objective of this chapter is to investigate:

- what is controlling the reaction of C_3A at this stage?
- why does filler enhance this reaction?
- what is the impact of sulfate on C-S-H?

1. Literature review	68
1.1. The second aluminate dissolution in cement paste	68
1.2. Interaction between sulfate and C-S-H	70
1.3. Effect of SCMs on the second C_3A reaction	72
2. Mixes studied	73
3. Results	74
3.1. Control of C_3A reaction by gypsum	74
3.3. Effect of gypsum depletion on C-S-H	79
3.4. Discussion on the effect of gypsum on C-S-H	83
4. Summary	85
5. References	86

1. Literature review

The main peak of hydration in the calorimetry curve is mainly attributed to the silicate reaction. Figure 4.1 compares alite curve which corresponds to the silicate reaction and Portland cement curve. A small additional peak is visible at about 16 hours on the PC. This peak has been identified as the second dissolution of the aluminate (C_3A) [1-3].

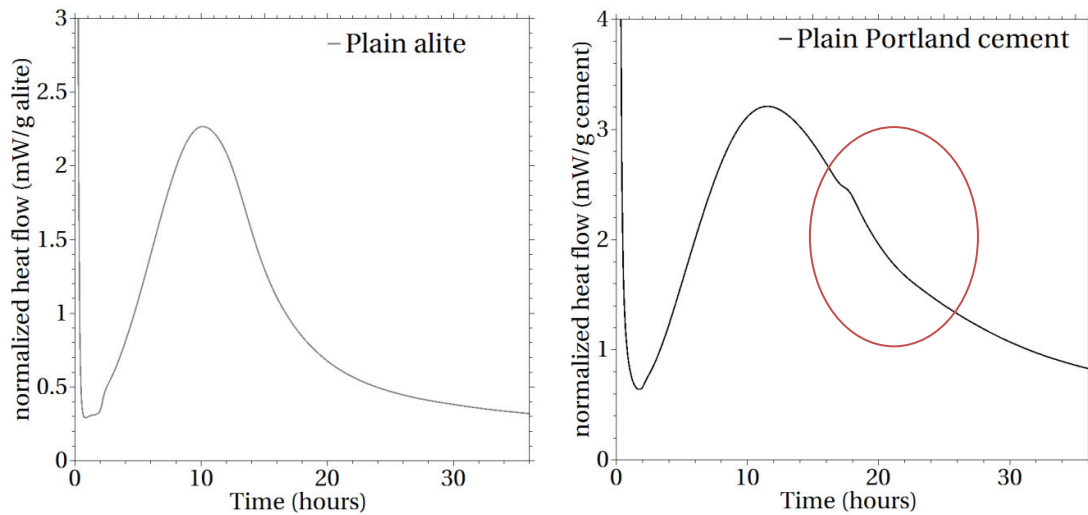


Figure 4.1: Comparison of the calorimetry curves of alite (left) and Portland cement (right). A small additional peak is visible in the PC curve which corresponds to the second dissolution of the aluminate phase

1.1. The second C_3A dissolution in cement paste

It has been shown in several works that the small peak during the deceleration period corresponds in PC to the second C_3A dissolution. XRD measurements in Figure 4.2 indicates that the C_3A phase starts to dissolve right at the beginning of the contact with water and then stops for a certain period before restarting at the time of this small peak.

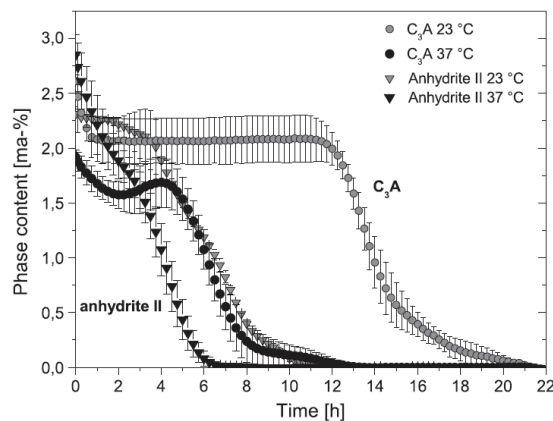


Figure 4.2: The renewal of C_3A dissolution at $20^\circ C$ corresponds to the anhydrite depletion. From Hesse et al.[3]

Several theories have been suggested to explain the retardation of the C_3A dissolution. The first hypothesis was that the C_3A is surrounded by a protective membrane, usually reported as ettringite[4, 5]. Many works have disproved this theory [1, 3, 6, 7] and suggested that the adsorption of sulfate on C_3A is rather the retardation mechanism. It is still not clear where the sulfate is adsorbed, probably on coordination sites which would be occupied by H or OH group in absence of sulfate[8, 9].

The content of sulfate in the pore solution decreases with hydration time[10]. Figure 4.3 shows the concentration of sulfate ions measured in the pore solution at early age. The formation of ettringite and the adsorption of sulfate ions on C-S-H are the main sources of sulfate consumption [2]. The amount of sulfate therefore decreases with hydration time as hydrates continue to form. A sudden decrease of SO_4^{2-} ions in the solution occurs after about 10 hours, as shown for example in the data from Rothstein in Figure 4.3. At this stage all the solid gypsum has been dissolved and the sulfate concentration in solution drops as the formation of ettringite is still ongoing and consumes sulfate which is not replaced[10, 11].

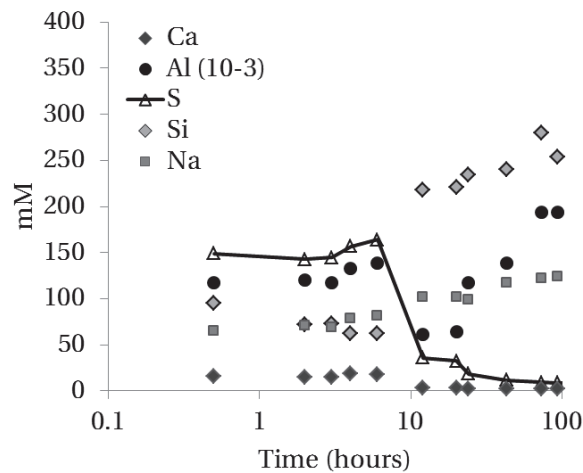


Figure 4.3: Concentrations in the pore solution in PC at w/c 0.35. Adapted from Rothstein[10]

The dosage of sulfate in the OPC is very important in practice. There is an optimum of sulfate with respect to the compressive strength which changes with the age of testing. Addition of gypsum beyond the optimum will also lead to a decrease in the strength at early ages, because the second aluminate reaction is delayed and the hydrates formed from this are not contributing to the strength [9, 12] (Figure 4.4). It is important that the aluminate reaction occurs during the deceleration period to contribute to the strength development by one day.

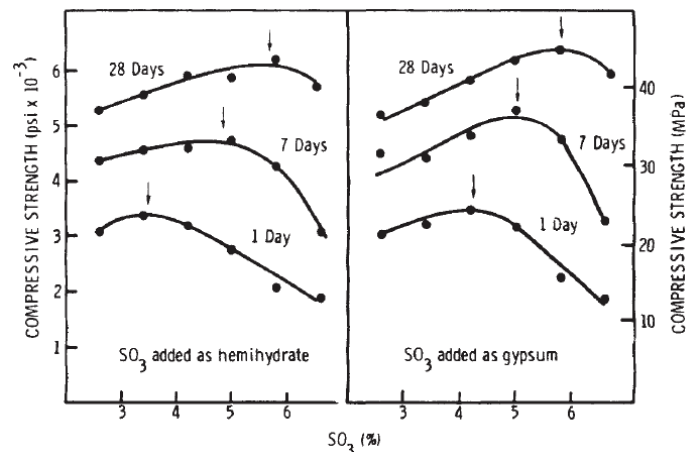


Figure 4.4: Optimal gypsum content on the mechanical strength. From Gartner[9]

The small peak on the calorimetry curve is often attributed to AFm formation. In pure C_3A system, this is the case. However in Portland cement, the peak comes from the high exothermic dissolution of the aluminate phase[13] and continued formation of ettringite using the sulfate previously adsorbed by the C-S-H [2, 3, 14].

1.2. Interaction between sulfate and C-S-H

Lerch[1] was the first to suggest an interaction between sulfate and C-S-H. Subsequently several studies have demonstrated that sulfates ions are able to be adsorbed on C-S-H [2, 15-17].

C-S-H structure

Calcium Silicate Hydrate (C-S-H) has a layered structure. Calcium sheets are bordered by silicate chains on either side and separated by an interlayer of water molecules or some mobile calcium ions. The silicate chains in C-S-H are formed of dimers linked with bridging Si tetrahedra. This configuration is called a “dreierketten structure”. Experiments and atomistic simulation have indicated that the 14Å Tobermorite is a good model for the C-S-H structure[18, 19].

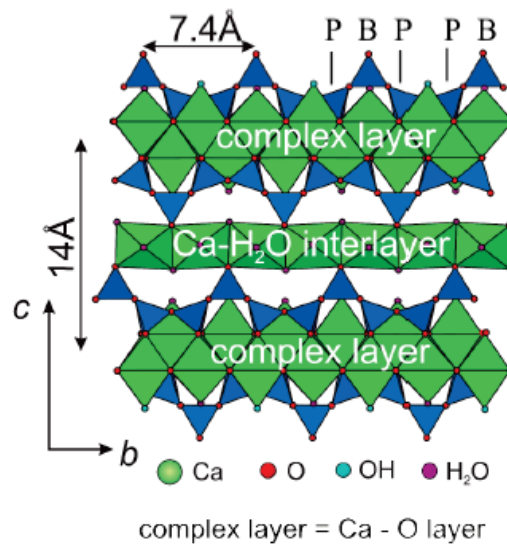


Figure 4.5: 14Å Tobermorite structure. From Garbev[20]

The surface of C-S-H is charged. The silicate tetrahedra end with an oxygen atom that forms a silanol group $\equiv\text{Si-OH}$. In the cement paste, a high pH is reached and leads to the deprotonation of the silanol group. Thus the surface of C-S-H becomes negatively charged.

Adsorption

Zeta potential experiments on C-S-H with increasing sulfate concentration in solution have shown that sulfate is adsorbed on the surface of C-S-H[16]. It has been shown that there is a coupled adsorption of sulfate and calcium ions [15, 21]. Figure 4.6 illustrates the complexation $\equiv\text{SiO}$ sites.

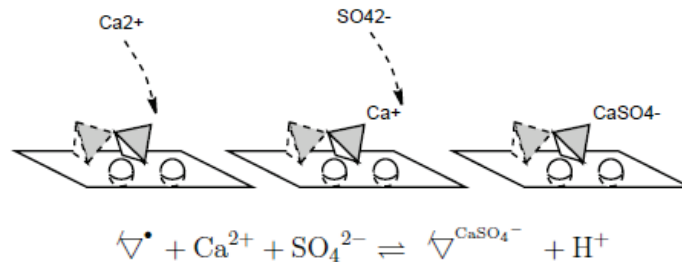


Figure 4.6: Mechanisms proposed by Barbarulo for sulfate adsorption on C-S-H surface sites [15]

The amount of sulfate was found by several workers to increase with the Ca/Si ratio of the C-S-H [15, 17, 22] which was supported by the Barbarulo model. This confirms that the sulfate does not incorporate in the atomic structure of the C-S-H unlike aluminum for instance. Sulfate is adsorbed on the surface sites of C-S-H and can be easily desorbed. Microanalysis on the C-S-H showed that the sulfate content measured as S/Ca ratio decreases during the deceleration period[2]. Thus sulfate ions desorb when the sulfate concentration in solution drops, due to the depletion of gypsum, and can form ettringite. Thus ettringite continues to precipitate despite the calcium sulfate being depleted [2, 3].

Microstructure

The similarity of the shape of the kinetics curves between systems with sulfate (PC) and without sulfate (alite or C_3S) indicates that the interaction of sulfate with C-S-H does not affect the mechanisms of the silicate hydration. Nevertheless several researchers have described changes of the microstructure between these systems [23, 24]. In presence of sulfates, Portlandite precipitates as hexagonal platelets[25]. The preferential growth of the [00.1] surface of Portlandite might be caused by the formation of a calcium-sulfate complex [26]. According to atomistic simulations, the growth on the [00.1] surface is controlled by the Ca concentration and the calcium-sulfate complex might decrease the calcium to hydroxide ratio in the solution that would favor its growth.

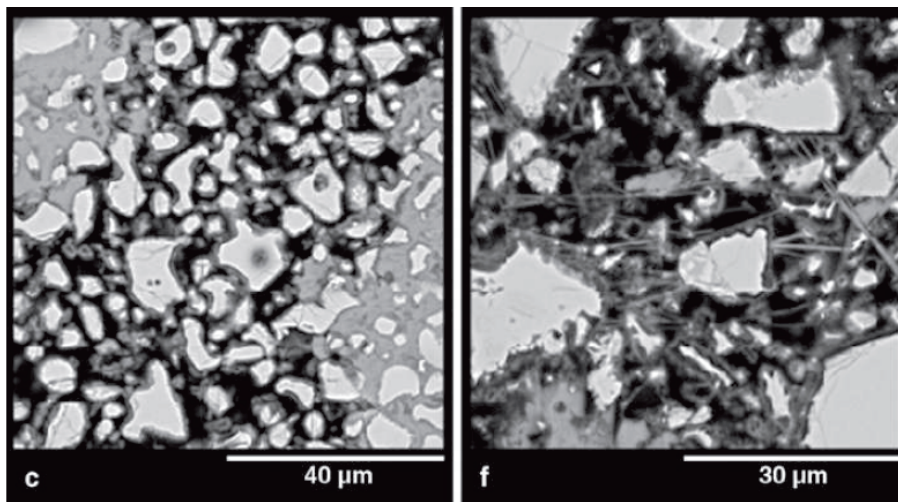


Figure 4.7: Microstructure at 16 hours of c) C_3S paste and f) PC. The presence of sulfates changes the microstructure. From Gallucci [23]

The impact of sulfates on the C-S-H morphology is rarely reported although several authors have suggested that calcium sulfate might change the growth of C-S-H [27-29]. The change of zeta potential of C-S-H might have consequences on the growth mechanism[21].

1.3. Effect of SCMs on the second reaction

In blended systems, the peak of the second C_3A dissolution has sometimes been considered as marking the beginning of the reaction of SCM [30-32]. Indeed, many authors observed that increasing the slag or other SCM addition lead to a more pronounced peak. Therefore they concluded that it was the results of the reaction of SCM. However this is not correct as similar enhancements are also observed with inert particles such as corundum[33] or quartz[34].

Furthermore using a progressive addition amount of gypsum in a slag cement system, Kocaba showed that the peak is delayed and becomes broader (Figure 4.8). However the reaction of the C_3A was similar in all the systems[34] which shows that slag reaction is not responsible for the peak. Therefore solely the physical presence of particles affects the second reaction. However the mechanism behind this effect is not well understood.

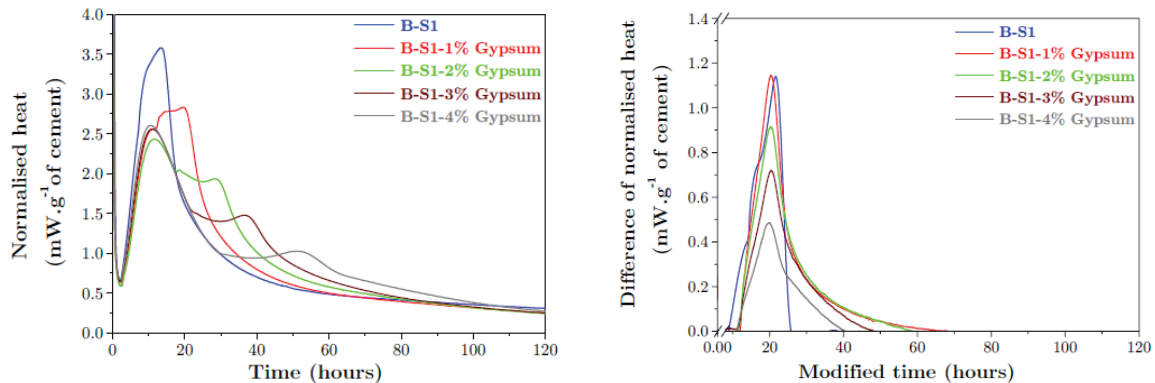


Figure 4.8: Effect of additional gypsum on 40% Slag PC systems (left) the C_3A peak is progressively delayed (right) the peak area is similar for all the systems. From Kocaba [34]

To summarize, the second aluminate reaction is affected by the sulfate content. It controls the second C_3A reaction and interacts with the C-S-H phase at a determinant stage for the microstructure development. The link between the SCM and the enhancement of the second C_3A reaction is not well understood.

2. Mixes studied

The aim of this section is to investigate the role of the SCM on the second aluminate reaction. As sulfate is controlling the C_3A reaction the first step is to analyse how the SCM affects the sulfate consumption throughout the hydration. At the beginning of the deceleration, SCM particles are still inert. So in this study we used quartz to simulate the inert SCM grains.

The effect of gypsum on the reaction was investigated by adding extra gypsum to the 70% quartz-cement system. High replacement was chosen to accentuate the second aluminate reaction (Figure 4.9). The 70% blend was also compared to Portland cement paste as reference sample.

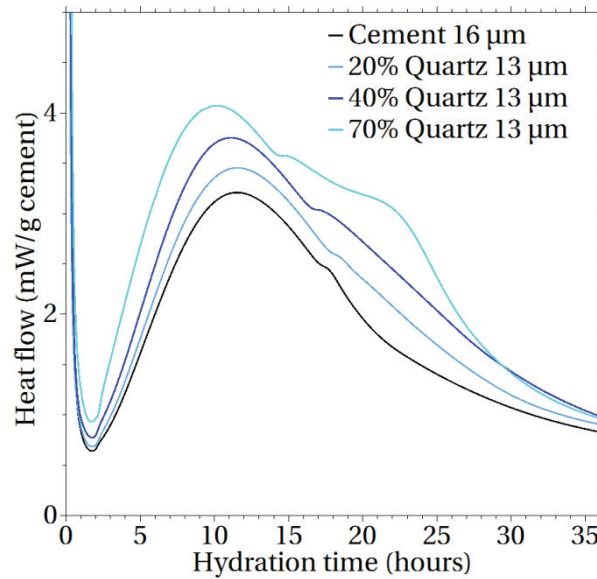


Figure 4.9: Isothermal calorimetry curves of quartz – cement paste showing the enhancement of the second C_3A dissolution

The four following systems were studied:

PC w/s 0.4 (reference)

70% Quartz – cement w/s 0.4

70% Quartz – cement + 2% calcium sulfate w/s 0.4

70% Quartz – cement + 6% calcium sulfate w/s 0.4

Some complementary mixes are shown to emphasize the effect of quartz replacement and of the SCM (slag, fly ash).

3. Results

3.1. Control of the C_3A reaction by gypsum content

Figure 4.10 shows the calorimetry curves during the first day of hydration of 70% quartz-cement pastes with different additional amount of gypsum.

The aluminate peak is characterized by the shoulder peak. The onset and kinetics are changed: the peak is delayed and becomes broader with increasing gypsum content in the system. It can be also noted that the underlying silicate curve is unaffected by the second aluminate reaction.

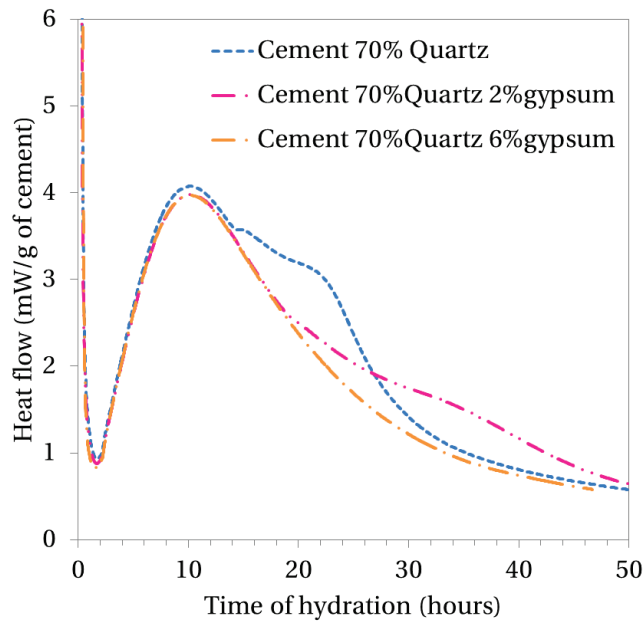


Figure 4.10: Effect of gypsum on the kinetics of 70% quartz-PC paste

Onset of the second C_3A reaction

The amount of gypsum was tracked by *in situ* XRD. The results are plotted in Figure 4.11. The rate of consumption of gypsum varies. The reasons of these changes of rate are still not clear and need further investigation.

The peak of the second C_3A reaction seems to start whereas a small amount of gypsum is detected in the paste. Thus, the C_3A reaction might start before the total depletion of gypsum. However it is possible that remaining gypsum as large pieces become isolated from the solution by the formation of hydrates.

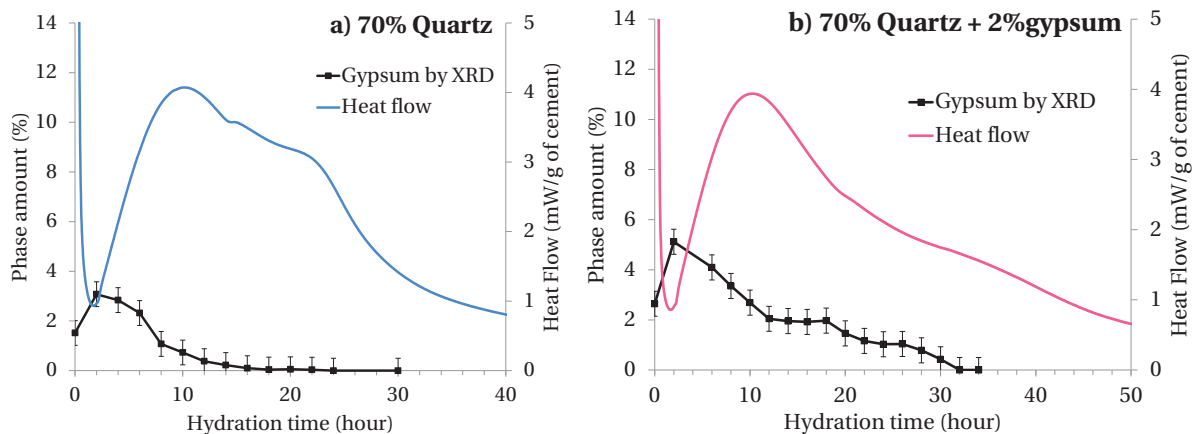


Figure 4.11: Gypsum content detected by *in situ* XRD (a) 70% Quartz PC (b) same system with 2% additional gypsum

It was found that the onset occurred at a similar cumulative heat value for all the systems with same SO_3/C_3A ratio (Figure 4.12). At this stage the heat is mainly released by the silicate reaction. This means that the onset also depends on the silicate reaction.

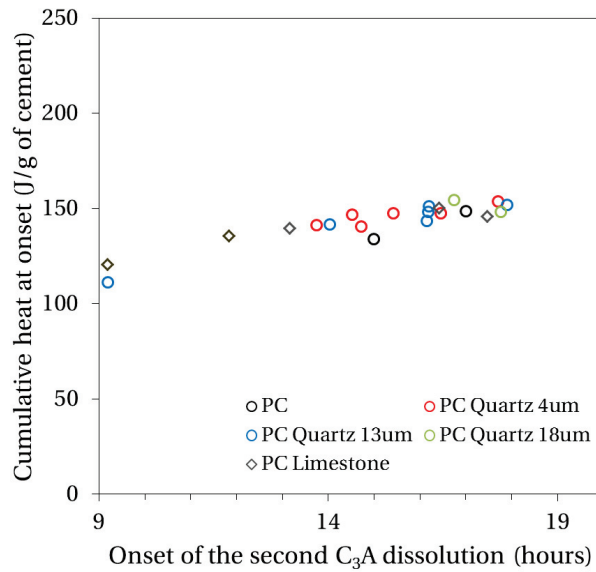


Figure 4.12: Cumulative heat as a function of the time of the onset of C₃A peak. Similar value of cumulative heat are observed in all the systems with same C₃A/sulfate ratio

This relation can be explained by the sulfate adsorption on the C-S-H formed by the silicate reaction. At early age sulfate is mainly consumed by the formation of ettringite and adsorption on the C-S-H structure. Figure 4.13 shows that there is a significant amount of sulfate detected by microanalysis in the C-S-H. Therefore the sulfate amount decreases with the increasing amount of C-S-H surface. As a consequence the critical level of sulfate, which becomes too low to control the C₃A, is reached earlier and the C₃A reaction starts again.

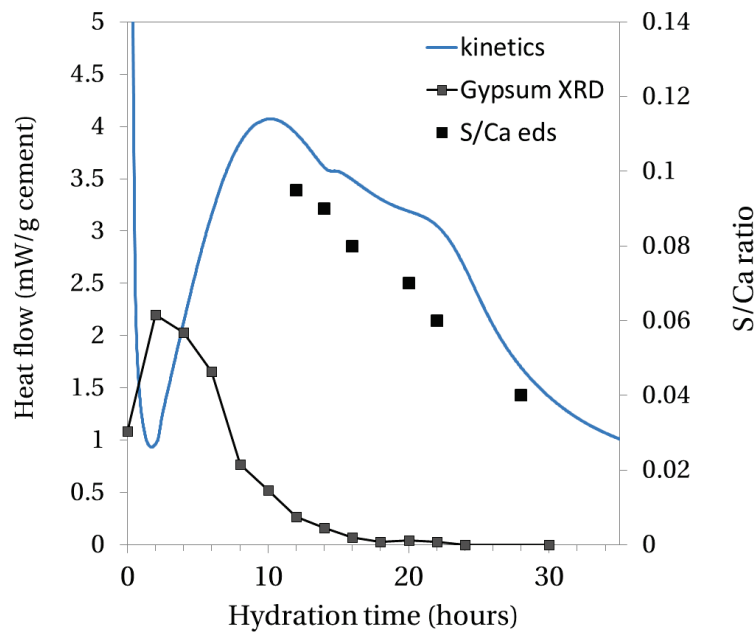


Figure 4.13: S/Ca ratio in 70% Quartz cement paste. Sulfate ions are adsorbed on the C-S-H structure and are released gradually during the deceleration period

Adsorption on quartz surface can be excluded as an explanation. Microanalyses measurement indicated that quartz does not significantly adsorb sulfate on its surface compared to cement grain (Table 4.1).

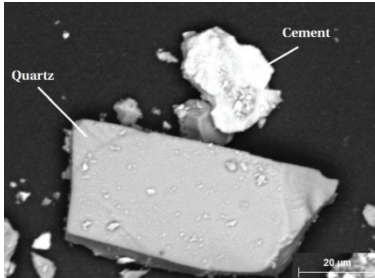


Figure 4.14: BSE image: quartz and cement grains

Table 4.1: Atomic percent of some elements on cement and quartz grains

	O	Si	Ca	Al	S
Quartz	66.04	32.02	0.17	0.75	0.01
Cement	55.91	12.39	25.28	1.30	0.29

Kinetics of the second C_3A reaction

The kinetics of the reaction is affected by the gypsum. Above we observed that increasing the gypsum content leads to a broader and thus slower reaction.

In Quartz-PC systems (Figure 4.15), a double peak was observed for systems with high replacement (>70%) or very diluted systems ($w/c > 1$).

The concentration of sulfate in the pore solution of systems with different kinetics of second C_3A reaction was measured by ICP. The results plotted in Figure 4.16 shows that high replacement level (here 70%) leads to a lower concentration of sulfate in the solution compared to the plain cement system. Such low amount is completely consumed before the end of the deceleration. At the same time, the exothermic peak appears. This suggests that the C_3A dissolves very rapidly (curve 70%Quartz).

In the case of the plain Portland cement, the sulfate concentration does not totally drop and a broad C_3A peak is visible. The remaining sulfate could still controlled some C_3A sites and leads to a slower reaction which correspond to the broader exothermic peak.

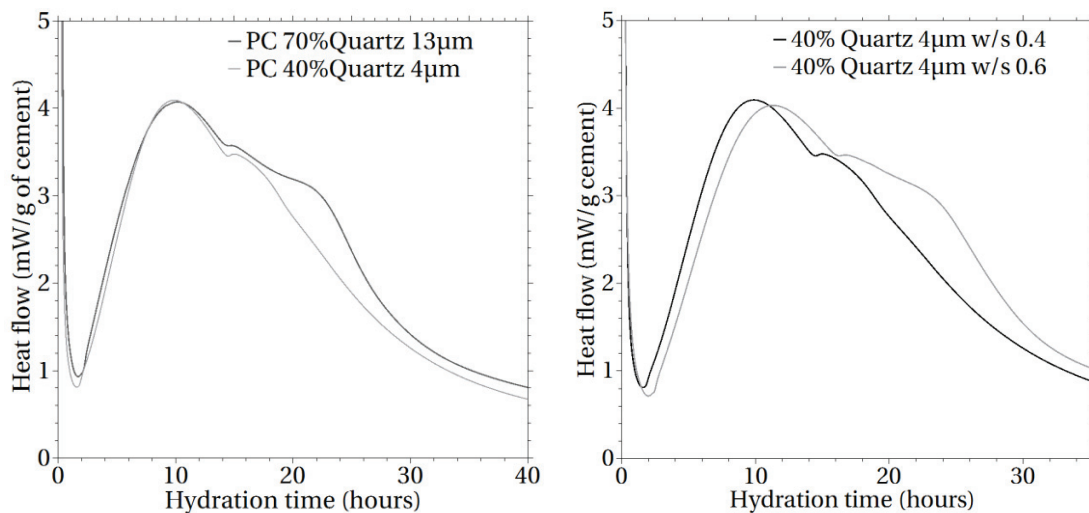


Figure 4.15: Isothermal calorimetry curves (left) acceleration does not affect the shoulder peak (right) water/solids ratio enhance the peak

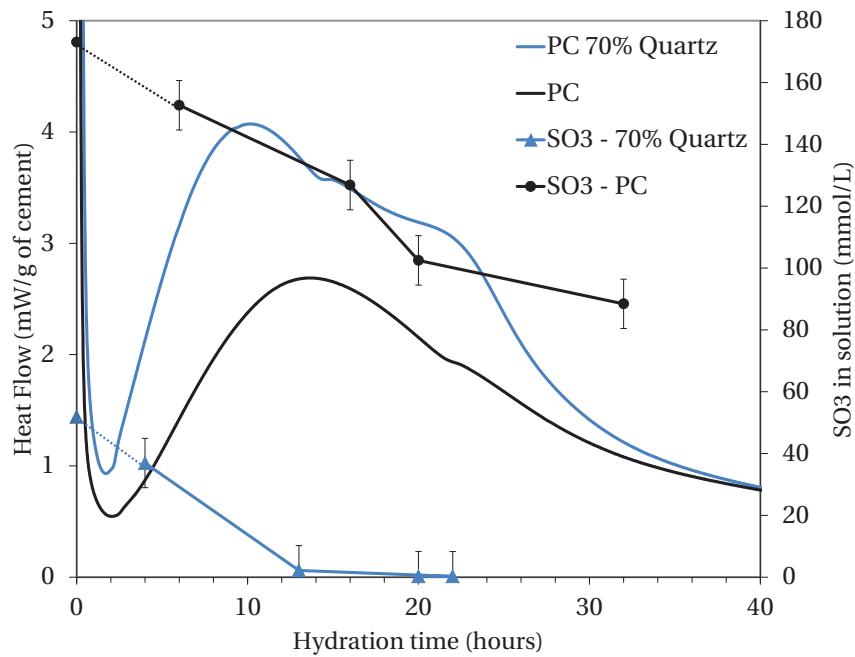


Figure 4.16: Sulfate content in the pore solution in cement paste and 70% quartz-cement paste. The initial amount was calculated from the XRF of cement. The total depletion of sulfate is observed in 70% quartz-cement system at the second C_3A peak.

Effect of Supplementary cementitious materials

The effect of the SCM is similar to the effect of quartz as at this stage most of the SCM have not yet started to react. The comparison of the effect of quartz and slag in Figure 4.17 shows that this is not related to any reactivity of the SCM but is purely a consequence of the physical replacement (i.e. *filler effect*). A similar effect is observed with fly ash which is much less reactive than slag (Figure 4.17). Nevertheless, for high replacement of slag it is not excluded that there may be a small amount of reaction of the slag at this stage and the species released from slag dissolution would participate to the reaction (such as aluminum, alkalis). This might explain the slight enhancement of the peak for 70% of slag replacement compared to the quartz curve.

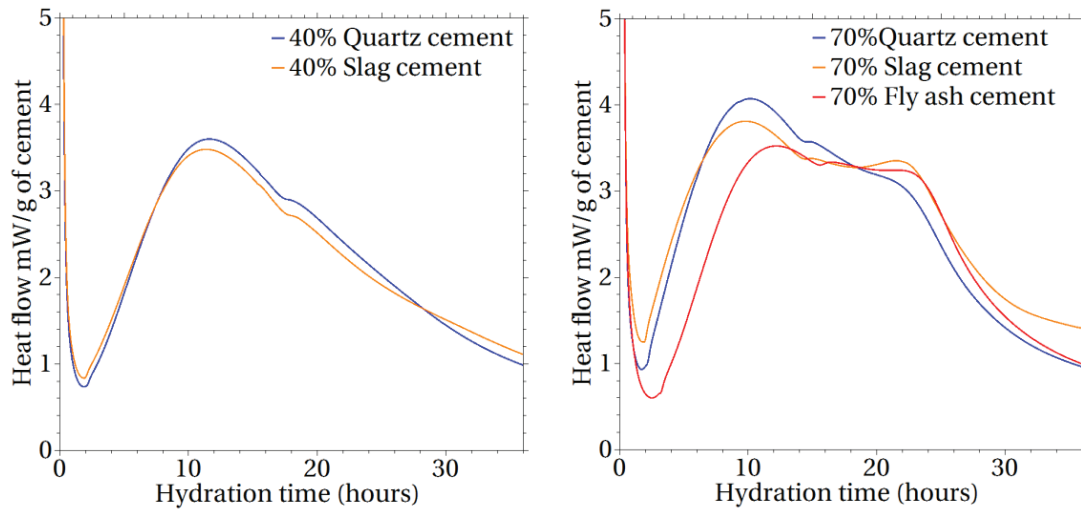


Figure 4.17: Comparison of the effect of quartz, fly ash and slag on the C_3A dissolution peak.

3.2. Effect of gypsum depletion on C-S-H

In this section we consider how the sulfate affects the C-S-H. We used a new technique 1H NMR coupled with SEM. 1H NMR quantifies the different water populations in the paste: free water, gel and intersheet water. Thus 1H NMR complements the observations made with SEM and gives information on the nanostructure of C-S-H.

1H NMR data of the Portland cement and the blends with 70% quartz with the different amount of gypsum were acquired. Figure 4.18 compares the water content (free water and water in C-S-H) between the four systems.

The first step is to compare the data from the Portland cement (a) with the blend with 70% Quartz (b). The filler effect caused by the replacement of quartz does not induce dramatic changes. In both systems capillary water decreases while C-S-H gel water and C-S-H intersheet water increase as C-S-H is forming. Gel water, in both systems, reaches a plateau. According to Muller et al.[35] a plateau in the gel water content accompanied by the continued formation of C-S-H corresponds to the densification of the bulk C-S-H. The size of the capillary pores when the densification starts, is indicated in Figure 4.18. Capillary pores are much bigger in the 70% Quartz PC system than in the plain cement. This suggests that the densification related to the cessation of the formation of gel pores, is not caused by the lack of available space. It can be also noted that the gel water/ gel intersheet ratio of C-S-H is increased in the quartz-cement system.

The gypsum has a significant effect on the repartition of the water populations. The amount of C-S-H gel water is reduced with increasing the amount of gypsum in the paste. The C-S-H gel water seems almost not able to form in the system with the highest level of gypsum (Figure 4.18(d)). Thus, the gel water/intersheet ratio is decreased. More systems need to be explored to determine if the limitation of the gel formation is caused by the presence of gypsum or the by the delayed C_3A dissolution.

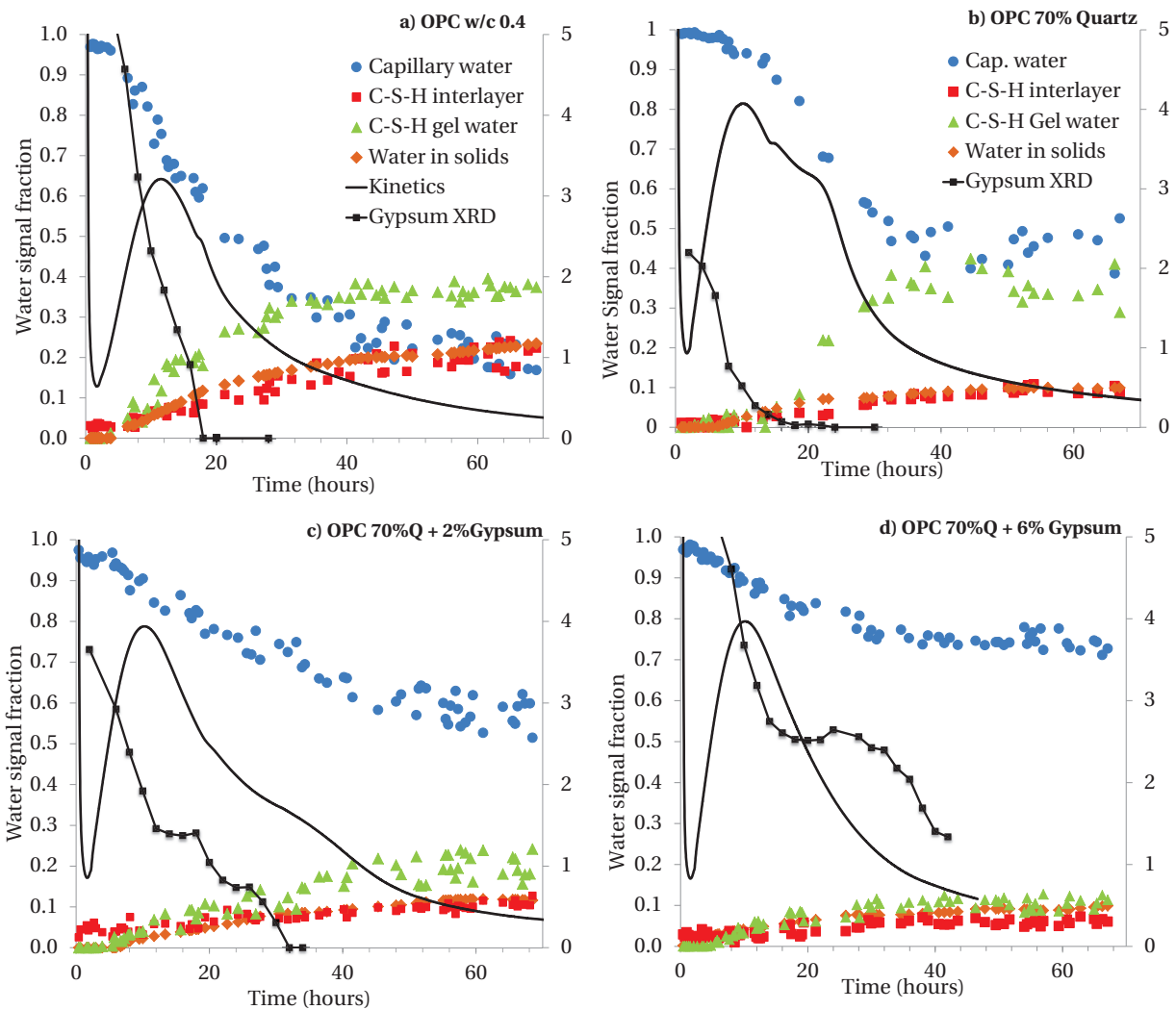


Figure 4.18: Evolution of the different water populations (capillary water, interlayer water, gel water and water in the solids including Portlandite, AFt AFm). The gypsum content is indicated with black squares.

The four systems were observed in the SEM: before, during and after the sulphate. Details of the gypsum consumption are indicated in Figure 4.23 and micrographs are shown in Figure 4.19 to 4.22. It can be seen that over the course of the deceleration period all the systems show a change in the morphology of the C-S-H. Before the depletion, C-S-H has a structure of diverging needles (Figure 19,20,21,22 on the left), by the end of the deceleration period the needles seem to be merge together (Figures on the right). The transition in morphology corresponds to the depletion of gypsum from XRD measurements (Figure 4.23). At this stage we see from the EDS data plotted in Figure 4.24 that the S/Ca ratio is significantly decreasing. This indicates that the sulfates adsorbed on the C-S-H structure are released and may induce this change of morphology.

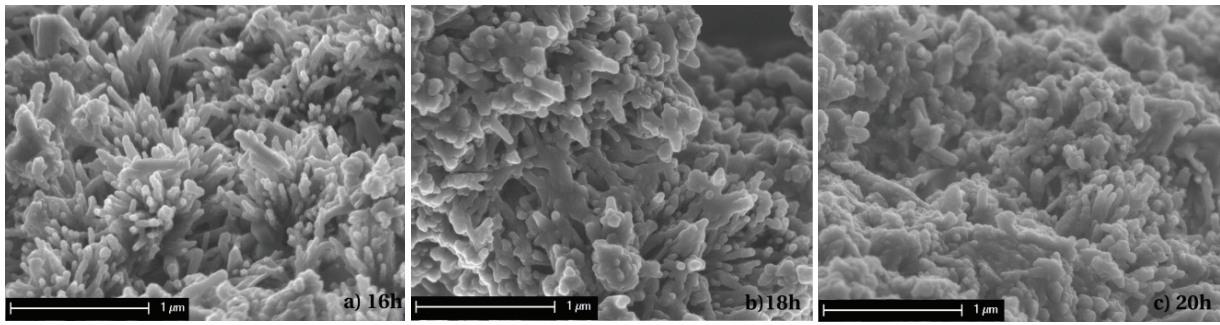


Figure 4.19: Change of C-S-H morphology in plain cement a) before b) at c) after the depletion of gypsum

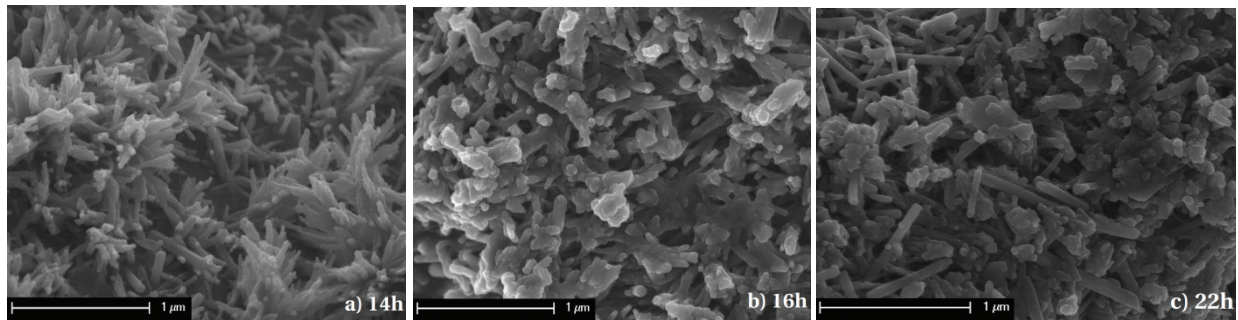


Figure 4.20: Change of C-S-H in 70%Quartz PC a) before; b) at c) after the depletion of gypsum

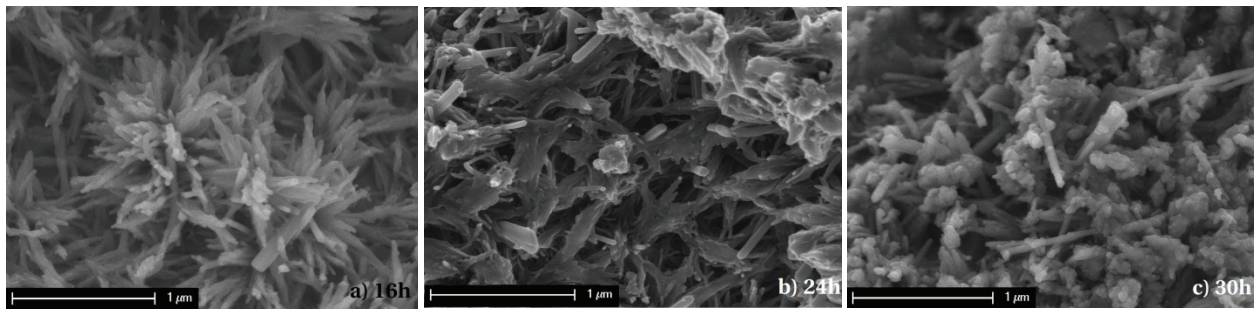


Figure 4.21: Change of C-S-H in 70%Quartz PC with 2% Gypsum a) before: b) at c) after the depletion of gypsum

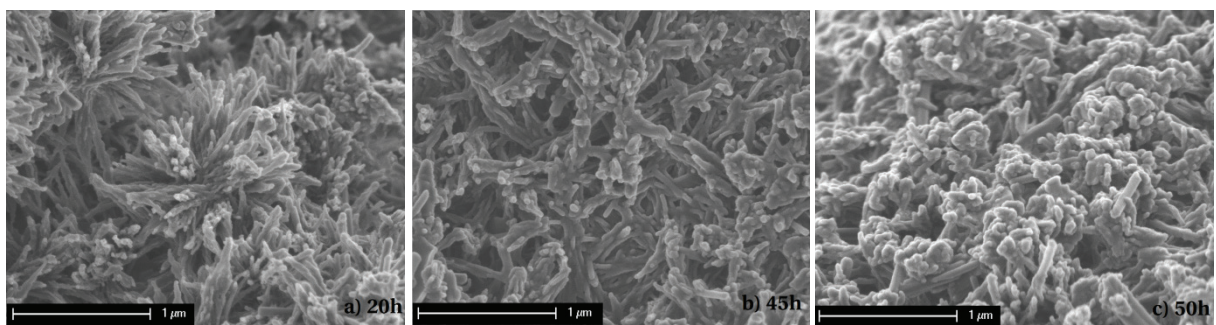


Figure 4.22: Change of C-S-H in 70% Quartz PC with 6% Gypsum a) before b) at c) after the depletion of gypsum

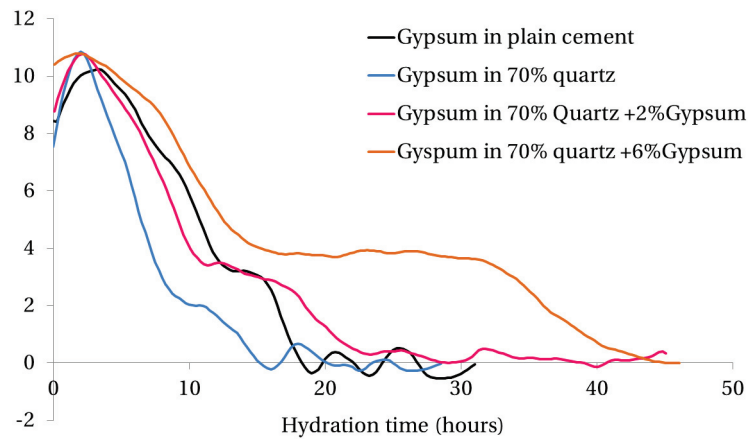


Figure 4.23: Evolution of the gypsum content from XRD. The depletion of sulfate is marked for each system.

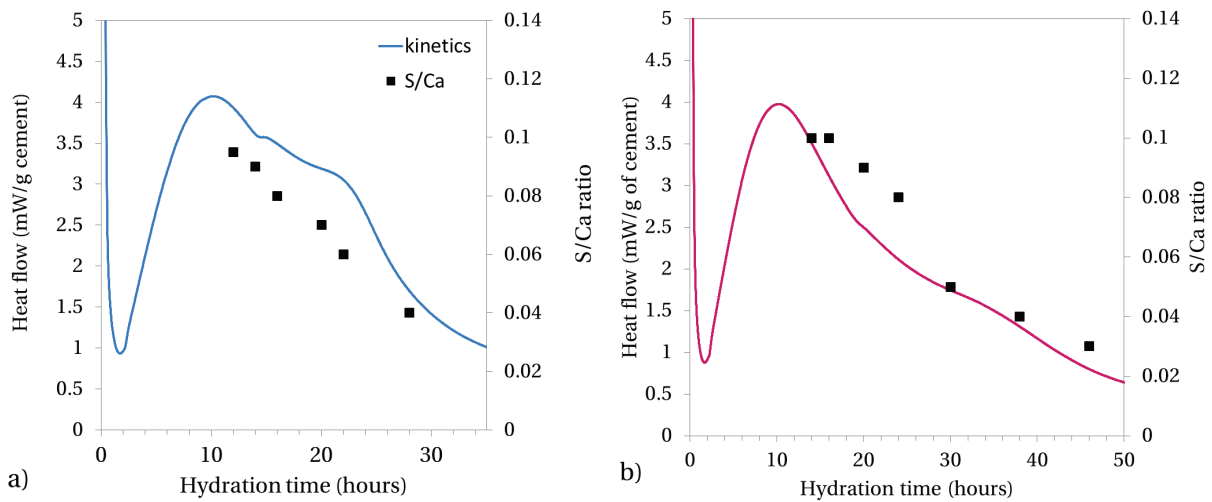


Figure 4.24: S/Ca ratio in a) PC 70% Quartz and b) PC 70% Quartz + 2% Gypsum added

Our results indicate that the adsorbed sulfate affects the C-S-H morphology and this is not caused by the lack of space as from NMR data there are still large capillary pores present in the systems studied. It seems that when gypsum is desorbed the needles stop growing at the end. This effect can be compared with the results on the different growth of C-S-H in alite paste and cement paste (Chapter 3) where we reported that the C-S-H needles in alite paste (no sulfate) were growing side by side whereas in cement paste (presence of sulfate) the diverging structure was dominant. The role of gypsum on the C-S-H growth is supported by recent work [36] where it was observed that addition of gypsum to alite system makes the C-S-H growing with the diverging structure.

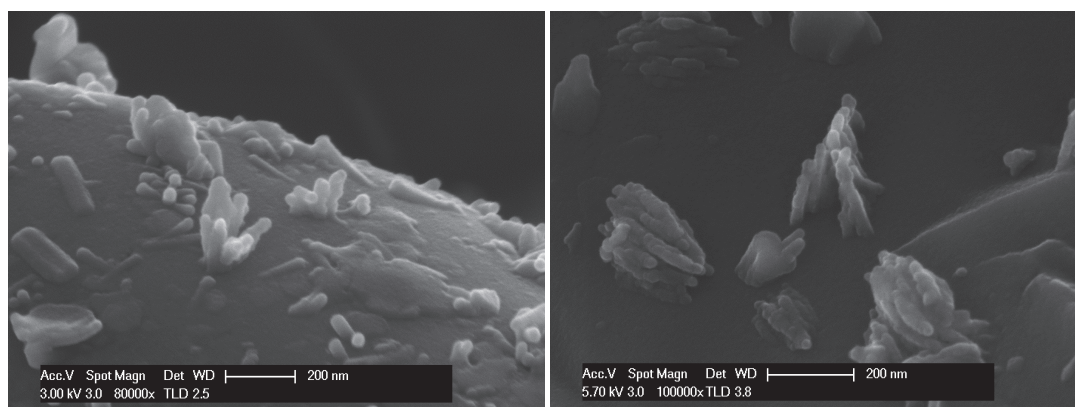


Figure 4.25: Morphology of the C-S-H in PC (left) compared in alite i.e. no gypsum (right)

3.3. Discussion on the gypsum effect on C-S-H

Adsorption of sulfate

This work indicates that as long as gypsum is present, the C-S-H grows as divergent needles. Once the sulfate starts to desorb from C-S-H, the C-S-H needles seem to fused together. At the same time the amount of gel porosity increases so this does not correspond to the formation of dense C-S-H. From ^1H NMR data, the densification of C-S-H occurs later and is rather dependent on the water/cement ratio than on the gypsum content.

Gartner explained the diverging structure or the “sheaf of wheat” structure by defects (silicate vacancies) in the structure which will induce the sheets to curve and form this shape [37]. However our results show that adsorption of sulfate is rather responsible of the diverging structure.

Jennings model [38] explains the diverging fibril structure as an artefact of the sample preparation. His model is based on the aggregation of nanoglobules. Thus the sulfate might change the arrangement of these globules.

Sulfate and gel water formation

^1H NMR data shows that the systems with high amount of sulfate do not form much gel water. The gel water/ intersheet ratio is thus changed but this does not affect the kinetics neither the morphology of C-S-H (i.e. whether the ratio, needles are forming). Two options can be explored: either the formation of C-S-H gel water becomes limited or the C-S-H gel water is not stable and transforms rapidly into intersheet water.

From our results and the literature, the interaction between sulfate and C-S-H is occurring at the interface. Therefore, the mechanism which might obtrude the gel water formation should be related to the access of water. The voluminous sulfate ions (3.68 Å for S ion against 2Å for Ca ions) might restrain the access of water and avoid water to be trapped between the nanocrystalline layers.

The influence of the adsorption of sulfate on the C-S-H might also perturb the ^1H NMR signal. For example if the sulfate increase the relaxation time of water then the gel water might be detected as capillary pores which correspond to longer relaxation time. This point needs further investigation.

4. Summary

The deceleration period is quite complex to study due to the overlapping of the silicate and aluminate reactions. By adding gypsum the reactions can be better separated. The results presented here clarify several issues:

Aluminate reaction

- Inert filler and SCM affect the deceleration period by enhancing the second C_3A reaction. This is the result of two main changes related to the sulfate content. First the presence of filler increases the hydration of cement which leads to a higher volume of C-S-H on which sulfate is adsorbed. Therefore, the sulfate content decreases more rapidly and the C_3A dissolution restarts earlier. The second change is that cement is diluted due to the replacement. Thus there is less sulfate present for the same content of water. This leads to a greater depletion of sulfate in the pore solution during the deceleration period. This could explain the faster reaction C_3A in blended systems. The proposed mechanisms are illustrated in Figure 4.26.

C-S-H

- Sulfate ions affect the morphology of C-S-H. The adsorption of sulfate promotes the growth as needles diverging from nucleation sites. In the absence of sulfate the C-S-H needles grow more in parallel. This effect is also observed in alite paste where sulfate is present.
- Gypsum seems to have a marked effect on the gel pores formation: few gel pores are formed in presence of sulfate. This might play a role in the occurrence of an optimum sulfate content from a point of view of mechanical strength.
- However, the reason for the limited gel formation is not well understood. Does the sulfate adsorbed at the C-S-H/solution interface impede the formation of gel water or modify the 1H NMR signal? Further investigation on the effect of sulfate on the NMR results is needed.

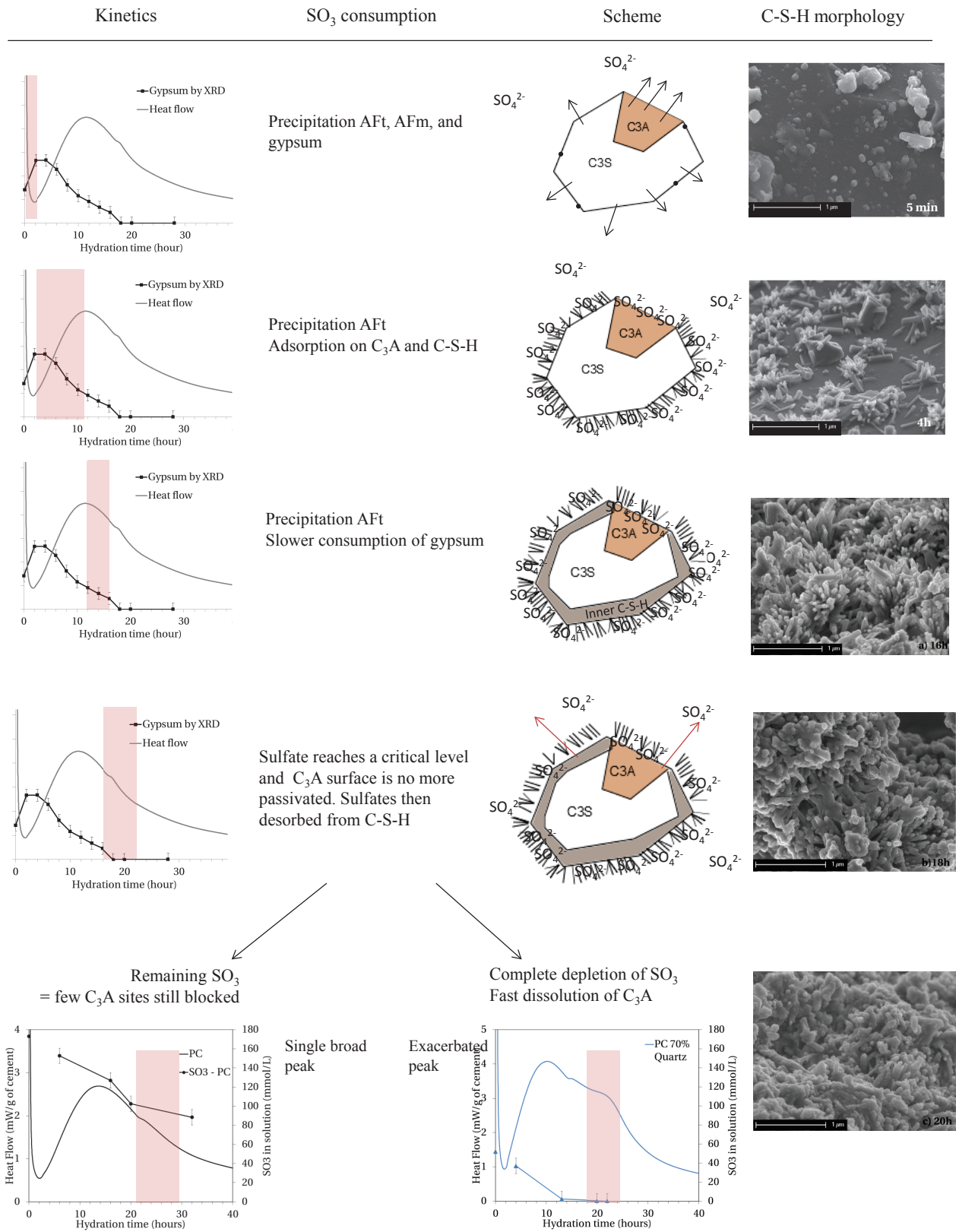


Figure 4.26: Effect of sulfate on the kinetics of second reaction of C₃A. Proposed mechanisms to explain the kinetics and the microstructure

5. References

1. Lerch, W., *The influence of gypsum on the hydration and properties of Portland cement pastes*. 1946: Portland Cement Association.
2. Quennoz, A. and K.L. Scrivener, *Interactions between alite and C3A-gypsum hydrations in model cements*. Cement and Concrete Research, 2013. **44**(0): p. 46-54.
3. Hesse, C., F. Goetz-Neunhoeffler, and J. Neubauer, *A new approach in quantitative in-situ XRD of cement pastes: Correlation of heat flow curves with early hydration reactions*. Cement and Concrete Research, 2011. **41**(1): p. 123-128.
4. Collepari, M., et al., *Retardation of Tricalcium Aluminate Hydration by Calcium Sulfate*. Journal of the American Ceramic Society, 1979. **62**(1-2): p. 33-35.
5. Pommersheim, J. and J. Chang, *Kinetics of hydration of tricalcium aluminate in the presence of gypsum*. Cement and Concrete Research, 1988. **18**(6): p. 911-922.
6. Minard, H., et al., *Mechanisms and parameters controlling the tricalcium aluminate reactivity in the presence of gypsum*. Cement and Concrete Research, 2007. **37**(10): p. 1418-1426.
7. Quennoz, A. and K.L. Scrivener, *Hydration of C3A-gypsum systems*. Cement and Concrete Research, 2012. **42**(7): p. 1032-1041.
8. Feldman, R. and V.S. Ramachandran, *The influence of CaSO₄ · 2H₂O upon the hydration character of 3CaO · Al₂O₃*. Magazine of Concrete Research, 1966. **18**(57): p. 185-196.
9. Gartner, E., et al., *Hydration of Portland cement*. Structure and performance of cements, 2002. **13**: p. 978-0.
10. Rothstein, D., et al., *Solubility behavior of Ca-, S-, Al-, and Si-bearing solid phases in Portland cement pore solutions as a function of hydration time*. Cement and Concrete Research, 2002. **32**(10): p. 1663-1671.
11. Lothenbach, B., et al., *Effect of temperature on the pore solution, microstructure and hydration products of Portland cement pastes*. Cement and Concrete Research, 2007. **37**(4): p. 483-491.
12. Chowaniec, O., *Limestone addition in cement*, in *Faculté des Sciences et Techniques de l'Ingénieur*. 2012, Ecole Polytechnique Fédérale de Lausanne: Lausanne.
13. Gallucci, E., P. Mathur, and K. Scrivener, *Microstructural development of early age hydration shells around cement grains*. Cement and Concrete Research, 2010. **40**(1): p. 4-13.
14. Jansen, D., et al., *The early hydration of Ordinary Portland Cement (OPC): An approach comparing measured heat flow with calculated heat flow from QXRD*. Cement and Concrete Research, 2012. **42**(1): p. 134-138.
15. Barbarulo, R., H. Peycelon, and S. Prene. *Experimental study and modelling of sulfate sorption on calcium silicate hydrates*. in *Annales de chimie*. 2003: Lavoisier.
16. Nachbaur, L., et al., *Electrokinetic Properties which Control the Coagulation of Silicate Cement Suspensions during Early Age Hydration*. Journal of Colloid and Interface Science, 1998. **202**(2): p. 261-268.
17. Divet, L. and R. Randriambololona, *Delayed Ettringite Formation: The Effect of Temperature and Basicity on the Interaction of Sulphate and C-S-H Phase*. Cement and Concrete Research, 1998. **28**(3): p. 357-363.
18. Bazzoni, A., *Study early hydration mechanisms of cement by mean of electron microscopy*, in *LMC*. 2014, Ecole Polytechnique Fédérale de Lausanne: Lausanne.
19. Galmarini, S., *Atomistic Simulation of Cementitious Systems*, in *Faculté des sciences et techniques de l'ingénieur*. 2013, Ecole Polytechnique Fédérale de Lausanne: Lausanne.
20. Garbev, K., et al., *Cell Dimensions and Composition of Nanocrystalline Calcium Silicate Hydrate Solid Solutions. Part 2: X-Ray and Thermogravimetry Study*. Journal of the American Ceramic Society, 2008. **91**(9): p. 3015-3023.

21. Medala, P., Labbez, Nonat. *Investigations of the interacting forces between Calcium Silicate Hydrate (C-S-H) particles: influence of sulphate sorption on C-S-H in Cement and Concrete Science Conference*. 2009. Leeds.
22. Matschei, T., et al., *The distribution of sulfate in hydrated Portland cement paste*. Proceedings of the 12th ICCO, Montreal, Canada, 2007: p. 9-12.
23. Gallucci, E. and K. Scrivener, *Crystallisation of calcium hydroxide in early age model and ordinary cementitious systems*. Cement and Concrete Research, 2007. **37**(4): p. 492-501.
24. Kjellsen, K.O. and H. Justnes, *Revisiting the microstructure of hydrated tricalcium silicate—a comparison to Portland cement*. Cement and Concrete Composites, 2004. **26**(8): p. 947-956.
25. Berger, R. and J. McGregor, *Influence of admixtures on the morphology of calcium hydroxide formed during tricalcium silicate hydration*. Cement and Concrete Research, 1972. **2**(1): p. 43-55.
26. Galmarini, S., et al., *Changes in portlandite morphology with solvent composition: Atomistic simulations and experiment*. Cement and Concrete Research, 2011. **41**(12): p. 1330-1338.
27. Gunay, S., *Influence de la cinétique d'hydratation des phases aluminates en présence de sulfate de calcium sur celles des phases silicates : conséquences sur l'optimum de sulfatage des ciments*. 2012, Université de Bourgogne: Dijon.
28. Bentur, A., *Effect of Gypsum on the Hydration and Strength of C3S Pastes*. Journal of the American Ceramic Society, 1976. **59**(5-6): p. 210-213.
29. Sauvaget, C., *Influence du rapport molaire SO₃/K₂O du clinker sur sa réactivité chimique et son ouvrabilité* 2001, Université de Bourgogne: Dijon.
30. De Schutter, G. and L. Taerwe, *General hydration model for portland cement and blast furnace slag cement*. Cement and Concrete Research, 1995. **25**(3): p. 593-604.
31. Utton, C.A., et al., *Effect of Temperatures up to 90°C on the Early Hydration of Portland–Blastfurnace Slag Cements*. Journal of the American Ceramic Society, 2008. **91**(3): p. 948-954.
32. Wu, *Early stage hydration of slag cement*. Cement and Concrete Research, 1983. **13**(2): p. 277-286.
33. Le Saout, G.S.K. *Early hydration of Portland cement with corundum addition*. in *16th Internationale Baustofftatung*. 2006. Weimar.
34. Kocaba, *Development and evaluation of methods to follow microstructural development of cementitious systems including slags*. 2009, EPFL: Lausanne.
35. Muller, A.C.A., et al., *Densification of C–S–H Measured by 1H NMR Relaxometry*. The Journal of Physical Chemistry C, 2012. **117**(1): p. 403-412.
36. Mota B., M.T., Scrivener K., *Impact of alkali salts on cement hydration*, in *Workshop on Cement Hydration*. 2014: Villars.
37. Gartner, E.M., *A proposed mechanism for the growth of C-S-H during the hydration of tricalcium silicate*. Cement and Concrete Research, 1997. **27**(5): p. 665-672.
38. Jennings, H.M., *A model for the microstructure of calcium silicate hydrate in cement paste*. Cement and Concrete Research, 2000. **30**(1): p. 101-116.

Chapter 5

Hydration at later ages (> 1 day)

Due to their slower reaction, the SCMs only contribute significantly to hydration after the main clinker reaction i.e. after 1 day. During this later period both SCMs and cement are reacting. In this chapter we investigate the impact of SCMs on the hydration at later ages. The first step was to investigate the cement reaction at later ages. The mechanism(s) controlling the kinetics at later ages are still not well understood. The work presented in this chapter aims to elucidate the following points:

- What are the kinetics of the SCM reaction at later ages?
- How do the cement hydration and SCM reaction act on each other?
- How is the microstructure changed by the SCM reaction?
- How do the hydrates fill space?
- How is the porosity modified?

Part of the results of this chapter has been submitted for publication untitled “Evolution of Pore Structure in Blended systems” in Cement and Concrete Research

1. Literature review	90
1.1. Kinetics and mechanisms	90
1.2. Impact of SCM on the microstructural development	93
2. Mixes studied	94
3. Factors controlling the later hydration	97
3.1. Cement paste	97
3.2. Blended systems	101
4. Evolution of the pore structure	113
4.1. Phase assemblages	114
4.2. Filling ability	115
4.3. Discussion	120
5. Summary	121
6. References	123

1. Literature review

1.1. Kinetics and mechanisms

The later ages period is usually referred as to the “final slow down” or stage V (Figure 5.1 [1]). The beginning of this stage is not clearly marked as stages IV and V both show a gradual decrease of the heat release.

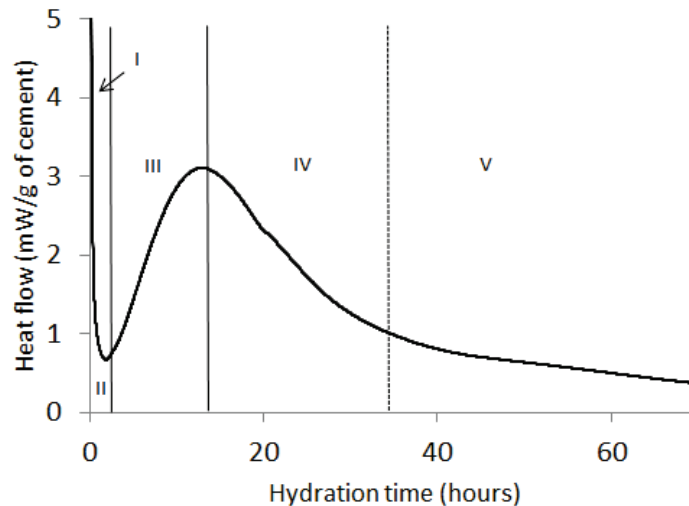


Figure 5.1: Stages over the course of cement hydration. Stage IV and V represent the slow-down of the reaction

The mechanisms controlling these two regimes are still debated. The main question is whether the two stages are controlled by two distinct processes or only one. Indeed similar mechanisms have often been proposed for both regimes:

1. The rate becomes controlled by diffusion as hydration products form a thick layer around the reactive cement grains [1, 2]
2. Based on Avrami equation the decrease of the surface of the new phase created slow down the growth (i.e. C-S-H starts to impinge) [3]
3. There is a change of the C-S-H growth due to the lateral impingement [4]
4. All the small particles are consumed and only larger grains are left which have slower dissolution rate [5, 6].
5. Water is less available making the hydration rate lower [6].

These mechanisms are discussed below in the light of our current knowledge

Diffusion control

For a long time, diffusion was considered as the controlling mechanism of the stages IV and V. The thick product layer shown in Figure 5.2(left) was thought to increase the path for the reacting species and slow down the transport. However, the micrograph in Figure 5.3(right) shows that most of the grains during the deceleration period have a gap between the product layer and the grain. In a diffusion controlled regime the gap should be filled first since it is near to the reacting grains. Others experiments [7-9] and recent simulations [10] have demonstrated that the diffusion control cannot explain for the deceleration period.

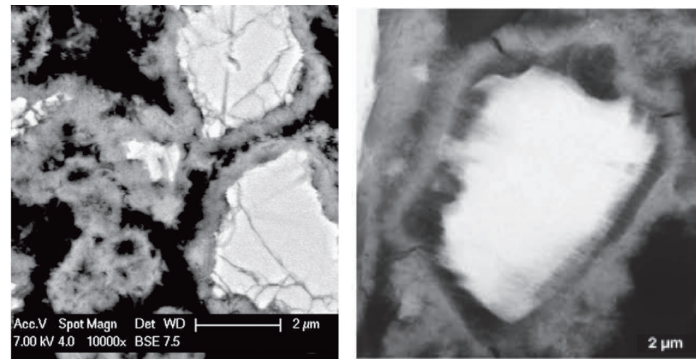


Figure 5.2: (left) Hydrated C_3S grains at the main peak. C-S-H layer is covering the whole surface of the grains. From Costoya[11] (right) Formation of the gap between the silicate phase and the product layer at 24 hours. From Gallucci [7]

Impingement

Other studies explained the slow-down of the kinetics by the reduction of the available space for the growing C-S-H due to their impingement. However, Bishnoi demonstrated that the impingement of C-S-H with a uniform bulk density cannot explain the deceleration rate: the density of C-S-H was too high. Instead he proposed that C-S-H has variable density over hydration time. A low density C-S-H at early age was suggested and observed in other work [7, 12]. In the Bishnoi model [10] the C-S-H with a low density fills a large fraction of the pore space by the maximum of the main peak and then densifies (Figure 5.3).

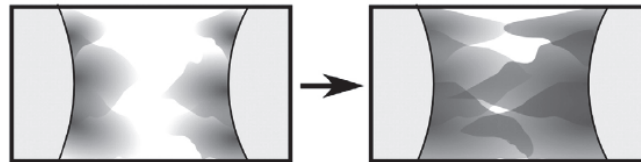


Figure 5.3: Impingement of the hydrates between two grains. From Bishnoi [10]

However Kirby and Biernacki [13] showed that when the water/cement ratio was increased, and thus increases the space to fill between the grain, the maximum heat released was not significantly changed. This indicates that it is not the lack of space which induces the slow-down of the kinetics.

It has been proposed that lateral impingement of nuclei growing on the surface of grains rather perpendicular impingement of product from two adjacent grains is responsible for the slow-down [4, 14]. TEM observations have revealed that at the maximum of the main heat peak the surface of the C_3S grain was completely covered with C-S-H needles of similar length. Consequently at the peak the only space for C-S-H to grow was from the end of the needles. However the C-S-H needles were not observed to grow much further while inner C-S-H started to form. The theory of Bazzoni is illustrated in Figure 5.4. Bazzoni explained the slow down as a result of the restriction of the lateral grow at the maximum of the peak. The C-S-H growth becomes limited and continues in the inner space.

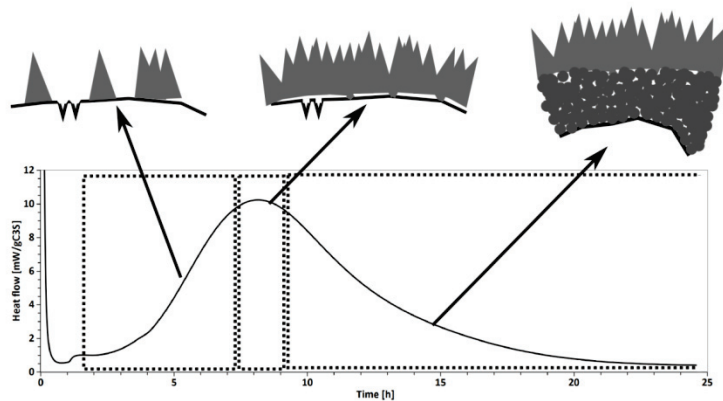


Figure 5.4: C-S-H growth at the different stage of hydration. From Bazzoni[4]

Restriction of water

The lack of water has been suggested to explain the slow-down of the kinetics. However recent advances in H^1 NMR technique on cement hydration have shown that capillary free water is still present and continues to decrease during the deceleration period [15]. The capillary water represents the free water which is easily available compared to gel water for instance. Therefore the restricted access to water cannot be the cause of this slow-down in the hydration kinetic.

In summary, the transition from the acceleration to the deceleration seems best explained by the lack of surface on the grains for nucleation of new C-S-H needles. As a consequence the product starts to grow in the inner space. Thus the kinetics during the deceleration could still be related to the growth of C-S-H. The question is does another process become more limiting over the rest of the course of the hydration and justify stage V? This point is not solved. However during the later period the amount of space available seems to play a critical role.

Blended system

In blended systems, there is the reaction of the SCMs in addition to the reaction of the clinker phase. The rate of reaction of SCMs is slower than clinker. However once this reaction starts, the subsequent hydraulic or pozzolanic reaction may affect the cement hydration. The reaction of slag is in general faster than that of fly ash. Although their reactivity depends on several factors, their reaction at 20°C, in general, starts at respectively 2 days[16] and 5-7 days [17, 18].

It is easier to measure the reaction of cement than to measure the degree of reaction of a SCM. Few techniques are able to quantify the sole contribution of SCM in the blend. For pozzolans such as fly ash, the degree of reaction is often estimated from the Portlandite consumed. The amount of Portlandite in the fly ash system is compared to the amount in a reference sample containing quartz at similar replacement level than fly ash. This technique is currently used [17, 19] in preference to selective dissolution which is not considered very accurate [20, 21]. The development of image analysis on full spectra imaging has also proved to be a good technique to quantify the degree of hydration of fly ash [20, 22].

Image analysis can be used to measure the reaction of slag if coupled with a mapping of the magnesium. However the accuracy will decrease for low replacement level. From the work of Kocaba [21], the most

promising technique is based on calorimetric measurements. The calorimeter records continuously the heat released from the sample. The difference between the cumulative heat curve of slag system and the curve of the quartz system with a similar amount of slag, isolates the contribution of slag to the heat evolution. Based on this method she found that the slag reaction was not significantly affected by the type of cement. Others methods of quantification have been used. Richardson used ^{29}Si MAS NMR and observed after 2 years of hydration, slag reacted less in systems with high replacement level [23]. Other authors have also reported this effect [24, 25].

1.2. Impact of SCM on the microstructural development

SCMs have a different chemical composition to cement, however the hydrates formed are similar to those formed in plain Portland cement pastes. Thermodynamic models enable the stable phases to be predicted from the chemistry of the components.

Phase assemblage

In general SCMs are materials richer in silica and aluminum than Portland cement. The main hydrate resulting from the SCM reaction and the Portland hydration is C-S-H although its composition may be different in blended systems. The Ca/Si ratio is usually lower than in PC while the Al/Si ratio is increased [16, 26, 27]. The aluminum from the SCM dissolution is incorporated in the C-S-H structure and the designation C-A-S-H is therefore more suitable.

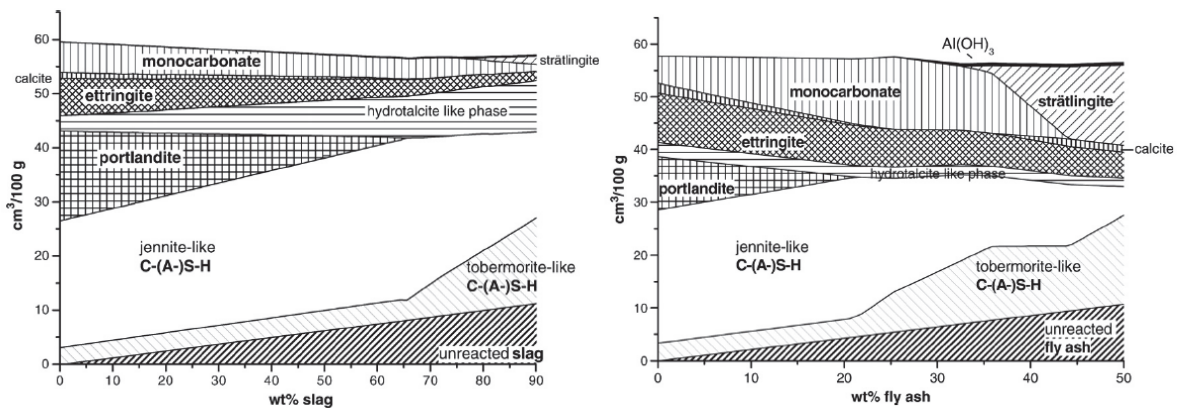


Figure 5.5: Prediction of the phase assemblage by thermodynamics of a cement paste with increasing slag content and fly ash content. From Lothenbach et al. [28]

Figure 5.5 shows the prediction from thermodynamic modelling with the GEMS- PSI software of a cement paste blended with slag and fly ash [28]. The chemistry of the SCM used changes mainly the proportion of the phases produced. In both graphs two kind of C-S-H are distinguished. This arises from the way the model deals with C-S-H solid solution. In fact, only one C-S-H or variable composition may be formed.

Using TEM images the morphology of C-S-H in cement or alite paste has been observed as fine fibrils [26, 29]. In presence of high amount of SCM a different morphology has been identified. Richardson reported that a foil-like morphology of C-S-H was observed in systems containing a high amount of slag.

The foil-like morphology was thus attributed to the slag reaction as it became the predominant structure with increasing the proportion of slag.

A recent study [26] has shown that the presence of foils is related to the absence of Portlandite. The link between CH and C-S-H also explained the different chemical composition of each type: fibril C-S-H has Ca/Si ratio of 1.50 and higher whereas foil-like has lower Ca/Si ratio up to 1.50 [26]. Figure 5.6 shows the two type of C-S-H and indicate that the two types can coexist.

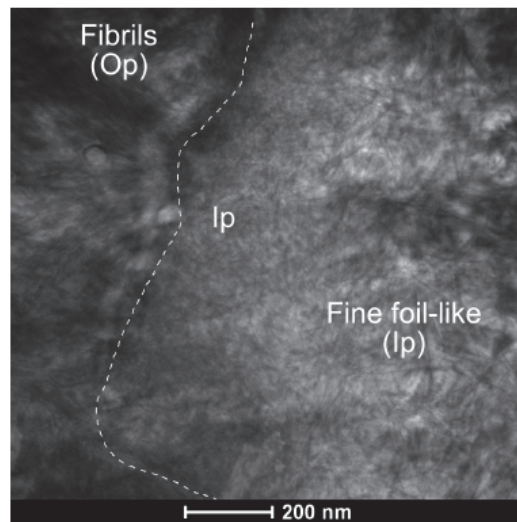


Figure 5.6: Interface fibrils / foil-like morphology in the Fly ash-cement paste after 3 years. From Rossen [26]

Pore structure

The pore structure is an important parameter for the durability properties. Thermodynamics is very helpful to understand the hydrates formed in the blended systems but does not give information on the spatial distribution of the hydrates in the space.

The size of the pores in hydrated cement varies from the micron to the nanoscale. Powers and coworkers modeled the pore populations in cement paste.

Using water sorption, Power et al. observed that a part of the water in C-S-H was lost at low relative humidities. This was called gel pore water. This led to a model based on the volumetric variation of five components: the unreacted cement, the hydrates and the capillary pores, gel water and non-evaporable water which is currently called interlayer water. Recent advances in the technology have enabled refinement of this model[15]. Using ^1H NMR the nanoporosity of the C-S-H has been characterized[15]. Four water populations are differentiated: the capillary pores, the gel water, the C-S-H intersheet water and the solid water. It appeared from the work of Muller et al.[15] that the gel water does not increase linearly with the degree of hydration (Figure 5.7). Indeed the experiments showed that the C-S-H is growing first as a loose-packed product made of gel pores and sheets which supports the idea proposed by Bishnoi [10]. The amount of gel pores and sheets grow rapidly until the capillary pores reach a critical size of about 10 nm. From this point no more gel pores are formed even though C-S-H is still forming as indicating by the increase in the amount of intersheet water. The water populations measured by ^1H NMR are shown in Figure 5.7. Another interesting observation from this data is that after 40 days the C-S-H sheet water increases gradually while the amount of the gel water starts to decrease.

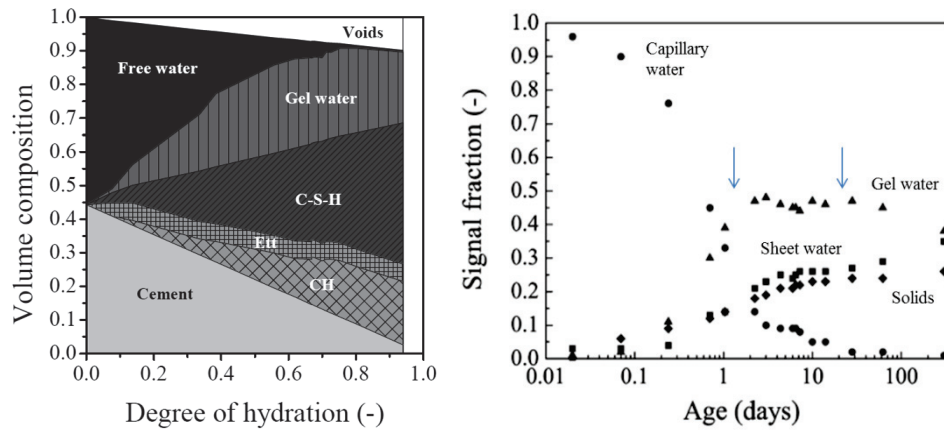


Figure 5.7: Water populations (left) volumetric composition of cement paste (right) water populations from ^1H NMR. Adapted from Muller et al.[15]

There are many studies reporting on porosity measurements in blended systems. However the contribution of the SCM reaction and its space filling properties are not well understood. The authors agree that blended systems have a higher total porosity at early age compared to plain OPC [30-32]. At later ages the effect of slag and fly ash on the total porosity is not clear from the literature. Generally, studies report similar or smaller pore entry sizes for blended cements [30, 31, 33, 34], but the vast majority of studies used severe drying methods. Figure 5.8 shows the pore structure from MIP measurements of cement and blended systems reported by Moreira. The total porosity is higher than cement for blended pastes while the threshold radius reaches at later age similar value than for cement paste. Thus the porosity is refined in blended systems. Several authors have underlined this phenomenon and have suggested that SCM fill the porosity differently than clinker reaction [28, 35, 36].

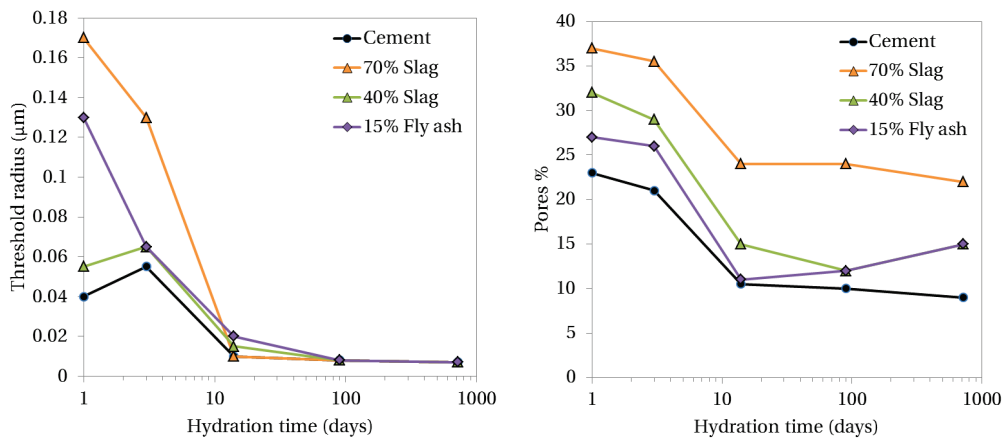


Figure 5.8: Pore structure development in blended systems. Adapted from Moreira [30]

2. Mixes studied

The first part of this chapter investigates the factors controlling the kinetics during later hydration. The first step was to study the kinetics in cement paste and quartz-cement paste to verify the influence of parameters such w/c and w/s that can be distinguish in blended systems.

Table 5.1: Mixes for the study of kinetics of cement hydration Varying w/c and w/s ratios

	Mix	Weight	
		w/c	w/s
100%	PC	0.4	0.4
100%	PC	0.6	0.6
40%	Quartz (13um)	0.67	0.4
Add 40%	Quartz (13 um)	0.4	0.3

To investigate the effect of slag and fly ash and their interaction with cement, we use five systems with 40% replacement varying the proportion of the SCM and the quartz. This method isolates the effect of the SCM reaction as quartz is inert, and keeps the water/cement and water/solids constant.

The mix design is detailed in Table 5.2 and Figure 5.9

Table 5.2: Mixes used to isolate the effect of SCM

Systems	%weight					%volume				
	Clinker	SCM	Quartz	Water	w/s	Clinker	SCM	Quartz	Water	w/s
100% PC	71.4	-	-	28.6	0.40	43.1	-	-	56.9	1.32
40%Slag	44.2	26.3	-	29.5	0.4	25.9	17.2	-	56.9	1.32
30%Slag-10% Qz	44.5	19.9	6.0	29.7	0.4	25.9	12.9	4.3	56.9	1.32
20% Slag 20% Qz	44.8	13.3	12.0	29.9	0.4	25.9	8.6	8.6	56.9	1.32
10% Slag 30% Qz	45.1	6.7	18.1	30.1	0.4	25.9	4.3	12.9	56.9	1.32
40% Quartz	45.4	-	24.3	30.3	0.4	25.9	-	17.2	56.9	1.32
40% Fly ash	39.5	26	-	34.5	0.4	25.9	17.2	-	56.9	1.32
30%FA-10% Qz	44.16	17.8	6.2	31.3	0.4	25.9	12.9	4.3	56.9	1.32
20% FA- 20% Qz	44.28	11.9	12.4	31.4	0.4	25.9	8.6	8.6	56.9	1.32
10% FA - 30% Qz	44.21	5.9	18.5	31.4	0.4	25.9	4.3	12.9	56.9	1.32

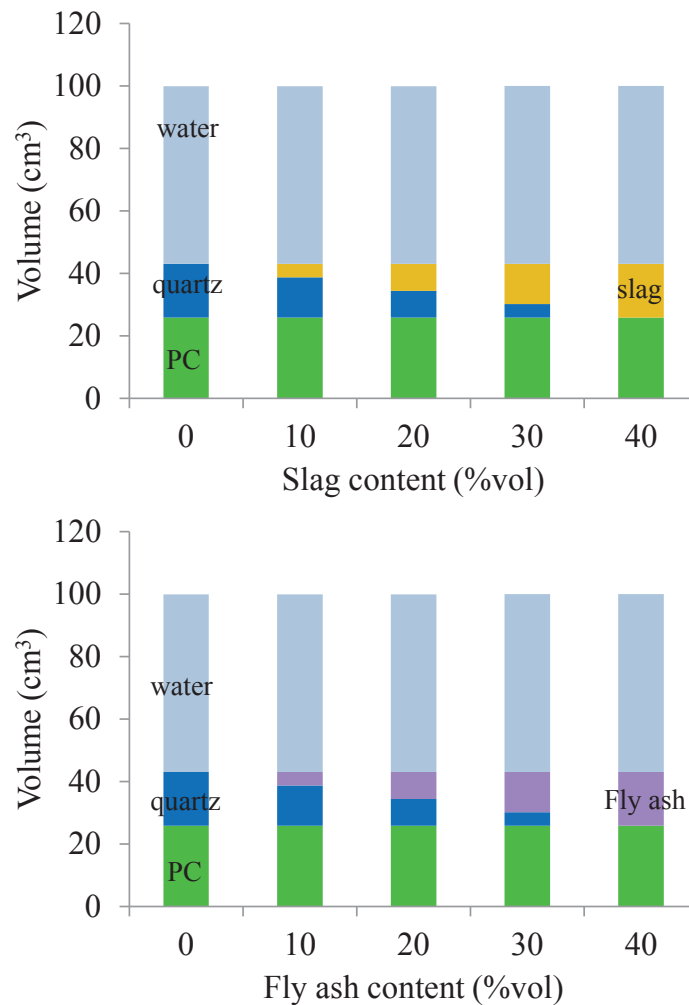


Figure 5.9: Initial proportion of the mixes of the slag - quartz - cement and fly ash - quartz cement systems

3. Factors controlling the later hydration

3.1. Cement paste

In general, a change in kinetics may be linked to a change of the rate controlling-mechanism. Figure 5.10 shows the cumulative heat and the heat flow of cement paste over 28 days on a logarithmic scale. Three different kinetic regimes can be defined. The deceleration period corresponds to the linear part of the curve. Then there is a transitory period followed by a later age regime. The kinetics in the transitory regime decreases gradually while the later ages is characterized by a very slow rate. This rate seems to continue for a long time as data from the chemical shrinkage in Figure 5.11.

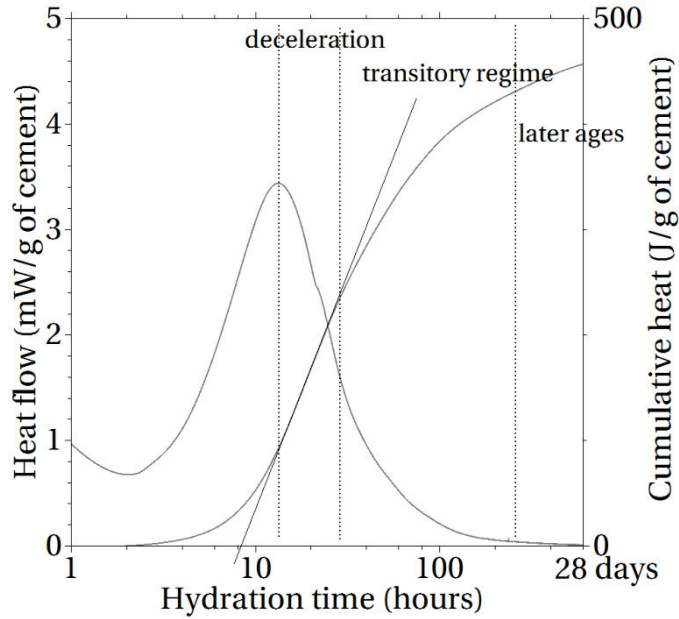


Figure 5.10: Proposed delimitation of the kinetics regimes

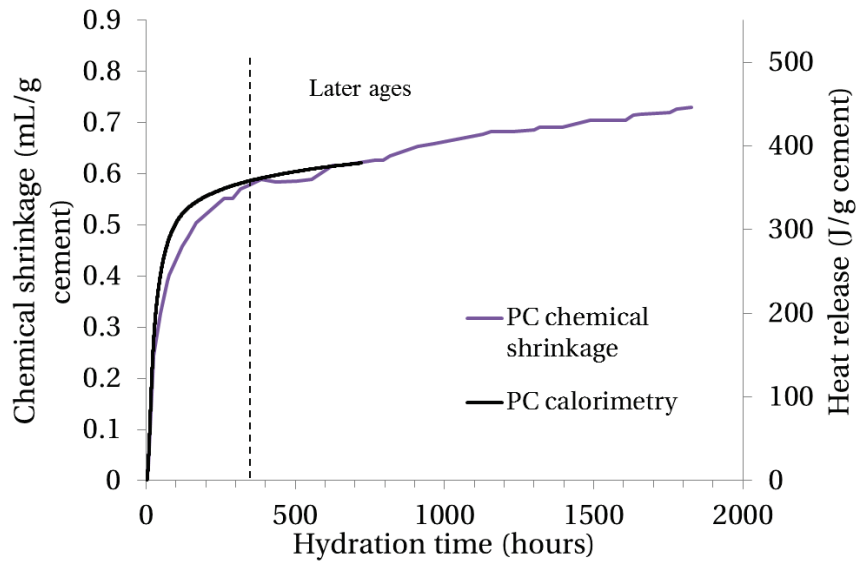


Figure 5.11: Correlation between calorimetry and chemical shrinkage of cement paste w/c 0.4. The later age has a constant rate

3.1.1. Deceleration period

Figure 5.12 shows the calorimetry curve of systems with different water/cement ratio. The systems with similar water-to-cement ratio eventually converge. In all the systems presented in Figure 5.12, only cement is hydrating (quartz is inert). We suggest that the availability of large water filled pore where hydrates can grow in it would play a role in this stage.

Recent study support this hypothesis [4]. Bazzoni showed that the deceleration is still governed by C-S-H growth in inner and outer space.

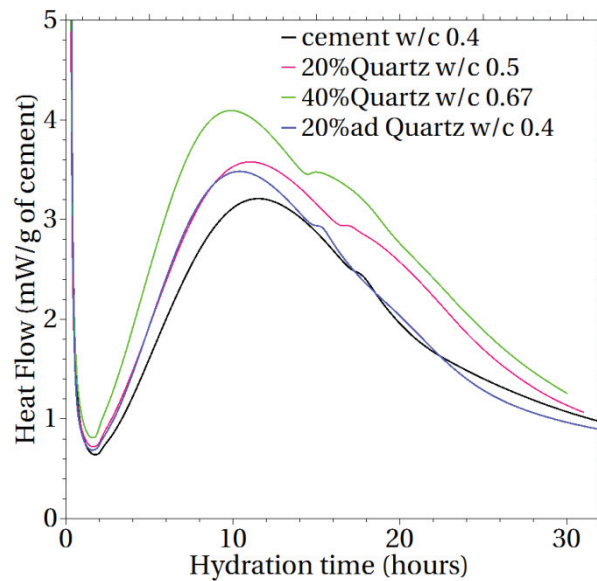


Figure 5.12: Deceleration rate dependent on the water/cement ratio

3.1.2. Transitory regime

The transitory regime is characterized by a gradual decrease in the rate. For systems which have a low water/solids ratio, the transition is more marked. As an example in Figure 5.13 the system with 40% of additional quartz (w/c 0.4 and w/s 0.3) the curve in the transition regime shows a sharper decrease than for the systems with w/s 0.4 or 0.6. This seems to indicate that the kinetics of the transitory regime is dependent on the space to fill between the grains.

The micrographs in Figure 5.14 show the microstructure of cement paste w/c 0.4 at 7 days (i.e. end of the transitory regime). The microstructure is well filled with hydrates, there are no visible capillary pores except within remains shells of hydration product from small grains while in cement paste w/c 0.6 at 7 days (Figure 5.14) large capillary pores are left that explains the more gradual transitory regime: space still can be filled. This suggests that the transitory regime is controlled by the filling of the space by the hydrates, mainly C-S-H.

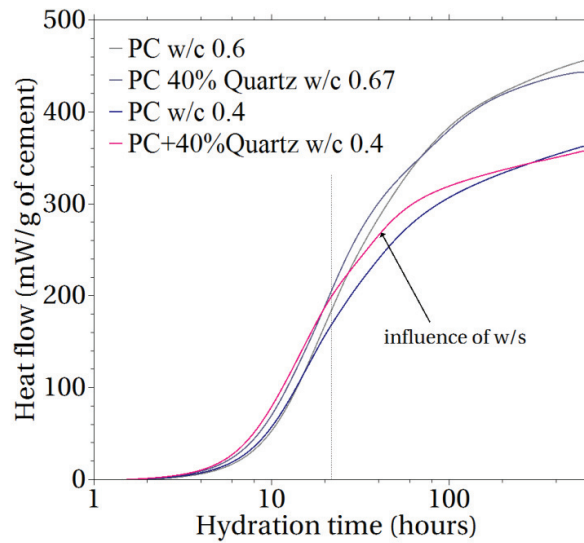


Figure 5.13: Effect of the water/cement and water/solids ratios

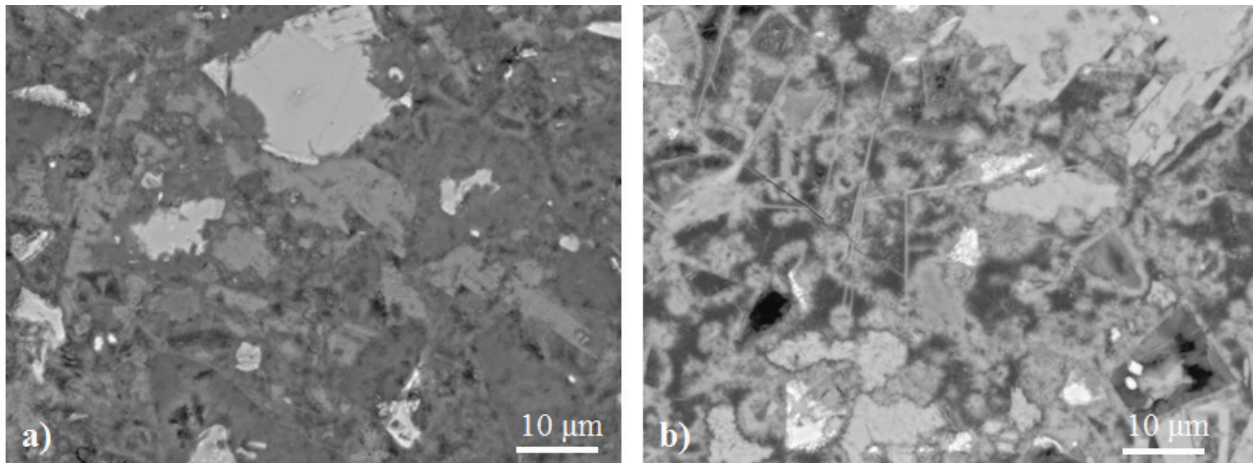


Figure 5.14: Micrographs at 7 days of hydration of a) PC w/c 0.4; b) PC w/c 0.6. At this stage the PC 0.4 paste is already well filled whereas in PC 0.6 some outer space remains.

3.1.3. Very late age regime

The beginning of the late age regime corresponds from Figure 5.11 to the slow and continuous increase in chemical shrinkage data (about 350h = 14 days). The rate suggests that the mechanism controlling the kinetics at this stage is not affected by the state of the microstructure. This is incompatible with a diffusion limitation mechanism which would reduce as the layer of hydrates increases.

Figure 5.15 shows the pore structure development over the course of cement hydration. From 14 days, the total porosity decreases slowly and the critical radius in the systems remains at ~6-8 nm. The reaction is thus continuing but the hydrates forming do not decrease the pore entry size anymore. Thus the deposition of C-S-H impacts the porosity in a different way than in early stages.

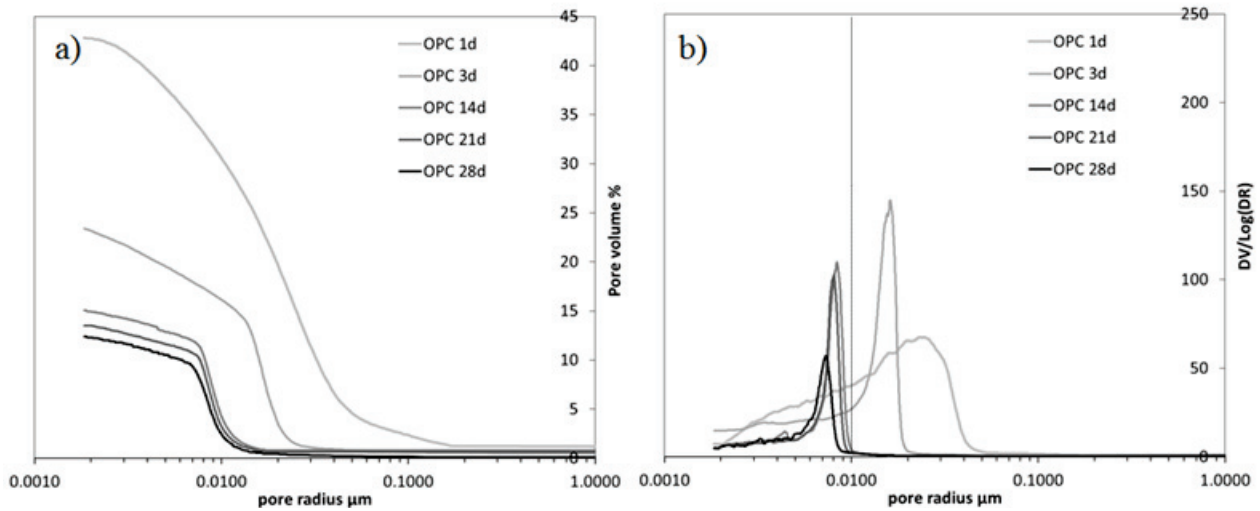


Figure 5.15: Pore structure development in cement paste w/c 0.4

The results indicate that the lack of space is limiting the hydration and leads to rate changes. In blended systems in addition to C-S-H from cement, hydrates from the SCM reaction are also filling the space that might affect the cement hydration.

3.2. Blended systems

The objective of this section is to study the kinetics in blended systems. More precisely, we want to know if the space filling limits the kinetics of SCM reaction as for cement.

Figure 5.16 shows the cumulative heat curves of quartz cement compared to slag and fly ash cement pastes. The major change caused by the slag reaction is during the transitory regime. In the fly ash systems the changes occur later due to the slower reaction of fly ash.

Calorimetry data indicates the overall heat release. However we need to quantify separately the reaction of each component: SCM and cement. To complement the information from calorimetry, XRD, TGA and SEM was used.

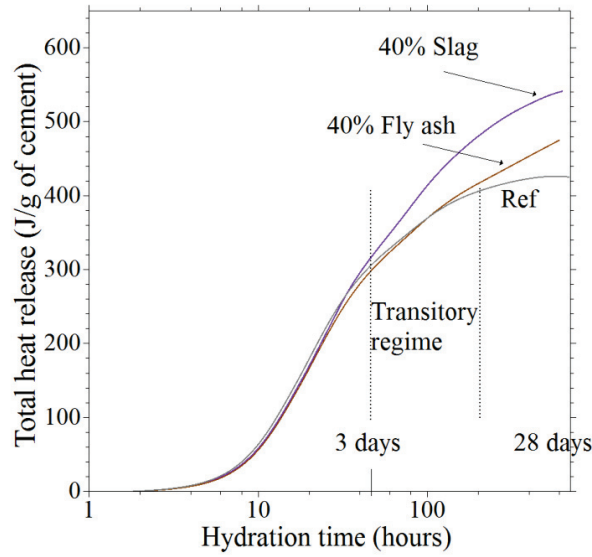


Figure 5.16: Cumulative heat curves of cement, 40% quartz PC, 40% Fly ash PC and 40% slag PC. The reaction of slag mainly affects the transitory regime while Fly ash reaction occurs later

3.2.1. Reaction of clinker phases in blended systems

The study of Slag – quartz PC and Fly ash – quartz PC systems with varying SCM and quartz proportions can be used to isolate the effect of the reaction of the SCM. Thus we can study how the hydration of the clinker phases is influenced with increasing the proportion of SCM in the blend.

Figure 5.17 shows the degree of hydration (DoH) of cement in slag – quartz PC systems measured directly by Rietveld analysis. The presence of slag has a significant effect on the hydration of clinker phases. We can see that increasing the level of replacement of slag decreases the reaction of clinker component. C_3S and C_2S are the phases the most affected. This indicates that the clinker phases and slag might compete.

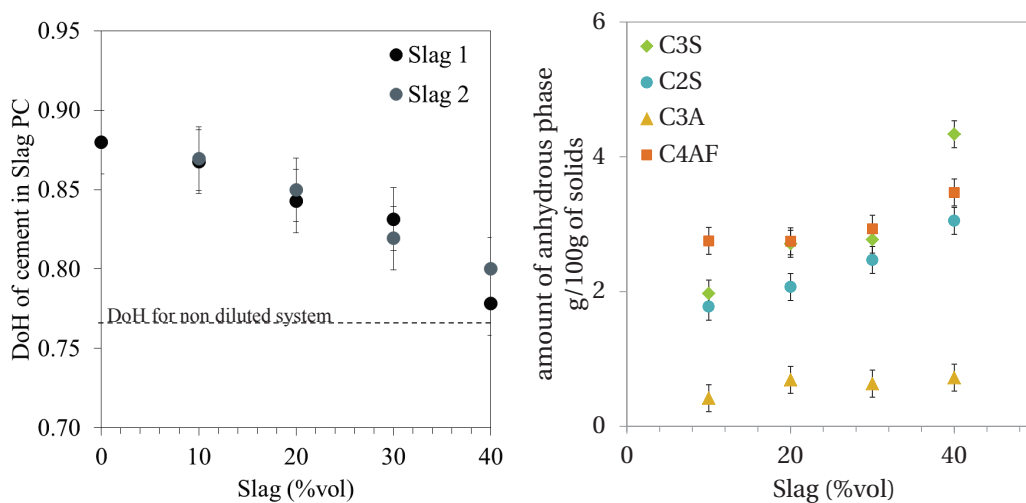


Figure 5.17: Degree of hydration of cement at 28 days with increasing the proportion of slag. Slag reaction affects mainly the C_3S and C_2S hydration

In the case of Fly ash – quartz PC systems, Figure 5.18 shows that varying the proportions of fly ash and quartz in the system does not change the degree of hydration of clinker component. However, the reaction is increased compared to the non diluted system (cement paste w/c 0.4) due to the filler effect.

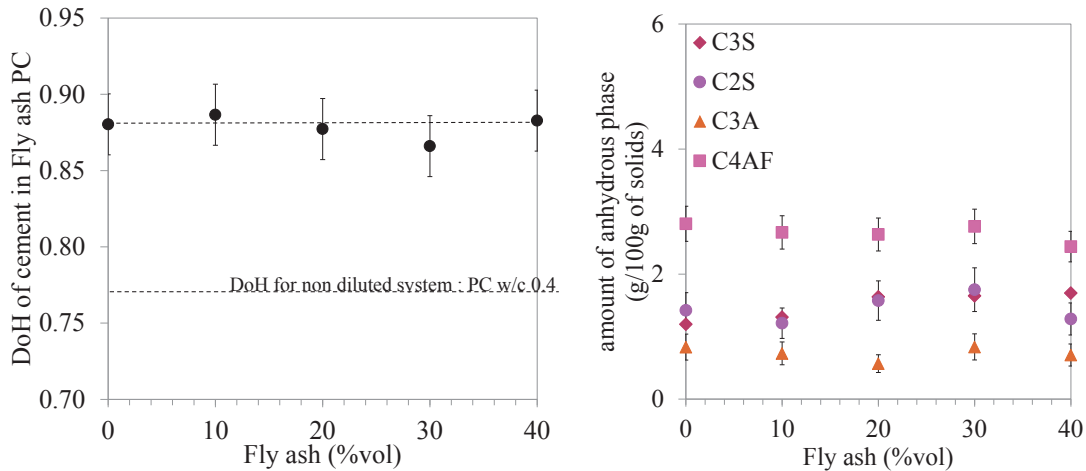


Figure 5.18: Degree of hydration of cement at 28 days with varying the proportion of fly ash. Fly ash reaction does not affect cement hydration

3.2.2. Reaction of SCM

In this section the progress of the SCM reaction through the cement hydration is studied.

Reaction of slag

Figure 5.19 shows the cumulative heat release of the four Slag – quartz PC systems with varying proportions of slag and quartz. The first observation is that the four curves are almost identical up to about 30 hours (i.e. end of the deceleration regime) and then progressively diverge. The total heat evolved at 28 days increases with slag content. Nevertheless the additional heat is not proportional to the slag content. For high replacement levels (more than 20%) the increase is quite small. This suggests that slag reaction becomes limited at higher additions.

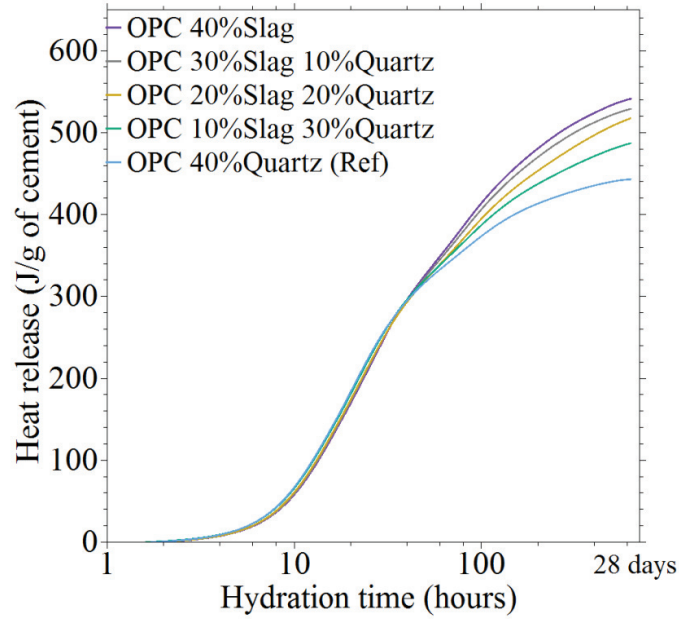


Figure 5.19: Calorimetry curve of slag-quartz-cement systems. The cumulative heat becomes limited

The measurement of the slag reaction is not straightforward. In this study we refined the method developed by Kocaba[16]. Kocaba deduced the effect of slag from the subtraction of a reference calorimetry curve (quartz) from the slag curve. This method assumes that the reaction of the clinker component is the same in the quartz-cement systems with same replacement level. However, above it was shown that the cement hydration is affected by the replacement of slag. Thus, we made an estimation of the slag reaction based on the heat released from the overall reaction and the degree of hydration of cement previously calculated. The calculated contribution of slag can be seen as a relative degree of slag reaction in the blend.

Therefore,

$$H_{slag} = \frac{H_{overall} - H_{cement}}{m_{slag}}$$

Where

H_{slag} is the heat released from the slag reaction per g of slag in the blend

$H_{overall}$ is the total heat released from the hydration of the blend. The value is determined from the cumulative heat released recorded by isothermal calorimetry.

H_{cement} is the heat released from the hydration of clinker phases. The amount of C_3S , C_2S , C_3A consumed were quantified by Rietveld analysis from XRD pattern and are assumed to react i:

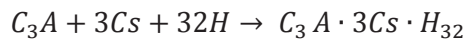
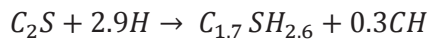
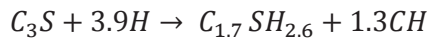


Table 5.3: Enthalpies of the three major reactions in cement hydration

Reaction	H (J/g)
C ₃ S	558
C ₂ S	362
C ₃ A	747

The results are plotted in Figure 5.20 and highlight that the slag reaction is limited at high replacement levels. From 7 days, the slag in the 10% slag-30%quartz PC system reacts more than in the 40% slag PC system. The restriction of the space seems responsible of the limited reaction as when the water to solids ratio was increased, the relative degree of hydration of slag is increased (Figure 5.21). Indeed the cumulative curve shows that from 0 to 7 days both systems have similar kinetics, indicating that space is not limiting the reaction during this period. Then from 7 days, we see that the reaction slows down in the lower w/s system with less space, while it continues in the higher w/s system

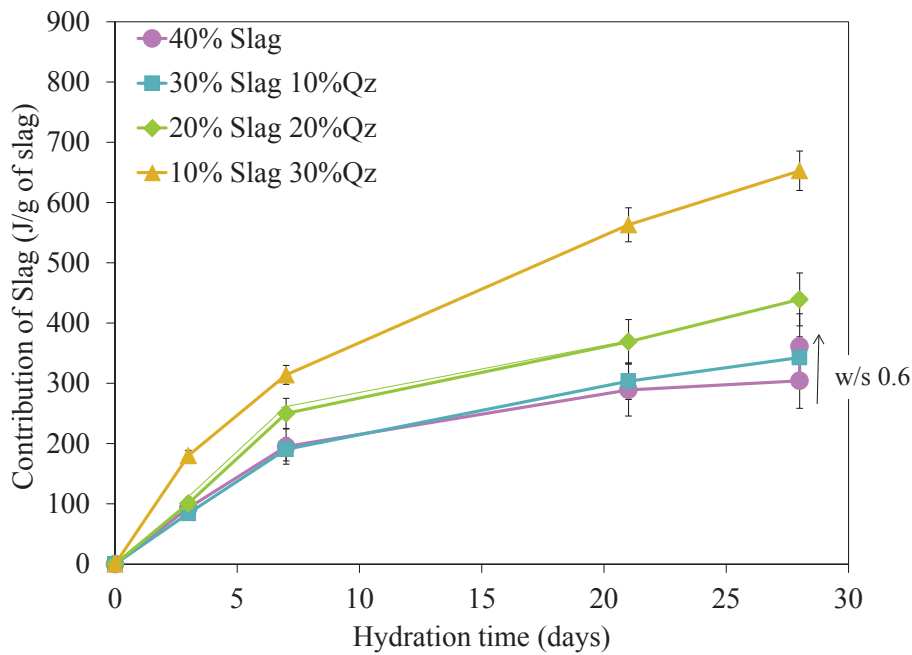


Figure 5.20: Contribution of slag in slag – quartz PC. Reaction of slag is limited from 7 days in the 40% Slag PC paste

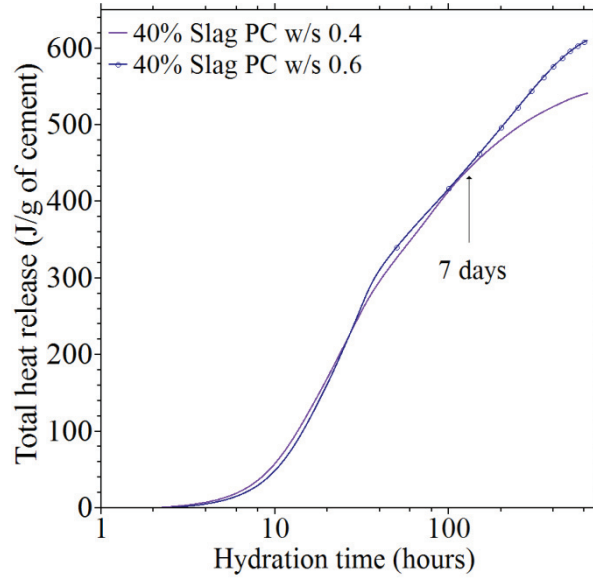


Figure 5.21: Effect of increasing the water/solids ratio in slag-cement systems. Significant effect is visible after 7 days

Reaction of fly ash

The degree of reaction of fly ash was estimated from the consumption of Portlandite measured by TGA technique assuming the following pozzolanic reaction:



Where $C_{0.1}A_{0.29}S$ represents the chemical composition of fly ash (from XRF data); x is the Ca/Si ratio and y is Al/Si ratio of outer C-S-H at 28 days. Both ratios were calculated from EDS measurements and are respectively 1.56 and 0.13.

Thus,

$$DoR (Fly ash) = 100 - \left(\frac{(M_{FA})_i - (M_{FA})_t}{(M_{FA})_i} \times 100 \right)$$

The degree of reaction of fly ash includes the amount of phases that should not react such as quartz and mullite. These phases represent 40% of the Fly ash (Table 2.13). Therefore maximum 60% of the overall fly ash may react.

The calculation does not take into account the calcium coming from the C-S-H initially formed by the reaction of the clinker phases which will have a Ca/Si ratio of around 1.7-1.8 [16].

Thermodynamic simulations with GEMS-PSI software were done to compare with the above results. The simulation was done for each system and time of hydration required. The amounts of the clinker phases from XRD were fixed and the reaction of fly ash was incremented. The degree of reaction of fly ash was deduced from the amount of Portlandite remaining in the system. This value should fit the amount of Portlandite measured by XRD at the required time.

The comparison with GEMS calculation shows that the values are comparable (Table 5.4).

Table 5.4: Comparison of the degree of reaction of fly ash from mass balance calculation and thermodynamic simulation

Systems	days	Degree reaction of fly ash	
		stoichiometry	GEMS
40% Fly ash	28	11%	12.0%
	60	14%	14.5 %
	90	14%	15.0%
10% Fly ash 30% Qz	28	26%	28.0%
	60	36%	38.0%
	90	39%	42.0%

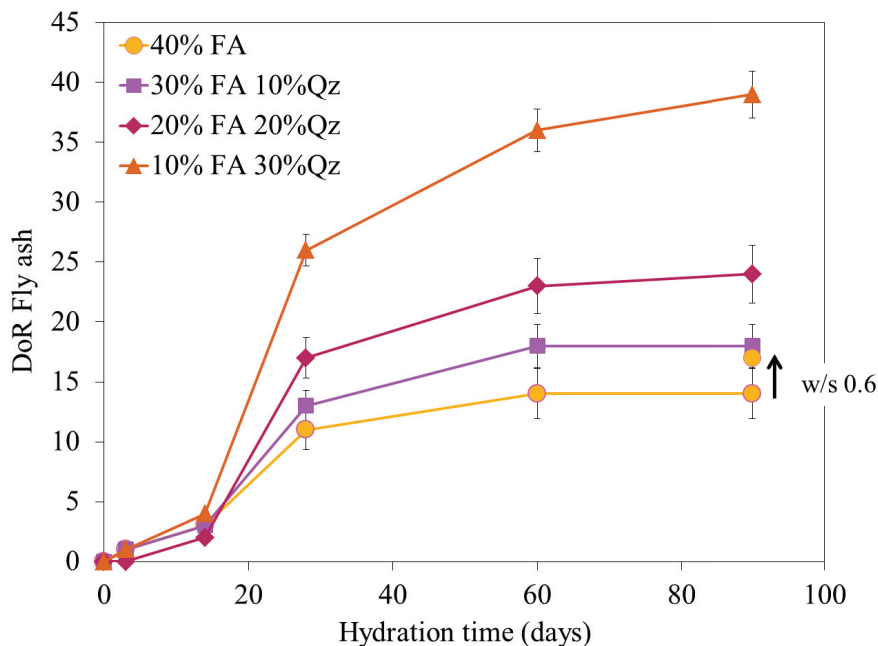


Figure 5.22: Degree of reaction of fly ash in Fly ash – quartz – cement systems with w/s 0.4, unless otherwise stated

The results of degree of reaction of fly ash are plotted in Figure 5.22.

A similar effect to that in slag – quartz PC systems is observed: the reaction of fly ash becomes limited at high replacement level. The degree of reaction of the system containing only 10% fly ash is roughly twice that in the system containing 40% fly ash. At 60 and 90 days the degree of reaction continues to increase for the systems with low fly ash content, but very little for those with high fly ash content.

Substantial amounts of calcium hydroxide remain even in the systems with the highest fly ash content (Figure 5.23) this indicates the reaction of fly ash is not limited by the lack of Portlandite.

Rather the lack of space seems the limiting parameter. For the 40% fly ash system at w/s equivalent of 0.6 the degree of reaction at 90 days is increased. These observations indicate that increasing the water-filled space in system with high replacement prolongs the reaction of fly ash.

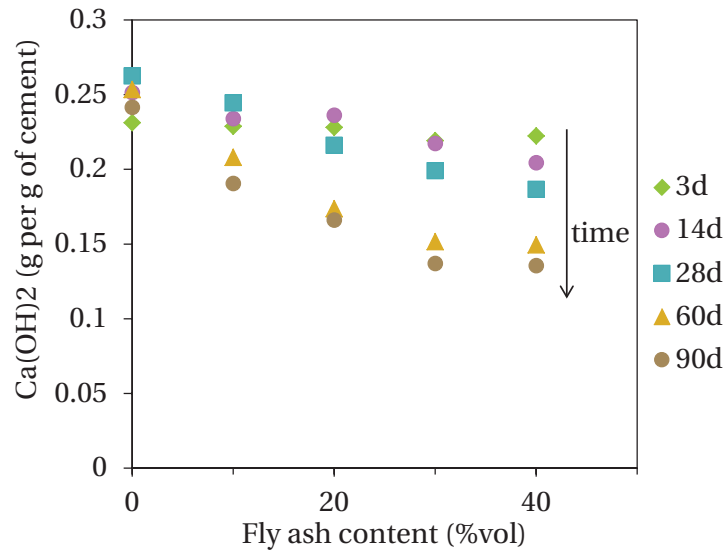


Figure 5.23: Portlandite content in the fly ash - quartz - PC pastes. Substantial amount remains after 90 days in all the systems.

Micrographs in Figure 5.24 and 5.25 support the hypothesis that space is the limiting factor for the reaction of slag and fly ash. The systems with limited reaction: 40% slag and 40% fly ash have a microstructure where the only space remaining is the hydration shells of small grains. Whereas in the systems where the reaction is still on-going (10% SCM – 30% Quartz PC) some large capillary pores are left (Figure 5.24(a) and Figure 5.25(a)).

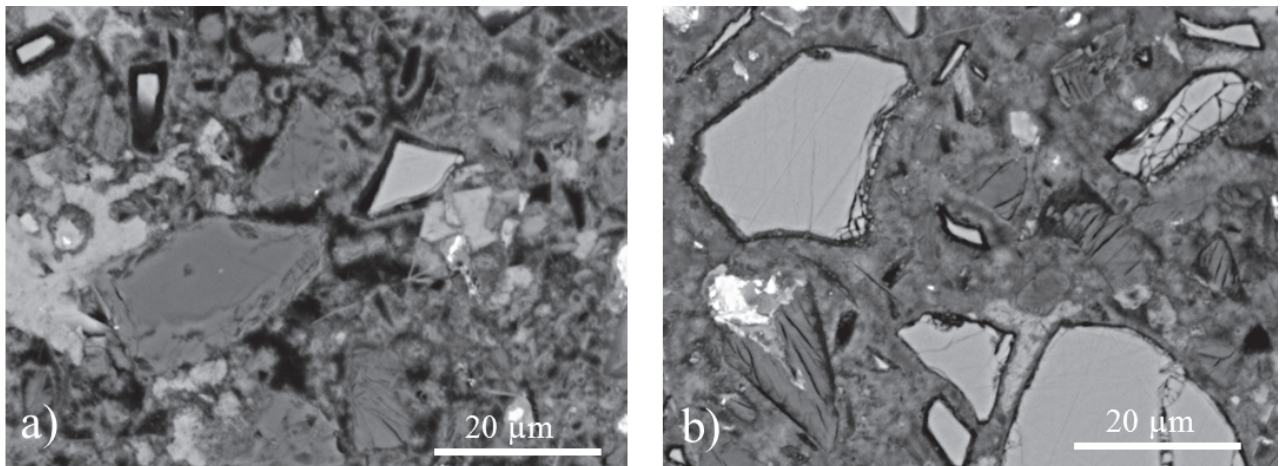


Figure 5.24: Micrographs at 28 days a) 10%slag-30%quartz cement b) 40% slag cement. The microstructure is well filled in the 40% Slag PC system which has the lowest reaction at 28 days.

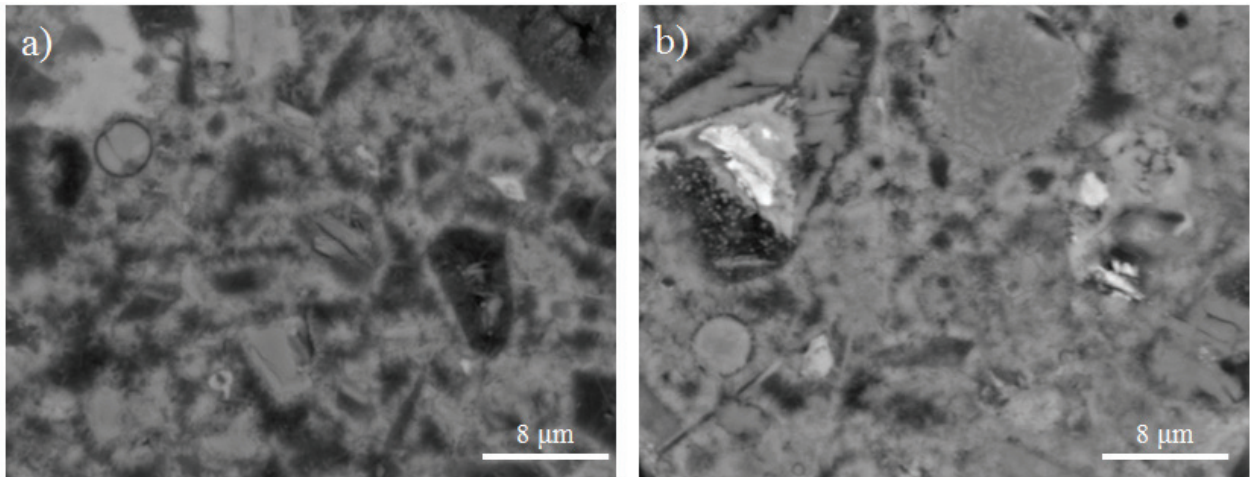


Figure 5.25: Micrographs at 28 days a) 10% Fly Ash PC b) 40% Fly ash PC. The microstructure is more filled in the 40% Fly ash system which has the lowest reaction at 28 days.

3.2.3. Characterization of the pore structure

Our results indicate that PC, slag and fly ash reactions are limited when the microstructure is full of hydrates. The SEM image has a quite low resolution to determine the porosity remaining. Mercury intrusion porosimetry quantifies the total accessible pore volume and the pore entry size of the pore structure. In this section we used this technique to quantify the porosity.

Figure 5.26 shows the MIP curves of the plain Portland cement, 40% slag-PC and 40% Fly ash-PC systems. The pore volume intruded by the mercury and the critical radius, both decreases with curing time as the hydrates are filling the pores.

In the case of the Portland cement, the pore volume decreases rapidly over the first 14 days and then decreases more slowly. The critical radius which corresponds to the maximum of the size distribution curve, decreases until 14 days. At this time, it reaches a size about 8-10 nm which does not decrease further with time. Porosity in systems with slag and fly ash show similar effect. Once the critical radius is about 7-8 nm it does not decrease further in size while the total porosity continues to decrease slowly. In other studies using MIP, a similar minimal pore entry radius (~7 nm) was reported for blended and plain cement systems [30].

Figure 5.27 shows the distribution of the pore size of the ternary systems (with slag and fly ash). The 40% slag system and 40% fly ash systems both have a critical radius about 6 nm and are the systems where the reaction is limited (Figure 5.20 and 5.22). Whereas in the systems with larger critical radius (e.g. 10% slag – 30% quartz) the reaction continues.

Therefore, in all the systems whether blended or unblended, C-S-H phase fills the pore space until the capillary pore reaches the size in the range of 6-8 nm. Afterward only the total porosity decreases.

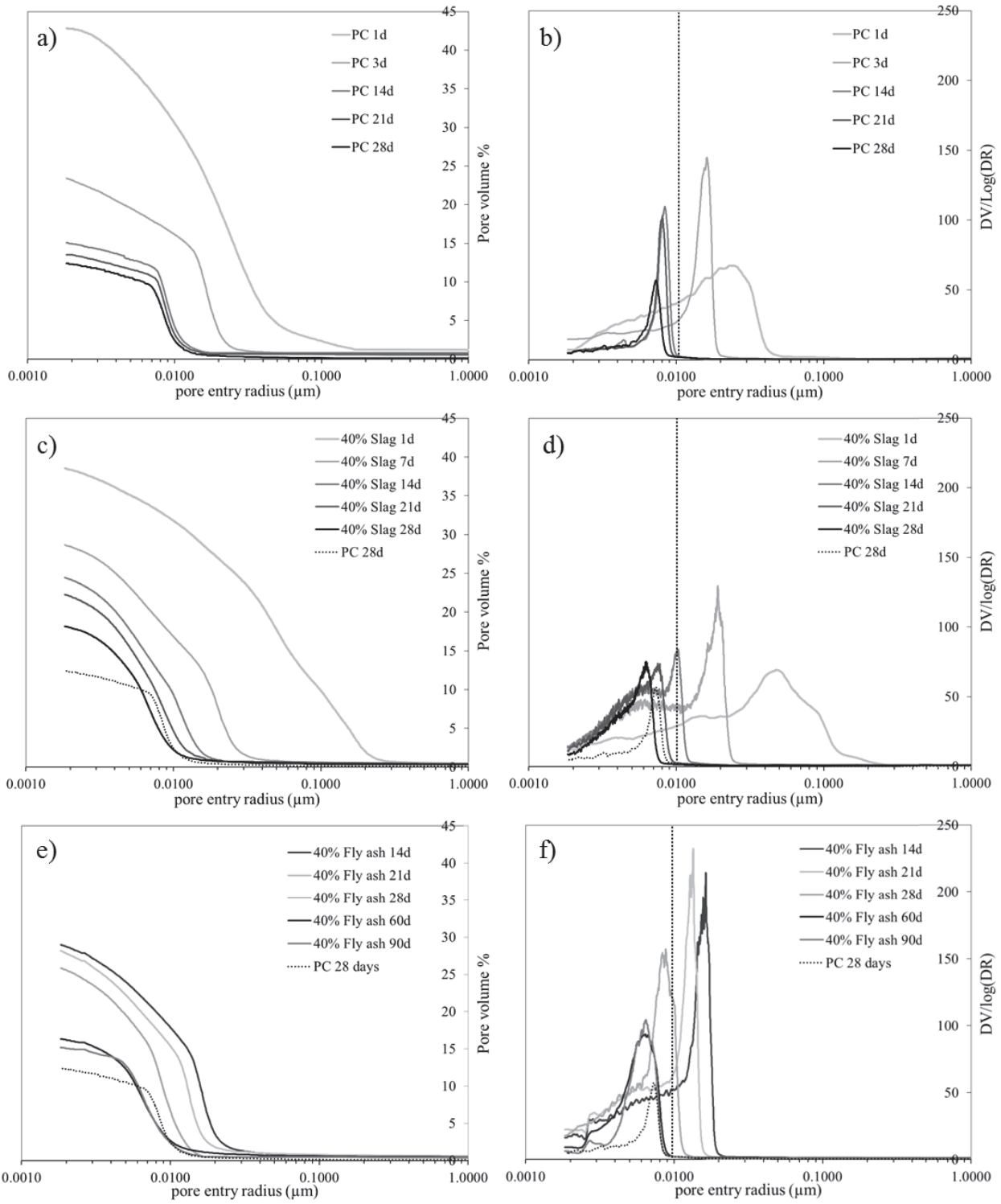


Figure 5.26: Cumulative and pore size distribution curves from MIP of a) and b) PC, c) and d) 40% Slag PC, e) and f) 40% Fly ash PC

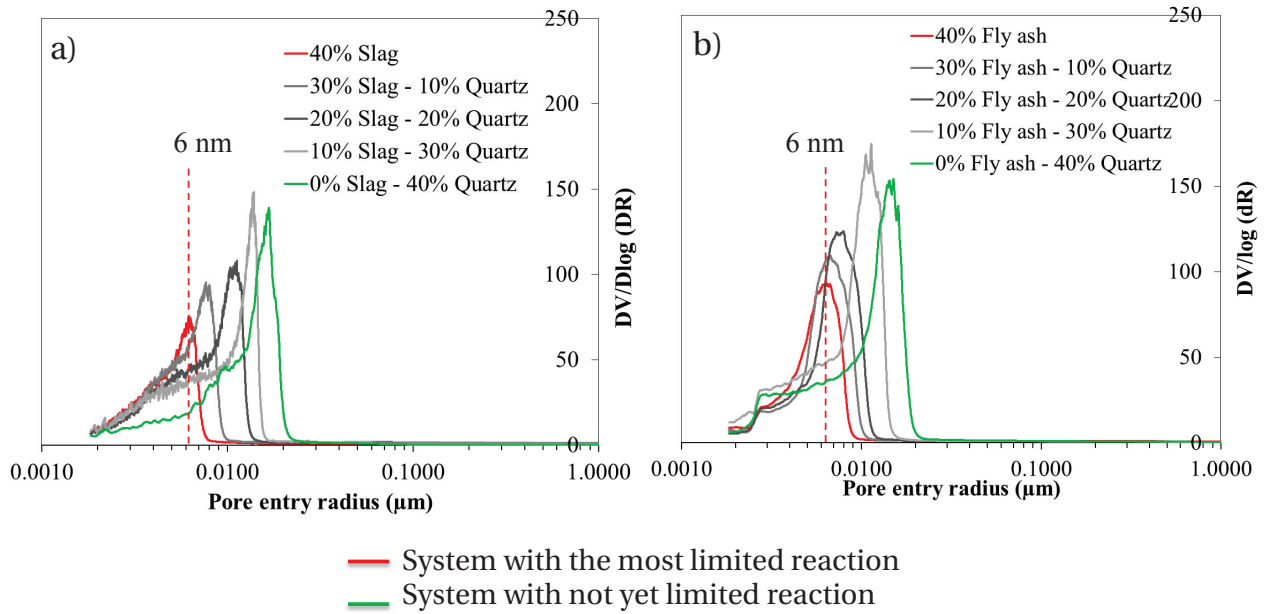


Figure 5.27: The reaction of slag (a) or fly ash (b) is limited in the systems where the critical radius reaches 6 nm

3.2.4. Kinetics

The presence of slag and fly ash changes the kinetics mainly during the transition regime (Figure 5.28). From this stage our results show that the slag and slightly latter the fly ash are reacting. Micrographs and calculations of the degree of reaction showed that cement, slag and fly ash reactions are limited by space restriction. C-S-H is filling the capillary pores and reduces the space available for further formation of C-S-H. As a consequence the kinetics gradually slows down: it is the transitory regime. The rate of this regime is dependent on the space between grains.

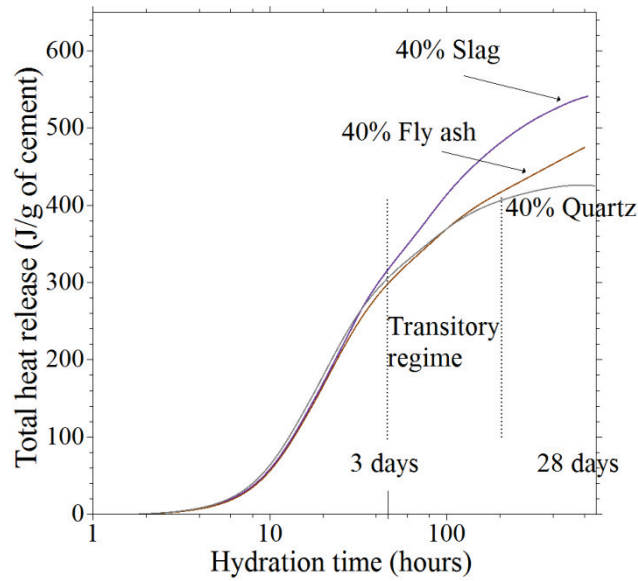


Figure 5.28: Cumulative heat curves of cement, 40% quartz PC, 40% Fly ash PC and 40% slag PC. The reaction of slag mainly affects the transitory regime while Fly ash reaction occurs later

The rate of the very late age was recorded with chemical shrinkage. Figure 5.29 compares the curves of cement paste and 40% Slag PC. The rate of very late regime was similar for both cement and slag cement systems, which suggests that similar mechanism is controlling the kinetics in both systems. Combining MIP results and chemical shrinkage curves we observe that the rate becomes constant when the pore entry size reached the minimal size (about 6-8 nm) which does not reduce further in size.

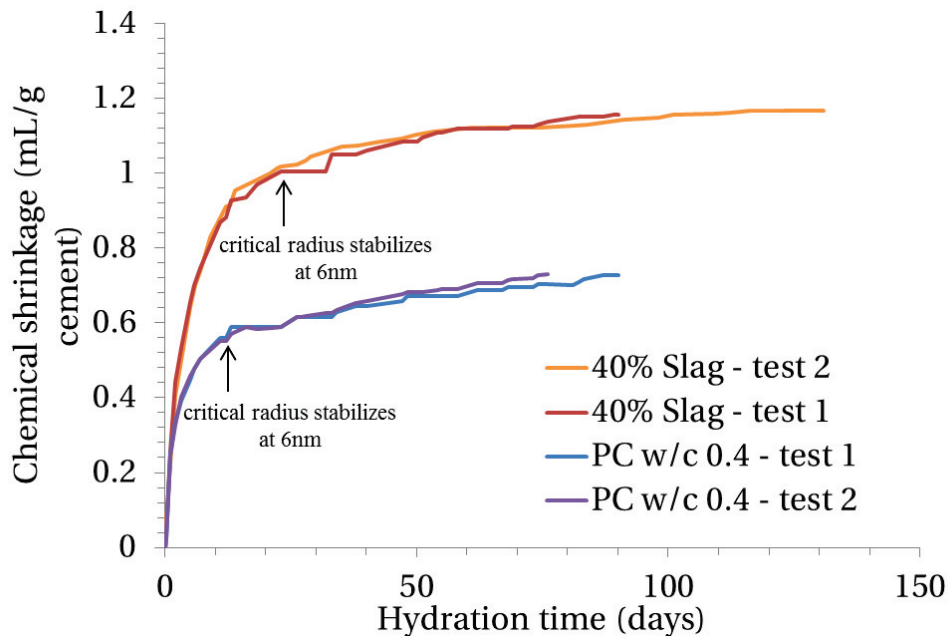


Figure 5.29: Kinetics slow down when the critical radius stabilizes

The stabilization of the kinetics and the size of the critical radius might be explained by the difficulty to grow in very small pores. Indeed, in a general sense, as the pore size decreases the solution needs to reach higher levels of supersaturation for precipitation to take place in it [37, 38].

Figure 5.30 shows the data for ettringite crystallization. For a radius of 6 nm, the Saturation index is significantly increased. C-S-H could be supposed to follow the same behavior. An estimation of the radius below which C-S-H cannot grow based on the Freundlich equation was 7.7 nm (details of the calculation in Appendix 2). This value matches well our MIP data. Thus the growth of C-S-H becomes more difficult with reducing the pore size and might explain the stabilization of the critical radius as well as the slow-down of the kinetics.

From our results the total pore volume accessible to mercury still decreases, this may be explained by the fact that MIP measures only the pore entry size and there may be “bigger” spaces beyond the pore entry which continue to be filled. In the smaller pores, we can suppose that C-S-H continues to growth by addition of extra intersheets to its bulk structure.

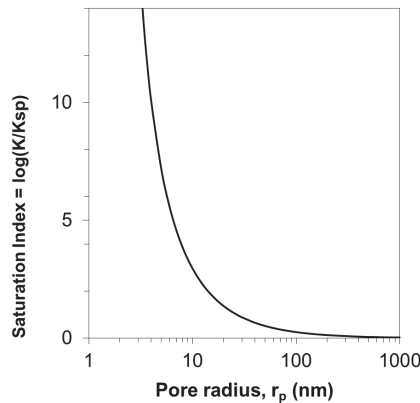


Figure 5.30: Decreasing pore entry radius, increase the pressure and thus the SI. Here the data correspond to ettringite crystallization. Adapted from Bizzozero[39]

At this stage, this is fairly tentative hypothesis and there could be other explanations for the stabilization of the pore size. For example, the increasing energy of the pore surfaces with higher curvature could also be important.

4. Evolution of the pore structure

The previous MIP results comparing cement, slag and fly ash systems showed a different development of the pore structure. This section focuses on the distribution of the hydrates from the SCM reaction (respectively hydraulic and pozzolanic from slag and fly ash) and the subsequent changes on the microstructure. We want to know if slag and fly ash fill the space like cement.

We used ternary systems combining inert filler (quartz), SCM (slag or fly ash) and cement in different proportion to investigate the sole contribution of the SCM.

4.1. Phase assemblages

The volume of the phase in cement, 40% slag and 40% fly ash at 28 days has been calculated with the GEMS thermodynamic model. We use the degrees of reaction previously measured. The C-S-H density in GEMS was 2.2 g/cm³ whether the origin of the C-S-H (from cement or SCM reaction). The results are plotted in Figure 5.31. Based on the GEMS assumptions, blended systems are expected to have a lower total volume of phase than in cement paste.

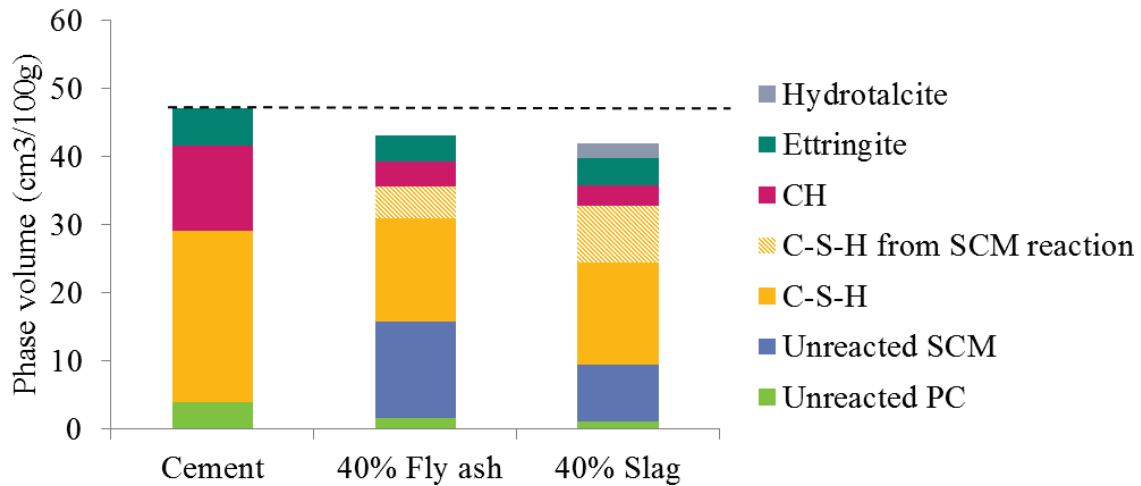


Figure 5.31: Comparison of the phase volume calculated from GEMS of PC at 28 days (DoH 0.88) ; 40% Fly ash PC at 90 days (DoR 0.15) and 40% Slag PC at 28 days (DoR 0.40)

Calculations at 90 days with fly ash – quartz cement systems indicate that we expect similar porosity in all the systems if the hydrates have similar filling ability (Figure 5.32). However, MIP data (Figure 5.33) show that the systems have different total porosity. The contradiction between the thermodynamic calculations and the porosity measured is probably caused by different filling ability of the C-S-H in those blended systems. Others works have revealed this inconsistency [28, 30, 35, 40].

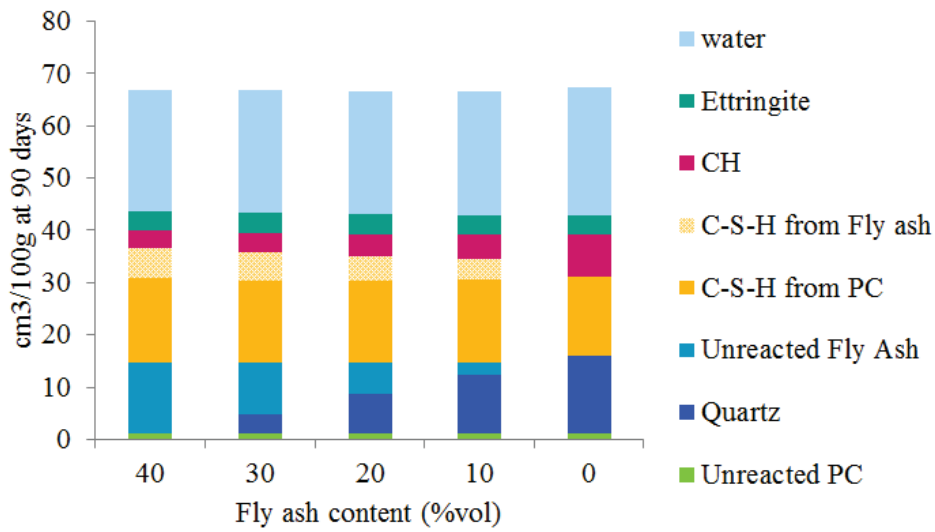


Figure 5.32: Volume of the phases in the Fly ash – quartz cement systems at 90 days

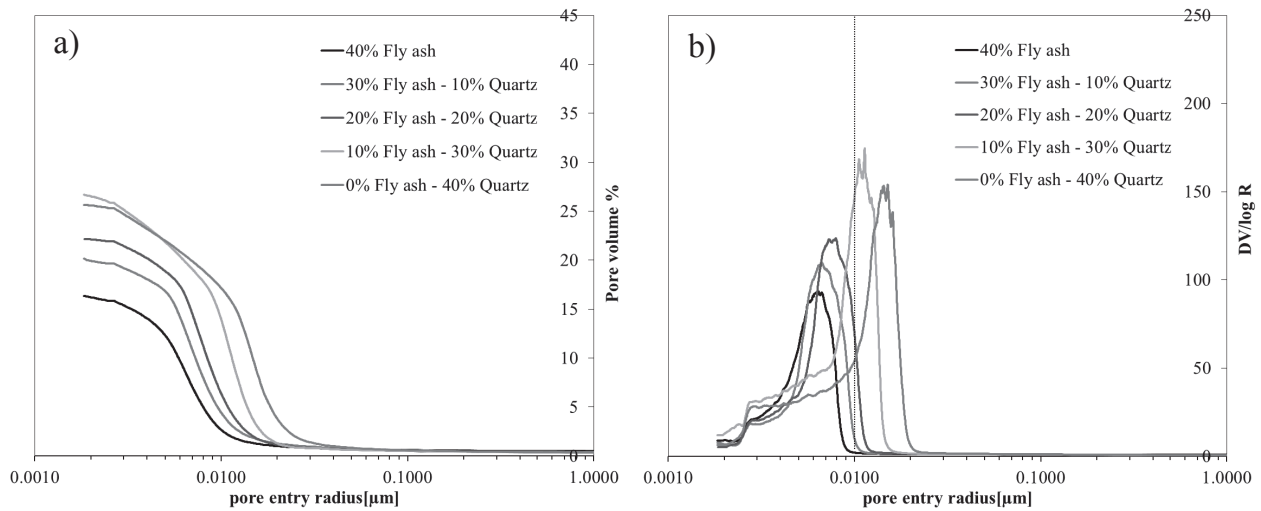


Figure 5.33: MIP curves of Fly ash – Quartz PC systems a) cumulative porosity b) Pore size distribution

4.2. Filling ability

Figure 5.34 summarizes the data of the pore volume as a function of the critical entry pore radius of fly ash, slag cement systems compared to cement systems. The results demonstrate clear differences in how the hydrates from the reaction of clinker, slag and fly ash fill space. The slag seems to be more effective in reducing the total porosity as well as the critical pore entry size than fly ash.

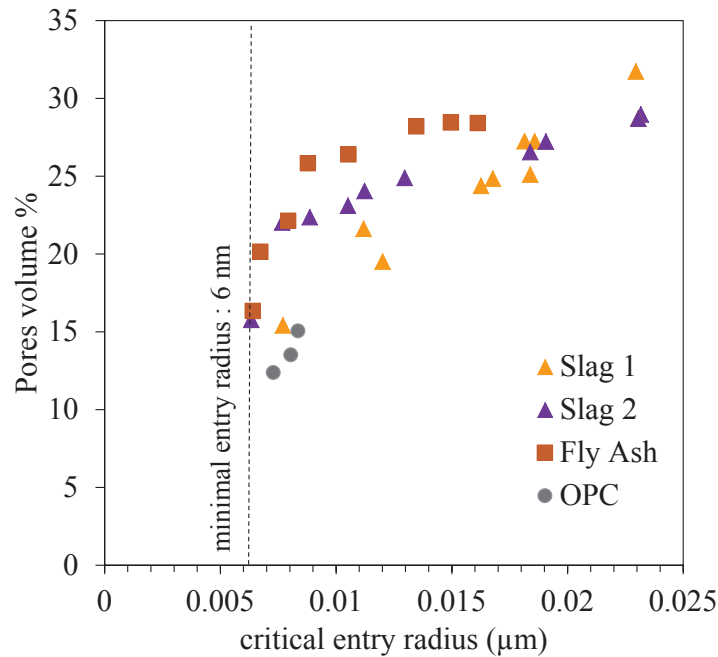


Figure 5.34: Pore volume in slag PC pastes as a function of the critical radius

In Figure 5.35 the reduction in total pore volume and the critical pore entry size are plotted as a function of the degree of reaction. Thus, we can compare the efficiency of cement, slag and fly ash in filling the pores. For the clinker the degree of reaction is measured directly by XRD, for fly ash it is expressed as the amount of calcium hydroxide reacted and for slag as the amount of extra heat by calorimetry.

Although the scales for degree of reaction are not strictly comparable clear differences in the trends emerge. Unsurprisingly, the clinker reaction is the most effective at reducing both total pore volume and critical pore entry size. The slag shows an almost linear reduction of the critical pore entry size with degree of reaction. While, the total porosity seems to reduce more slowly at the start and then more rapidly. Finally the fly ash is clearly less effective in modifying the pore structure. Although, the pore entry diameter reduces fairly consistently with degree of reaction, there is a latent period of reaction before the total pore volume decreases.

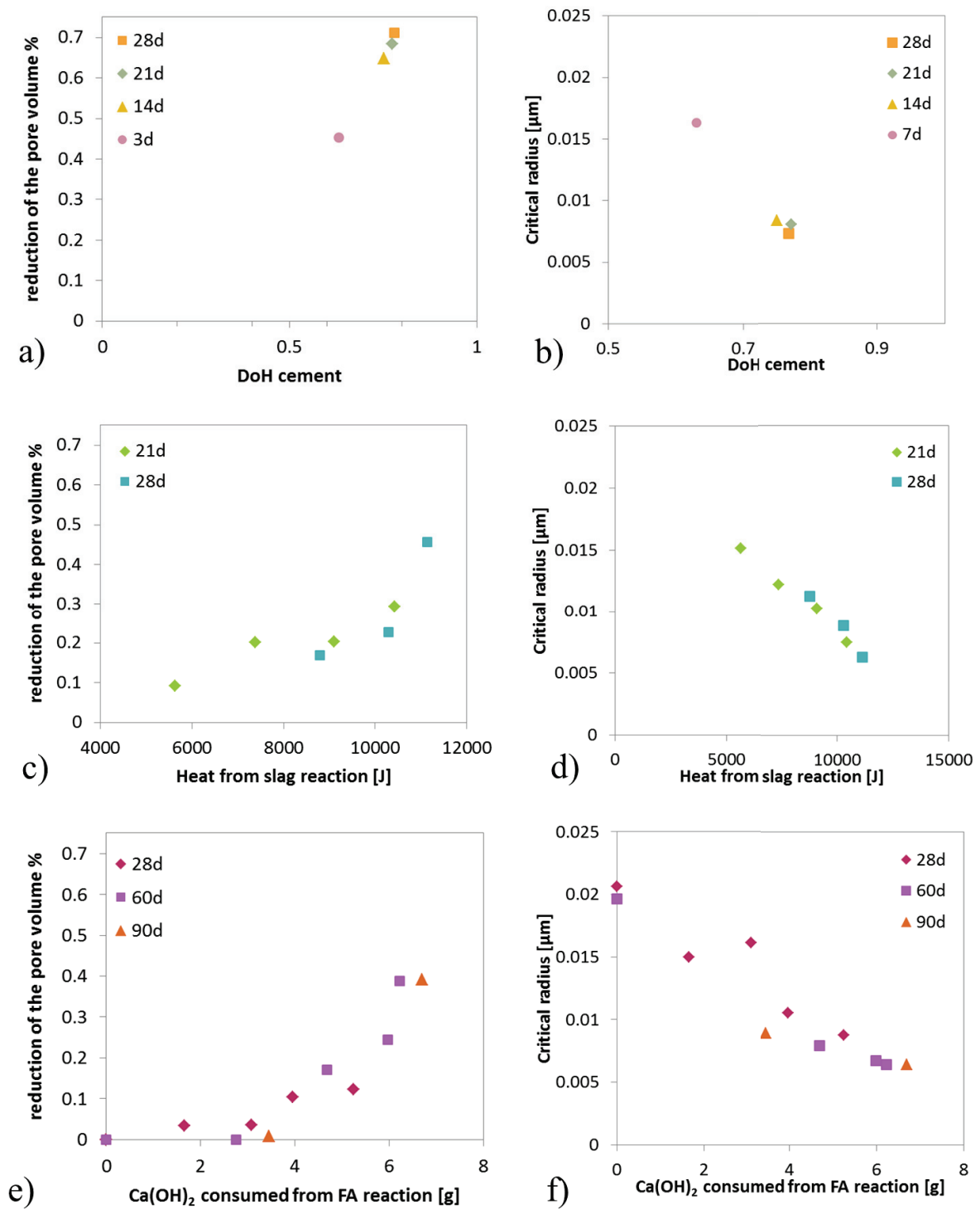


Figure 5.35: Pore volume reduction and critical radius a) and b) in cement paste; c) and d) in Slag-cement system e) and f) in fly ash cement system

Examination of the effect of water to cement ratio on the three systems also underlines the differences between plain cement paste and blends with slag and fly ash. The micrographs in Figure 5.37 compare the effect of the water/solids ratio (0.4 and 0.6) for PC, 40% slag and 40% fly ash. The effect of increasing the water/solids ratio is different in the slag/PC blend to the other systems.

For the slag pastes, although the water/solids ratio 0.6 provides more space, most of the capillary porosity seems to be filled. Large clumps of AFm phase are a notable feature in both systems. At higher water/solids = 0.6, these form in the spaces between particles, whereas in the system with w/s 0.4 these clumps occur in the shells of hydration product from small cement grains (Hadley grains), which would appear to be the only space available in this case.

These observations are supported by the MIP data from the same mixes show in Figure 5.36. At w/s 0.4 the systems all have the same critical pore entry size, while the systems with slag and fly ash have somewhat higher total porosities. When the water to solids ratio increases to 0.6 the critical pore entry radius increase for all the systems, but much less for the system with slag.

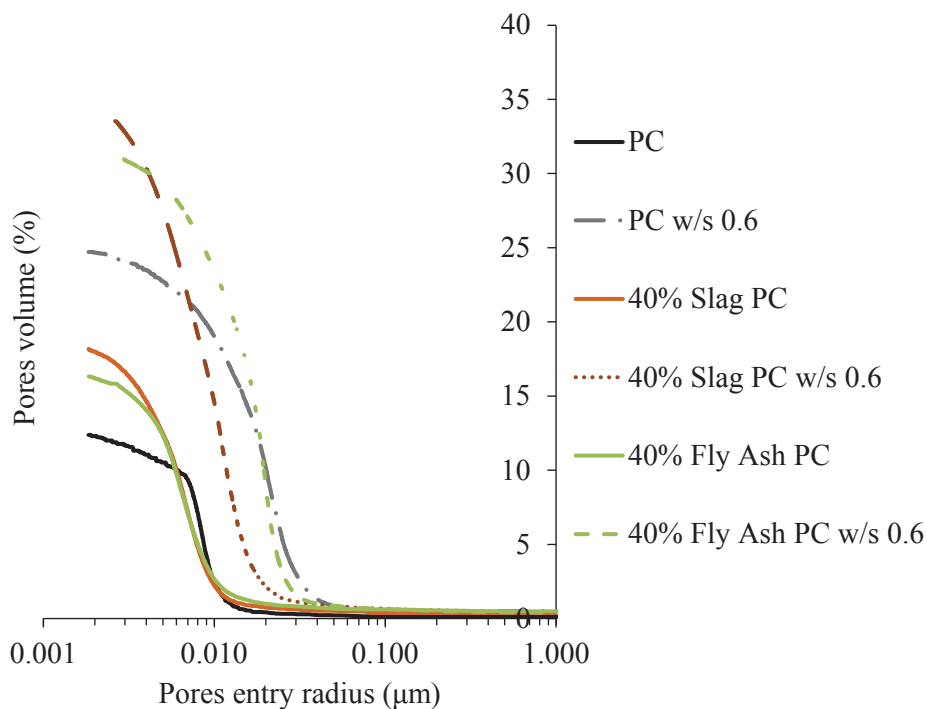


Figure 5.36: Effect of increasing w/s ratio on MIP curve at 28 days of PC, 40%Slag and 40% Fly ash systems at 60 days

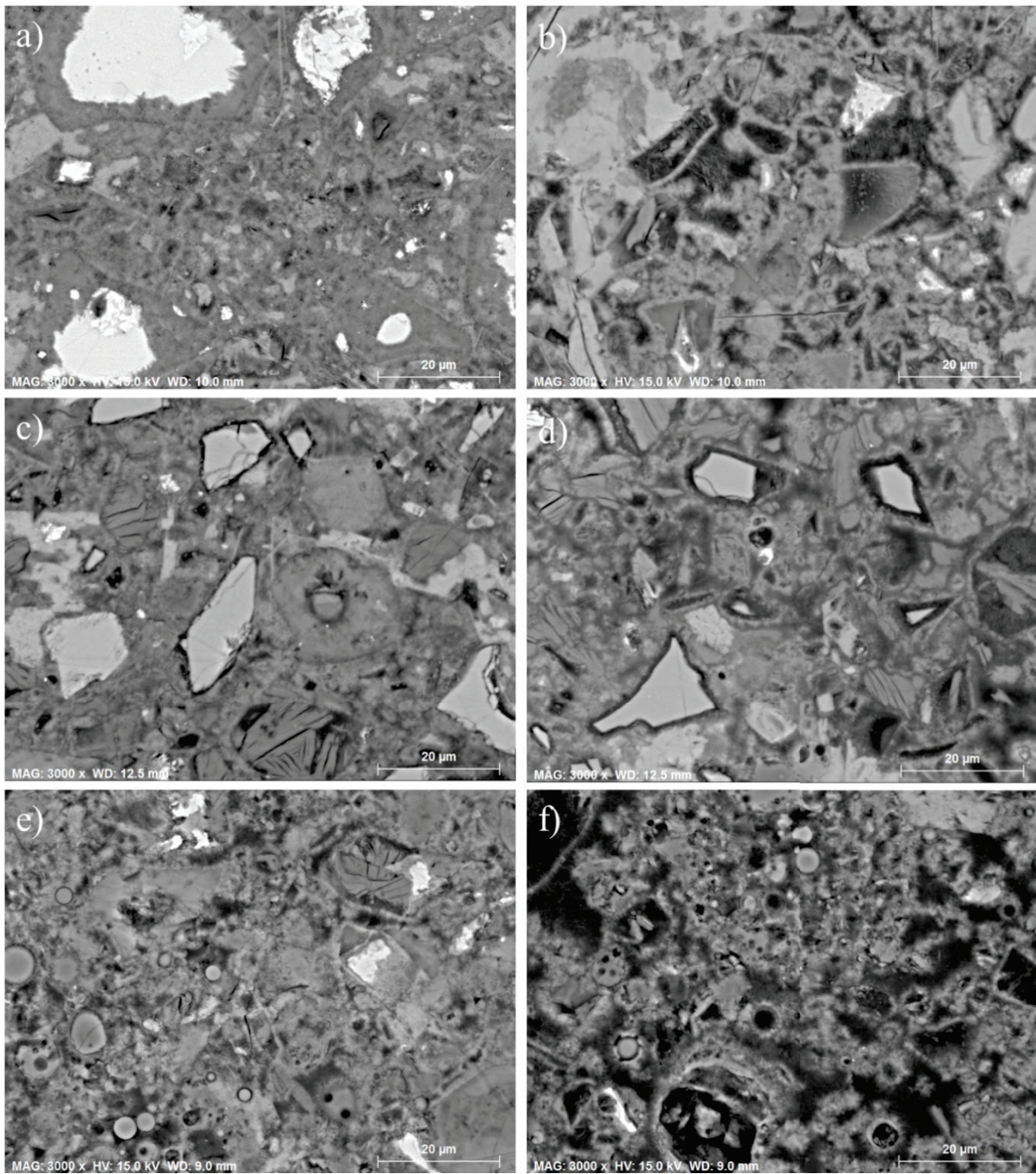


Figure 5.37: Microstructure of PC at 28 days a) w/s 0.4 b) w/s 0.6; 40% Slag at 28 days c) w/s 0.4 d) w/s 0.6; 40% Fly ash e) w/s 0.4 f) w/s 0.6

4.3. Discussion

Filling space

The ability to fill the pores is important for mechanical properties and durability. It has been suggested in some previous publications that the SCM's hydrates would fill the pores differently than cement. Our results demonstrate that slag, fly ash and cement have different filling ability. Portland cement is the most effective, the pore volume decreases with the critical radius through the hydration time.

Fly ash is less effective than slag. However they both present similarities. While the degree of reaction is increased, the critical radius is reduced whereas the porosity is slightly reduced in those blended systems. In other words, hydrates are forming, mainly C-S-H, they decrease the critical radius but not that much the total porosity. The explanation that we suggest is that the C-S-H is growing as needles which might create smaller pores but no significant reduction of the total porosity. There are two pieces of evidence to support this theory.

First the micrographs at high resolution show needles in the large capillary pores in the Slag and Fly ash PC systems (Figure 5.38). Secondly ^1H NMR data on the slag- quartz PC systems indicate that increasing the slag fraction decreases the gel water/ intersheet ratio (interlayer in Figure 5.39) [41]. A similar effect on C-S-H was found in the system where gypsum was still present. In those systems, the C-S-H was needles with diverging structure. Therefore it is plausible that C-S-H from SCM are needles that decrease the critical radius but nor much the total porosity.

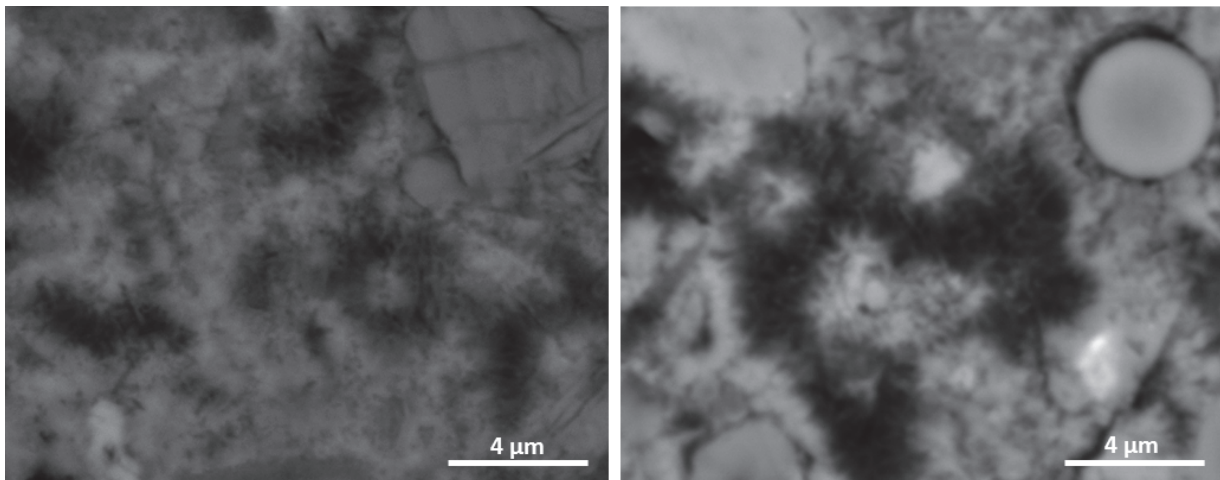


Figure 5.38: Detail of the microstructure (left) 40% Slag PC system at 28 days (right) 40% Fly ash PC system w/s 0.6 at 28 days. Needles are visible in both microstructures

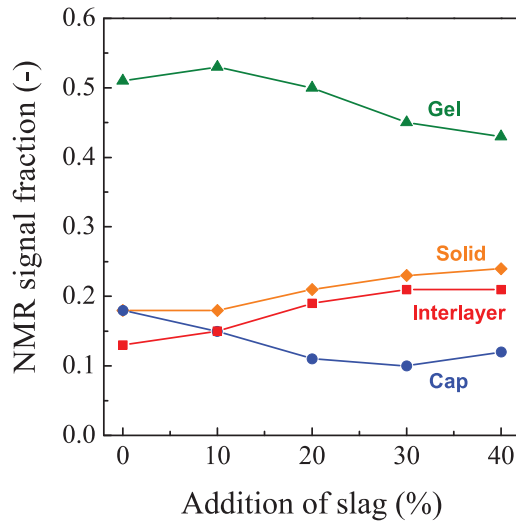


Figure 5.39: ^1H NMR on the Slag – Quartz PC systems. Gel water/interlayer ratio decreases with increasing slag amount

Growth of C-S-H at late age

The results show that the kinetics slows down when the pore entry size reaches $\sim 7\text{nm}$. In such small pores, the growth of C-S-H becomes difficult due to the increase of the SI. As a consequence the growth mechanism of C-S-H might change. Some elements suggest that it could be related to the formation of extra intersheet. The results indicate that this phenomenon would control the kinetics in all the systems blended or unblended.

5. Summary

The present work brings new insights on the mechanisms of hydration at later ages in plain and blended cements.

The link between the reaction of different components in blended cements and the evolution of pore structure has been clarified.

- Our results indicate that PC, slag and fly ash reactions are limited at later ages by the lack of capillary water-filled pores. This effect is significant for high replacement level in blended systems. Restriction of fly ash and slag reactions with increasing levels of replacement were reported by several authors [20, 23, 42]. However it could not be concluded if this restriction was due to the SCM itself or cement as the studies were done at different water/cement ratios. Fly ash does not appear to impact the degree of reaction of the clinker component, probably because the reaction is much slower. Slag on the other hand seems to compete with the clinker at later ages such that the degrees of reaction of both components are decreased.
- The reaction of slag seems to be more efficient than that of fly ash in modifying the porosity. The slag affects both pore entry size and total porosity in a similar way and, in addition,

introduces a new population of pores which are finer than those produced in plain cement paste. Different filling ability of the porosity has been observed for fly ash and slag systems. It also seems to be more effective at reducing the pore entry size at higher water to solids ratios. In fly ash systems it seem that a much higher degree of reaction is needed to have a significant impact on the total pore volume by MIP, even if there is an earlier impact on the critical pore entry size.

- In all the systems studied there seems to be a size for the critical pore entry which does not reduce further. When this size is reached the kinetics was observed to increase more slowly. The stabilization of the pore at about 6 nm can be explained by the increase of the saturation index for growth in the pore [37, 38]. The formation of interlayers or intersheets in the C-S-H structure, was also reported to occur at later ages. This might lead to a decrease of the total porosity but might not affect the reduction of the critical pore radius. Both explanations indicate that a change to slower growth is occurring at later ages.

This work brings more information on the mechanism controlling the kinetics after the main peak of hydration. Coupling data from micrographs, calorimetry, chemical shrinkage and MIP indicate that the kinetics might be controlled, up to the later age regime, by the formation of C-S-H. Afterwards, the kinetics of the later age need to be further investigated. However some elements suggest that it might be related to the growth of C-S-H by extra intersheets. The mechanism behind does not seem to be controlled by diffusion (Appendix 3). Figure 5.40 summarizes the main finding of this section.

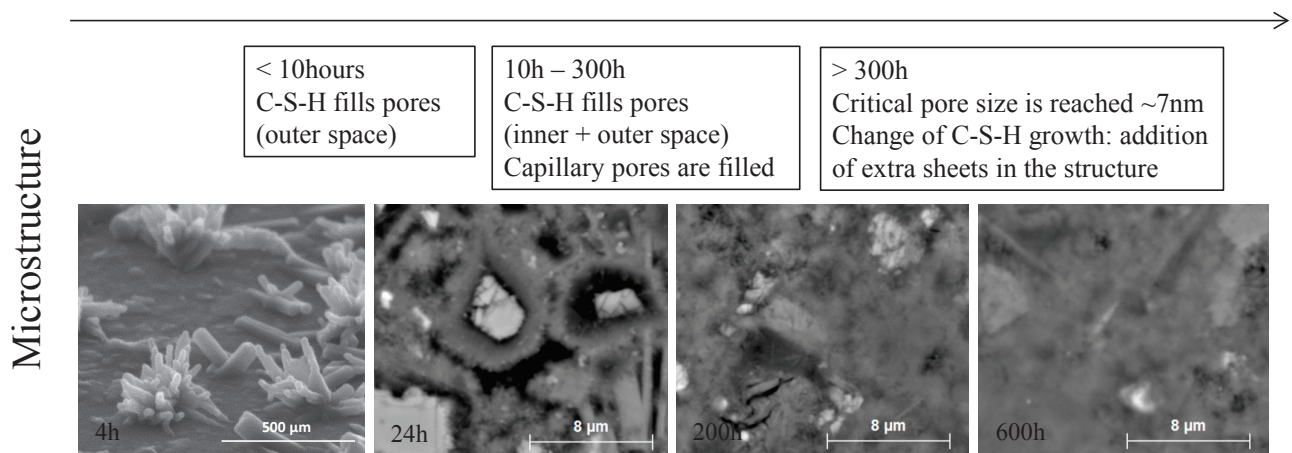


Figure 5.40: Microstructural development during the hydration

6. References

1. Gartner, E., et al., *Hydration of Portland cement*. Structure and performance of cements, 2002. **13**: p. 978-0.
2. Lea, F.M., *The chemistry of cement and concrete*. 1970.
3. Thomas, J.J., et al., *Modeling and simulation of cement hydration kinetics and microstructure development*. Cement and Concrete Research, 2011. **41**(12): p. 1257-1278.
4. Bazzoni, A., *Study early hydration mechanisms of cement by mean of electron microscopy*, in *LMC*. 2014, Ecole Polytechnique Fédérale de Lausanne: Lausanne.
5. Scrivener, K., *The development of microstructure during the hydration of Portland cement*, in *Metallurgy and Materials Science*. 1984, Imperial College of Science and technology: London.
6. Bullard, J.W., *Mechanisms of cement hydration*. Cement and Concrete Research, 2010.
7. Gallucci, E., P. Mathur, and K. Scrivener, *Microstructural development of early age hydration shells around cement grains*. Cement and Concrete Research, 2010. **40**(1): p. 4-13.
8. Costoya, M., *Kinetics and microstructural investigation on the hydration of tricalcium silicate*. 2008, EPFL: Lausanne.
9. Thomas, J.J., *A new approach to modeling the nucleation and growth kinetics of tricalcium silicate hydration*. Journal of the American Ceramic Society, 2007. **90**(10): p. 3282-3288.
10. Bishnoi, S. and K.L. Scrivener, *Studying nucleation and growth kinetics of alite hydration using μ ic*. Cement and Concrete Research, 2009. **39**(10): p. 849-860.
11. Costoya Fernández, M.M., K. Scrivener, and E. Gallucci, *Effect of particle size on the hydration kinetics and microstructural development of tricalcium silicate*. 2008.
12. Jennings, H.M., *A model for the microstructure of calcium silicate hydrate in cement paste*. Cement and Concrete Research, 2000. **30**(1): p. 101-116.
13. Kirby, D.M. and J.J. Biernacki, *The effect of water-to-cement ratio on the hydration kinetics of tricalcium silicate cements: Testing the two-step hydration hypothesis*. Cement and Concrete Research, 2012. **42**(8): p. 1147-1156.
14. Garrault, S., T. Behr, and A. Nonat, *Formation of the C-S-H Layer during Early Hydration of Tricalcium Silicate Grains with Different Sizes*. The Journal of Physical Chemistry B, 2005. **110**(1): p. 270-275.
15. Muller, A.C.A., et al., *Densification of C-S-H Measured by 1H NMR Relaxometry*. The Journal of Physical Chemistry C, 2012. **117**(1): p. 403-412.
16. Kocaba, *Development and evaluation of methods to follow microstructural development of cementitious systems including slags*. 2009, EPFL: Lausanne.
17. Deschner, F., et al., *Hydration of Portland cement with high replacement by siliceous fly ash*. Cement and Concrete Research, 2012. **42**(10): p. 1389-1400.
18. Sakai, E., et al., *Hydration of fly ash cement*. Cement and Concrete Research, 2005. **35**(6): p. 1135-1140.
19. Weerdt, D., *Hydration mechanisms of ternary Portland cements containing limestone powder and Fly Ash*. Cement and Concrete Research, 2011. **41**: p. 279-291.
20. Haha, M.B., K. De Weerdt, and B. Lothenbach, *Quantification of the degree of reaction of fly ash*. Cement and Concrete Research, 2010. **40**(11): p. 1620-1629.
21. Kocaba, *Methods for determination of degree of reaction of slag in blended cement pastes*. Cement and Concrete Research, 2012. **in Press**.
22. Paweł T. Durdziński, C.F.D., Mohsen B. Haha, Karen L. Scrivener, *A detailed study of the reaction of fly ash phases in hydrating cement paste*. submitted in cement and Concrete research.
23. R. Taylor, I.G.R., *Composition and microstructure of 20-year-old ordinary Portland cement-ground granulated blast-furnace slag blends containing 0 to 100% slag*. Cement and Concrete Research, 2010. **40**: p. 971-983.

24. Escalante, J.I., et al., *Reactivity of blast-furnace slag in Portland cement blends hydrated under different conditions*. Cement and Concrete Research, 2001. **31**(10): p. 1403-1409.
25. Lumley, J.S., et al., *Degrees of reaction of the slag in some blends with Portland cements*. Cement and Concrete Research, 1996. **26**(1): p. 139-151.
26. Rossen, J., *Composition and morphology of C-A-S-H in pastes of alite and cement blended with supplementary cementitious materials*. 2014, Ecole Polytechnique Fédérale de Lausanne: Lausanne.
27. Richardson, I. and G. Groves, *Microstructure and microanalysis of hardened cement pastes involving ground granulated blast-furnace slag*. Journal of Materials Science, 1992. **27**(22): p. 6204-6212.
28. Lothenbach, B., K. Scrivener, and R.D. Hooton, *Supplementary cementitious materials*. Cement and Concrete Research, 2011. **41**(12): p. 1244-1256.
29. Richardson, *The nature of C-S-H in hardened cements*. Cement and Concrete Research, 1999. **29**: p. 1131-1147.
30. Moreira, M., *Pore structure in blended cement pastes*, in *Department of Civil Engineering*. 2011, Technical University of Denmark.
31. Day, R.L. and B.K. Marsh, *Measurement of porosity in blended cement pastes*. Cement and Concrete Research, 1988. **18**(1): p. 63-73.
32. Hooton, R.D., *Permeability and pore structure of cement pastes containing fly ash, slag, and silica fume*. Blended Cements, ASTM STP, 1986. **897**: p. 128-143.
33. Feldman, R.F. and N.R.C.C.D.o.B. Research, *Pore structure formation during hydration of fly-ash and slag cement blends*. 1982: National Research Council Canada, Division of Building Research.
34. Taylor, H.F., *Cement chemistry*. 1997: Thomas Telford.
35. Whittaker, M., et al., *The role of the alumina content of slag, plus the presence of additional sulfate on the hydration and microstructure of Portland cement-slag blends*. Cement and Concrete Research, 2014. **66**(0): p. 91-101.
36. Scrivener, K.L. and A. Nonat, *Hydration of cementitious materials, present and future*. Cement and Concrete Research, 2011. **41**(7): p. 651-665.
37. Bizzozero, J., C. Gosselin, and K.L. Scrivener, *Expansion mechanisms in calcium aluminate and sulfoaluminate systems with calcium sulfate*. Cement and Concrete Research, 2014. **56**(0): p. 190-202.
38. Steiger, M., *Crystal growth in porous materials—I: The crystallization pressure of large crystals*. Journal of Crystal Growth, 2005. **282**(3-4): p. 455-469.
39. Bizzozero, J., *Hydration and dimensional stability of calcium aluminate cement based systems*, in *Faculté sciences et technique de l'Ingénieur*. 2014, Ecole Polytechnique Federale de Lausanne: Lausanne.
40. Scrivener, K. and A. Nonat, *Hydration of cementitious materials, present and future*. Cement and Concrete Research, 2011. **41**: p. 651-665.
41. Muller, A.C.A., *Charaterization of porosity and C-S-H in cement pastes by 1H NMR*, in *Faculté des Sciences et Techniques de l'Ingénieur*. 2014, Ecole Polytechnique Federale de Lausanne: Lausanne.
42. Lam, L., Y.L. Wong, and C.S. Poon, *Degree of hydration and gell/space ratio of high-volume fly ash/cement systems*. Cement and Concrete Research, 2000. **30**(5): p. 747-756.

Chapter 6

Conclusions & Perspectives

The objective of this work was to understand the impact of SCM on the kinetics and the microstructure development in blended systems. SCM were considered as inert materials (filler) and as reactive materials in the cement paste.

Important conclusions from this work are listed below:

1. Filler effect

- Fillers accelerate the hydration of the clinker phase in a blend, but this effect at early age cannot simply explained by the provision of extra surfaces for nucleation as formerly suggested. Our results show a clear relation between the inter-particle distance and the kinetics of the acceleration period. This can be explained by the shearing between particles which increases as the inter-particle distance decrease.
- During the deceleration period, the second C_3A reaction is occurring earlier and faster with increasing the replacement level of filler in the blend. It has been shown that this effect is caused by the faster depletion of sulfate ions, due to the faster reaction of clinker phases and faster formation of C-S-H.

2. Impact of Slag and Fly ash

- Due to the slower reaction of the SCMs, the SCMs only contribute significantly after the main clinker reactions. Nevertheless, it has been shown that during this inert period, the SCM particles act as filler and thus accelerate the kinetics.
- Slag and fly ash PC systems have similar C-S-H morphology and nucleation density to quartz-cement paste. This confirms that Slag and Fly ash act as inert particles in the early hydration stages.

- The reactions of slag and fly ash are limited at later ages by the lack of capillary water-filled pores. This effect is significant for high replacement level in blended systems. As a result a significant part of the SCM amount does not react. Thus a part of the SCM can be replaced by inert filler and still provide similar compressive strength.
- Slag reaction seems to compete with the clinker at later ages whereas fly ash does not appear to impact the degree of hydration of cement up to 90 days.
- MIP results have shown that slag and fly ash have a different filling ability than the clinker phases. The clinker phases are the most efficient in filling the pores while fly ash was the least effective. However, although the thermodynamic calculations predicted a higher porosity for blended systems, the MIP data showed that the total porosity was slightly higher for blended systems but the critical pore entry size was similar in all the systems (pure cement and blends). This emphasizes that the C-S-H from slag and fly ash fill the pores differently than C-S-H from cement. C-S-H from cement hydration becomes denser after about 2 days. Whereas the C-S-H from slag and fly ash seems less dense and could be present as needles which are efficient to decrease the critical radius but less to reduce the total porosity. ¹H NMR confirmed that the C-S-H structure in blended system at 28 days was modified compare in the cement paste: the gel water/C-S-H intersheet ratio was decreased with the proportion of slag in the blend.

3. Impact of Limestone

- Unlike slag and fly ash, limestone is dissolving from the very beginning of the hydration. As a consequence the induction is markedly reduced.
- Limestone has a larger accelerating effect on the acceleration due to the high number of C-S-H nucleation sites while the growth of C-S-H is not changed. A visible alignment of C-S-H on limestone surface seems to indicate that the effect of increased nucleation seems related to the arrangement of the atom at the limestone surface.

4. Nucleation and Growth of C-S-H

- Our results support the hypothesis that the acceleration is related to the nucleation and growth of C-S-H. The slope was steeper when a large density of small C-S-H particle growing was found.
- The microscopic observations of the quartz, slag, fly ash, limestone and cement surfaces confirmed that C-S-H is forming by a heterogeneous process and that the species are available everywhere in the pore solution.
- The effects of shearing and calcite surface indicate that the nucleation of C-S-H can be enhanced. Shearing may disturb the double layer surrounding the dissolving cement grains that

might better disperse the ions through the mix. It is also possible that the C-S-H nuclei are dislodged and displaced onto the surfaces during the mixing. The limestone effect may be related to the dissolution of this phase but also to a favorable surface structure.

- Increasing temperature does not favor the nucleation density of C-S-H. However the growth of the needles was enhanced (Appendix 1).
- The change of C-S-H morphology induced by the adsorption/desorption of sulfate ions on C-S-H does not appear to impact the kinetics. A similar effect is observed with alite and cement which leads to different C-S-H morphology. This indicates that the growth mechanism is not changed although the ^1H NMR measurements showed that C-S-H structure was modified with sulfate. The gel water/C-S-H intersheets ratio is decreased with increasing the amount of gypsum in the paste. Further NMR experiments are needed to explore this effect.

5. Later age

- Restriction of space limits the reaction of clinker phases, slag and fly ash. When the capillary pores reach a size of 6-8 nm with MIP, the kinetics switch to a slower rate. The space to fill is thus a determinant parameter for the kinetics at later ages. Information from the chemical shrinkage suggests that similar mechanism is controlling the kinetics of the later age for cement and slag-cement paste.
- The change to slower kinetics at later ages when the capillary pores reach 6-8 nm could possibly explained by the increase of the saturation index in such small pores. This would limit further growth of C-S-H and thus the filling in those pores. The formation of interlayers or intersheets in the C-S-H at later ages might also lead to a decrease of the total porosity with no significant impact on the critical pore radius. The increase of the energy of the pore surfaces with higher curvature could also be important.

Perspectives

Our study on the early hydration has brought new insights but also opened questions regarding the nucleation and growth of C-S-H.

In cement paste, the first growth of C-S-H are randomly distributed but there is always a distance between nucleation sites. The shearing during the mixing process, calcium carbonate surface or ions (such as Mg) are parameters that increase the number of nuclei and reduce the spatial distance between them. Thus the nucleation density can be increased, but also seems to be limited for some reason. What is limiting this process? It is still an outstanding and key question which is directly related to the mechanism of nucleation of C-S-H which is not yet well established. This still limits the scope of new materials whose the surface will be suitable for C-S-H nucleation.

The impact of sulfate on the morphology and structure of C-S-H also poses the question of the mechanism of growth of this hydrate. Especially as the diverging needles structure usually found in

presence of sulfate was not observed for C-S-H growing from the limestone surface. It is not clear if the morphology is dependent on the chemical composition of the pore solution and/or of the substrate. Atomistic modeling of the C-S-H structure coupled with experiments might bring useful information.

The formation of gel water in C-S-H was affected by the gypsum content and the presence of SCM. It might be interesting to investigate if these two components lead to similar mechanism that change the gel water/intersheet ratio. Does the adsorption of sulfate or incorporation of aluminate in C-S-H impede the formation of gel pores? The use of ^1H NMR is quite new in the cement field but might play a crucial role for the understanding of the C-S-H structure.

The work on blended systems at later ages has brought quantitative information on the ability to fill the space which might be useful for microstructural models. Recent modelling with μic has shown that the porosity can be simulated in cement paste. Currently efforts are done to improve the thermodynamic modelling of blended systems. These data combined with the filling ability of the hydrates should be improve the simulation of the microstructure development in cement and blended systems.

Slag and fly ash were the only two SCM used in this study, however systems containing limestone or even ternary systems may be the cements for tomorrow. Thus those systems should be considered for similar study.

The results showed that a part of the SCM is not reacting due to the lack of space. Thus, this part could be replaced by inert particle. Figure 6.1 shows that replacing 10% of the slag by inert quartz does not change the compressive strength from 10 days. Other properties might be verify, however these results are promising to optimize the replacement of slag which has limited resource.

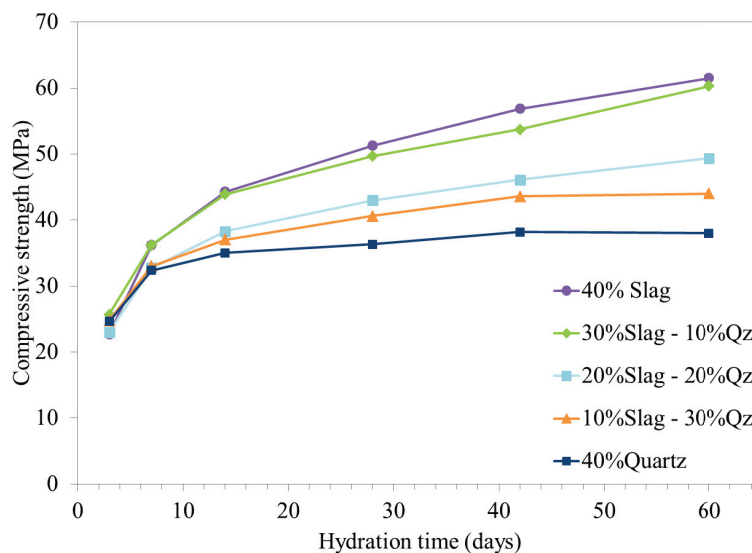


Figure 6.1: Compressive strength of Slag- quartz- PC system. 10% of slag can be replaced by inert filler while the mechanical property is maintained

Appendix 1

Effect of the temperature on nucleation and growth of C-S-H

The increase of energy caused by the shear between the particles may increase the temperature of the paste. Juilland[1] measured an increase of 5°C right after the mixing. Despite this slight increase was not enough to perturb the kinetics of hydration, we investigate in this section the effect of larger increase of temperature. The purpose of this study is to understand what happen when more energy is induced to the system.

Figure A1.1 shows the heat released from a cement paste at different curing temperature (5°C, 20°C, 60°C). The kinetics is significantly dependent of the temperature and the highest temperature the main reactions occur within 10 hours.

Although temperature above 50°C changes the phase assemblage and the density of C-S-H[2, 3], it can be seen on micrographs in Figure A1.2 that at 60°C similar C-S-H development is occurring on the cement surface than at 20°C. At 1 hour of hydration the cement grain is covered with C-S-H nucleation sites randomly dispersed. From Figure A1.2(a) and Figure A1.2(b) temperature does not seems to favor the number of nucleation sites on cement surface as they seems less numerous than at 20°C. After 2 hours at 60°C which corresponds to the end of the acceleration period, the grain is covered of C-S-H forming the sea-anemone structure. In contrast at similar time on the main heat peak at 20°C (Figure 3.9) the C-S-H present the sea-anemone structure but composed of less needles and their length appear shorter. Therefore the shorter needles cover less surface than at 60°C where they are longer.

Similar number of nucleation sites is observed on cement surface at 20°C and 60°C. Thus, the temperature favors the growth rate rather than the nucleation; this means that the activation energy for nucleation is higher than that for the growth of C-S-H.

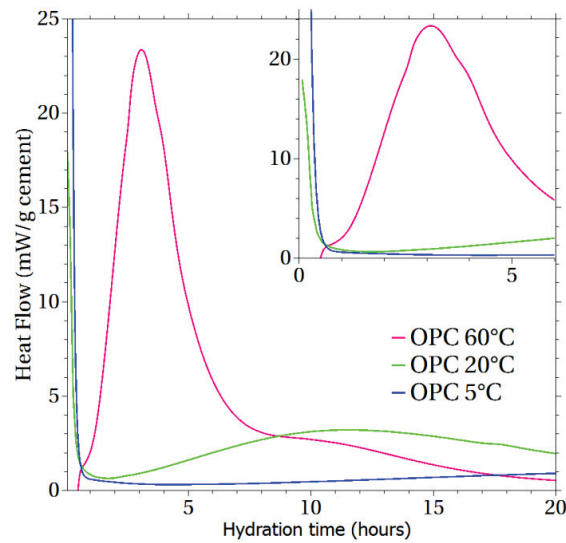


Figure A1.1: Calorimetry curves of cement paste at 5°C, 20°C and 60°C

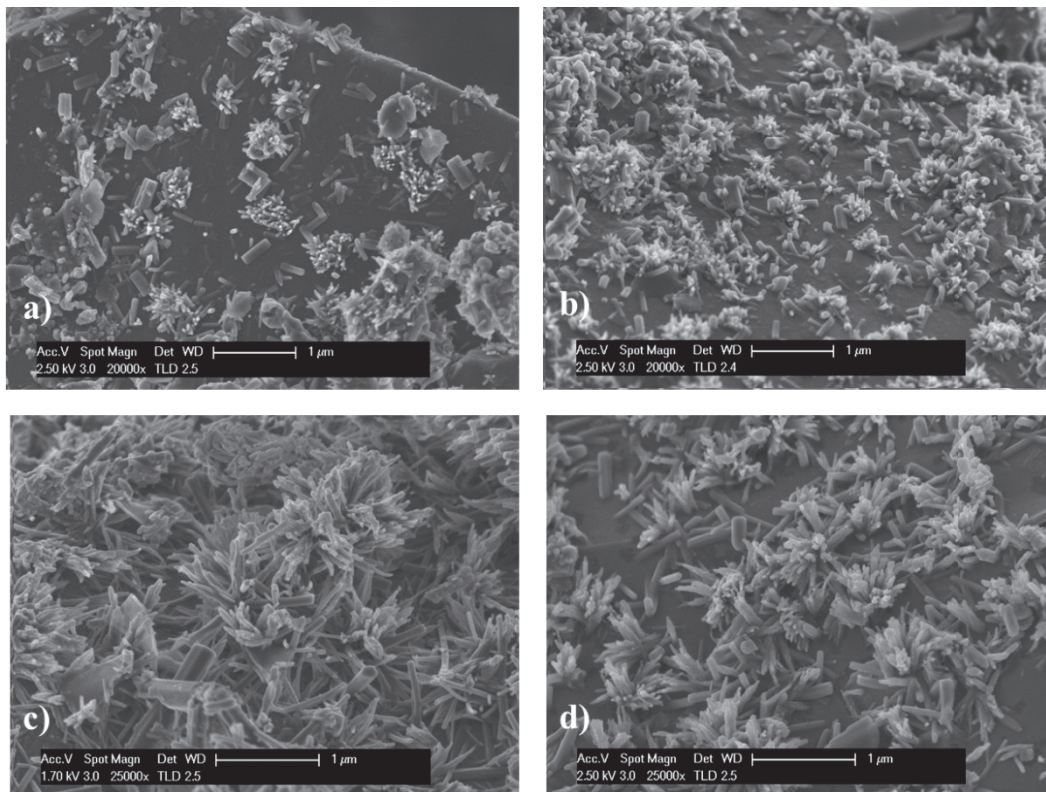


Figure A1.2: Micrographs of cement paste a) 60°C at 1 hour b) 20°C at 2 hours and c) 60°C at 2 hours d) 20°C at 8 hours

Bibliography

1. Juilland, P., et al., *Effect of mixing on the early hydration of alite and OPC systems*. Cement and Concrete Research, 2012. **42**(9): p. 1175-1188.
2. Gallucci, E., X. Zhang, and K.L. Scrivener, *Effect of temperature on the microstructure of calcium silicate hydrate (C-S-H)*. Cement and Concrete Research, 2013. **53**(0): p. 185-195.
3. Lothenbach, B., et al., *Thermodynamic modelling of the effect of temperature on the hydration and porosity of Portland cement*. Cement and Concrete Research, 2008. **38**(1): p. 1-18.

Appendix 2

Calculation of the supersaturation index of C-S-H and the minimal radius for precipitation

The saturation index SI is defined as:

$$SI = \log\left(\frac{K}{K_{sp}}\right)$$

Where K is the ion activity product and K_{sp} is the solubility product of the phase (here C-S-H)

When SI>0 the solution is supersaturated with respect to the crystal and then crystallization occurs

When SI=0 the solution is at equilibrium

When SI<0 the solution is undersaturated with respect to the crystal

We used the data of the pore solution extracted from a Portland cement paste w/c 0.5 from Lothenbach[1]. The data are duplicated in Figure A2.1.

Time [h]	K	Na	Li	Ca	Sr	Ba	Cr	Mo	Fe	Al	Si	S	OH ⁻
mM													
0.02	320	26	0.35	21.1	0.15	0.015	0.36	0.021	0.143	0.04	0.14	161	85
0.5	350	28	0.46	21.1	0.16	0.006	0.40	0.025	0.021	0.03	0.10	163	120
1	360	28	0.46	22.2	0.17	0.006	0.41	0.025	0.014	0.03	0.09	156	130
1.5	360	28	0.46	22.9	0.17	0.006	0.41	0.021	0.007	0.03	0.07	150	150
2	360	29	0.52	24.1	0.18	0.006	0.41	0.025	0.007	0.03	0.06	147	150
4	360	29	0.52	23.0	0.24	0.003	0.36	0.017	0.007	0.03	0.07	150	150
6	340	27	0.52	22.1	0.29	0.003	0.25	0.008	<0.007	0.03	0.06	139	150
7	350	30	0.63	21.3	0.30	0.006	0.22	0.008	<0.007	0.03	0.07	151	150
16	430	32	0.58	9.5	0.15	<0.003	0.10	<0.004	<0.007	<0.004	0.07	136	200
26	430	44	0.75	4.2	0.08	<0.003	0.07	<0.004	<0.007	<0.007	0.17	83	360
69	480	49	0.69	2.0	0.05	<0.003	0.04	<0.004	<0.007	<0.007	0.21	9	480
144	520	55	0.81	2.1	0.05	<0.003	0.05	<0.004	<0.007	0.09	0.24	10	520
336	510	56	0.86	1.9	0.05	<0.003	0.05	<0.004	<0.007	0.09	0.23	9	560
696	560	63	0.92	1.2	0.03	<0.003	0.05	<0.004	<0.007	0.12	0.27	11	540
2520	650	57	0.86	1.5	0.05	<0.003	0.06	<0.004	<0.018	0.04	0.21	17	570
7608	640	65	1.2	1.5	0.05	n.a.	0.06	n.a.	<0.018	0.11	0.21	16	590
Concentrations in filtered blank solutions													
	0.06	0.05	<0.006	0.03	<0.005	<0.003	<0.004	<0.004	<0.007	<0.01	0.01	0.04	-

The values for OH⁻ refer to the free concentrations measured in the pore solutions.

The measured concentrations of Zn and Mg were in all samples below the respective detection limits of 0.001 and 0.02 mM, respectively. Total S is determined by ICP-OES independent of its redox state. In pure OPC system investigated, S is present in the oxidized form as sulphate.

Figure A2.1: Concentration in the pore solution from a cement paste w/c 0.5

We used GEMS to calculate the SI of C-S-H in the paste at 28 days. The input data were the chemical composition of the pore solution at 696 hours.

The GEMS calculations give **SI_{C-S-H} = 0.58**

The Correns equation [2] describes the relation between the pressure and the concentration of the salt and is written as:

$$P = \frac{RT}{V_m} \ln \left(\frac{K}{K_{sp}} \right) = \frac{RT}{V_m} \ln(10^{SI})$$

Where R is the gas constant of 8.314J/K/mol

T is the temperature in kelvin units, here 293 K

V_m is the molar volume, for C-S-H V_m is estimated to 101 g/mol

For the supersaturation SI_{C-S-H} 0.58, the equation gives **P= 31 MPa**

Crystallisation pressure develops only when crystals grow in pores larger than a certain radius which corresponds to

$$P = \frac{2\gamma}{r}$$

Where γ is the interfacial energy between the crystal and the solution. This value has been calculated for C-S-H by Garrault[3] and is 0.12 J/m²

Thus, **r= 7.7 nm for 28 days**

Therefore, smaller pores than 7.7nm radius apply a pressure of 31 MPa which avoid the C-S-H to precipitate. This value is in good agreement with the MIP results.

The radius size does not decreases much from the calculations as **r= 7.1 nm for 100 days** (2520 hours).

Bibliography

1. Lothenbach, B. and F. Winnefeld, *Thermodynamic modelling of the hydration of Portland cement*. Cement and Concrete Research, 2006. **36**(2): p. 209-226.
2. Correns, C.W., *Growth and dissolution of crystals under linear pressure*. Discuss. Faraday Soc., 1949. **5**: p. 267-271.
3. Garrault-Gauffinet, S. and A. Nonat, *Experimental investigation of calcium silicate hydrate (C-S-H) nucleation*. Journal of Crystal Growth, 1999. **200**(3-4): p. 565-574.

Appendix 3

Fitting the kinetics at later age

Figure A3.1 shows the chemical shrinkage data of PC and 40% Slag PC systems. Both curves show a linear slow rate at late age. The mechanism controlling this stage is not well understood and often diffusion is assumed to be the controlled mechanism.

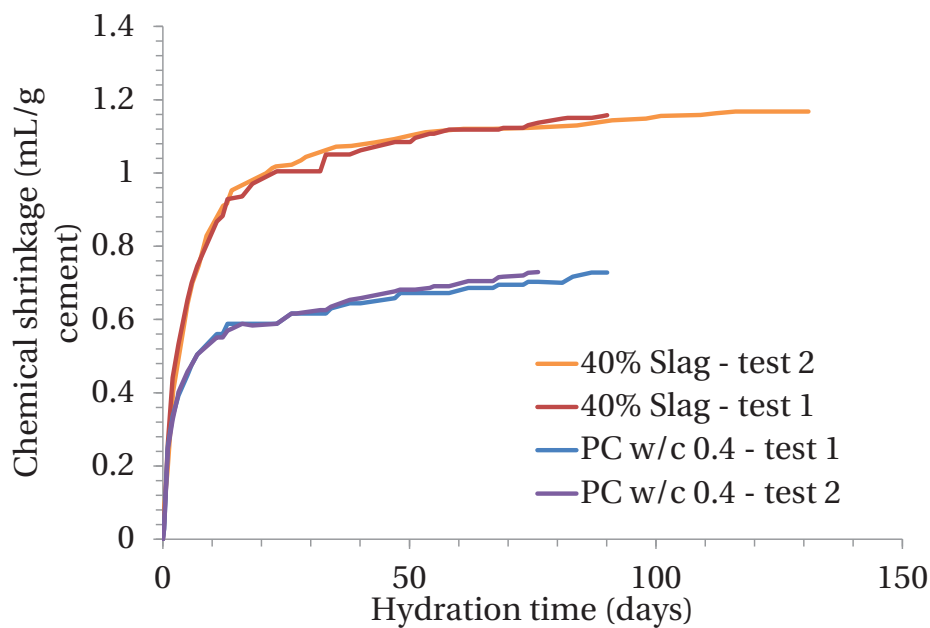


Figure A3.1: Chemical shrinkage curve of cement and 40% slag systems

When the supply of one of the reactant becomes limited then the reaction is diffusion controlled. The volume of the C-S-H phase will increase with time as:

$$V \propto (Gt)^{1/2}$$

Where v is the volume of the phase, G is the growth rate, t is the time.

Thus,

$$\log V \propto \frac{1}{2} \log G + \frac{1}{2} \log t$$

$$\log V \propto A + \frac{1}{2} \log t$$

Figure A3.2 shows the log of the chemical shrinkage as a function of the log time. The late age rate was fit with a simple $y = A + px$ behavior

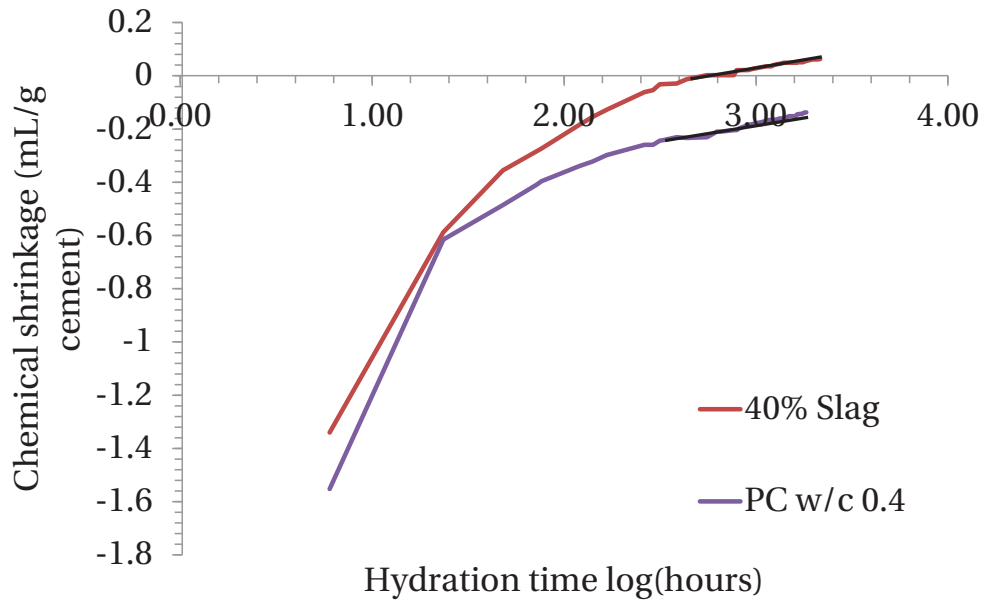


Figure A3.2: Fitting the late age rate

Table A3.1 shows the coefficients from the fitting of the curve at the late age. The slope of the curve (p) should be 0.5 if diffusion is controlling the reaction at this stage. The results indicate that the slope does not match the diffusion controlled value. Therefore, diffusion does not seem the mechanism controlling this period.

Table A3.1: Parameters derived from the fitting of $\log(\text{chemical shrinkage})$ and $\log(\text{time})$

	A	p
PC	0.55	0.12
40% Slag	0.21	0.09

Curriculum Vitae

Elise Berodier

Date of birth: 14th June 1986
Nationality: French

Education

- 2011- 2014 **PhD Thesis in Material Science:** Impact of the Supplementary Cementitious Materials on the Kinetics and Microstructural development of Cement Hydration - Laboratory of Construction Materials, Ecole Polytechnique Fédérale de Lausanne. Switzerland
- 2009-2011 **Master in Material Science (double degree)**
Master in degradation of materials - Industrial Engineering school of Barcelona - Politecnico University of Catalonia. Spain
- 2007-2011 Master in Material Science - Ecole Européenne d'Ingénieurs de Nancy – Institut National Polytechnique de Lorraine. France
- 2007-2005 **Bachelor degree** in Physics - University of Franche Comté. France
- 2004-2005 Preparatory course for National Polytechnique Institutes of France – National Polytechnique Institut of Grenoble. France

Professional Experience

- Switzerland - **EMPA** laboratory of Mechanics of Materials and Nanostructure
“Synthesis of silicon nanostructures by metal-assisted chemical etching”
Supervisor: Dr Michael Bechelany and Johannes Michler
- France – **SNC Lavalin** Engineering and Construction company, Lyon
Assistant of site manager
Supervisor: Nicolas Chateau
- Le Pavillon des Sciences** Scientific museum, Montbéliard
- Spain - **CIEFMA** Center of research of materials in Politecnico University of Catalonia
Wear of stainless steels in aqueous solution
Supervisor: Prof A. Mateo

Publications

Berodier, Scrivener, *Understanding the filler effect on the Nucleation and Growth of C-S-H*, J. Am. Ceram. Soc. 2014

Berodier, Scrivener, *Evolution of the pore structure in slag-cement systems*, Proceedings of the XIII International conference on durability of building materials and components, Sao Paulo 2014

Berodier, Bazzoni, Scrivener, *Study of nucleation and growth of C-S-H by means of electron microscopy* Workshop on Cement hydration, Villars 2014.

Berodier, Scrivener, *Filler effect at early age*, Rilem TC- SCM workshop. Dubendorf 2014

Berodier, Scrivener, *Microstructure development in blended system*, Proceedings of the 14th Euroseminar of Microscopy applied to Building Materials, Copenhagen 2013

Berodier, Scrivener, *Impact of filler on kinetics*, Proceedings of the 32nd Annual Conference on Cement and Concrete Science, Belfast 2012

Bechelany, Berodier, Maeder, Schmitt, Michler, Philippe, *New Silicon Architectures by Gold-Assisted Chemical Etching*. ACS Applied Materials & Interfaces, 2011. **3**(10): p. 3866-3873.

Dejeu, Bechelany, Berodier, Rougeot, Michler, Gauthier., et al., *Nanostructured Nonadhesive Surfaces for Micro- and Nanomanipulation*. The Journal of Physical Chemistry, 2012. **116**(28): p. 15117-